Dual Oxidant System for In Situ Treatment of Organic Contaminants

by

Yuyi Jin

A thesis
presented to the University of Waterloo
in fulfilment of the
thesis requirement for the degree of
Master of Applied Science
in
Civil Engineering

Waterloo, Ontario, Canada, 2017

Author's Declaration

I hereby declare that I am the sole author of this thesis. This is a true copy of the thesis, including any required final revisions, as accepted by my examiners.

I understand that my thesis may be made electronically available to the public.

Abstract

Recently, the potential catalytic properties of manganese dioxide have attracted attention as a means to activate persulfate. This focus of this research was on the potential ability of $MnO_{2(s)}$ solids synthesized through permanganate oxidation of organics to activate persulfate. A combined permanganate + persulfate (PM/PS) system is proposed for the treatment of organic compounds. In this system, a limited mass of permanganate is first introduced into a contaminated zone to generate $MnO_{2(s)}$ and then, after an appropriate reaction period, persulfate is delivered and activated by $MnO_{2(s)}$ for enhanced treatment.

$MnO_{2(s)}$ generated from non-aqueous phase trichloroethylene (TCE) and potassium permanganate were employed to activate persulfate for the treatment of 1-methylnaphthalene in a series of batch experiments at various $MnO_{2(s)}$ to persulfate mass ratios. The results from these batch experiments showed that $MnO_{2(s)}$ is capable of activating persulfate. The highest 1-methylnaphthalene degradation rate was achieved at a mass ratio 20 g $MnO_{2(s)}$ /g persulfate with synthetic groundwater. The mass of 1-methylnaphthalene removed increased with an increase in $MnO_{2(s)}$ dosage. The degradation of 1-methylnaphthalene using a mass ratio 5:1 (g $MnO_{2(s)}$: g PS) with Milli-Q water was slightly higher than for unactivated persulfate. The degradation kinetics of 1-methylnaphthalene by persulfate activated by $MnO_{2(s)}$ solids was one order of magnitude higher than that achieved by unactivated persulfate. The surface of $MnO_{2(s)}$ solids remained unaltered during the experiment period. The performance of the PM/PS system for the degradation of aqueous phase benzene and TCE was investigated in a series of batch reactors. The PM/PS system produced higher benzene degradation than unactivated persulfate for the same mass of PS consumed. Bench-scale stop-flow column systems that closely mimic *in situ* conditions were executed to evaluate the performance of the proposed PM/PS system for the treatment of a residual TCE and 1-methylnaphthalene mixture. The TCE and 1-methylnaphthalene mass removed in the PM/PS system was 11% and 25% higher than by only permanganate or persulfate, respectively. Based on the findings from batch and column experiments, the minimum permanganate to persulfate molar ratio for effective treatment is 13:1.

The results of this research confirm that $MnO_{2(s)}$ solids are able to enhance persulfate reactivity, and that the proposed PM/PS system is a promising remedy for the treatment of soil and

groundwater contaminated with organic compounds. The research efforts provide key insights into the design of a PM/PS system for ISCO.

Acknowledgements

I would like to show my greatest respect and gratitude to my supervisor Prof. Neil R. Thomson, for providing me the opportunity to join his research team and enjoy the most valuable research experience. He patiently supervised and guided me with my research over the past two years. Thank you, Neil, for your countless hours of revisions and advice on my thesis.

I also thank Prof. Hassan Baaj (Civil and Environmental Engineering) and Prof. Wayne Parker (Civil and Environmental Engineering) for being my committee members and generously offering your precious time and valuable comments on my thesis.

Financial support for this investigation was provided by a Natural Sciences and Engineering Research Council (NSERC) of Canada Collaborative Research and Development Grant (N.R. Thomson), and the American Petroleum Research Team.

I also would like to thank Felipe Solano, for helping me a lot in laboratory, sharing his experimental experience with me, and providing me with professional support for my research.

My sincere thanks to Mark Sobon and Shirley Chatten who advised and helped me with the column experimental setup and analytical methods.

I highly appreciate the lab assistance from Mark Merlau, Wayne Noble and Julie Taylor. I also would like to thank all those who helped in my research and lab work: Saeid Shafieiyoun and other colleagues on the Thomson Research Team.

I especially thank my parents for their great support and encouragement during the years of study! They gave me everything and support me to pursue my dreams throughout studies in China and Canada.

Table of Contents

List of Figures

List of Tables

Chapter 1

Chapter 1
Introduction

1

1.1 General

Groundwater and soil contamination by toxic organic chemicals released from various human activities are a risk to the natural environment and human health. As of September 2016, the National Priority List (NPL) released by the USEPA indicated 1338 active contaminated sites with more than 1000 of them suffering from groundwater and soil contamination (USEPA 2016). Volatile and semi-volatile organic compounds (VOCs and SVOCs) are the most widespread (Siegrist et al. 2011) and have been observed at > 60 % of these sites (USEPA 2013).

About 70% of the VOC impacted sites have non-aqueous phase liquids (NAPLs) present which as a long-term source of contamination to the groundwater system (Newell et al. 1995; Pivetz 2012; Siegrist et al. 2001). Halogenated solvents, fuel hydrocarbons (i.e., benzene, toluene, ethylbenzene, and xylene (BTEX) compounds), as well as polycyclic aromatic hydrocarbons (PAHs), are often found in these NAPL source zones (USEPA 2013). Trichloroethylene (TCE) is the most common halogenated solvent observed, and is denser than water and will not readily degrade in the subsurface environment (Huling and Weaver 1991; Liang et al. 2003). Due to the widespread use of fuel, benzene is commonly found in the subsurface and is volatile, highly soluble and hence very mobile in groundwater (ATSDR 2007). 1-methylnaphthalene is a PAH and is a common co-contaminant at many contaminated sites (USEPA 2013). Exposure to these compounds even at low concentration levels pose a carcinogenic risk to humans and thereby complete removal of the NAPL source zone and contiguous plume is generally required to satisfy regulatory standards (Siegrist et al. 2011).

Remedy approaches include institutional controls (ICs), on-site containment, *in situ* treatment (e.g., *in situ* bioremediation or chemical treatment), *ex situ* treatment (e.g., pump and treat (P&T)), and monitored natural attenuation (MNA) (USEPA 2013; Xu 2006). According to the *Superfund Remedy Report (SRR) 14th Edition*, the groundwater remedies selected by the Superfund remedial program have been a mix of primarily P&T, *in situ* treatment, MNA, and some ICs. P&T can be

used for primary hydraulic containment, but its high cost and inability to treat VOCs in NAPL source zones limits its application. MNA has a low cost but very slow removal rates. The percentage of sites where P&T or MNA have been selected has decreased, but the selection of *in situ* treatment remedies, which are effective to address the NAPL source zones, continues to rise from 30 % during 2005-08 to 38 % during 2009-11. Of these *in situ* treatment technologies, *in situ* bioremediation and chemical oxidation (ISCO) were the most frequent selected remedy approach to address NAPL source zones (USEPA 2013). The increasing application of ISCO at contaminated sites suggests the need for evolving innovation and optimization of this technology is required.

Strong oxidants generate reactive species (including free radicals) which are capable of transforming or degrading organics (Siegrist et al. 2011). In general, an ISCO system delivers strong oxidants at varied concentrations and mass loading rates into the subsurface as a solution to degrade and hence reduce the mass of the organic contaminants to less harmful species (Huling and Pivetz 2006; Siegrist et al. 2011; Watts et al. 2006). ISCO has the advantage of immediately destroying contaminants in place and enhancing the mass transfer of NAPLs to the aqueous phase which accelerates mass removal (Siegrist et al. 2011). The most common oxidants applied are hydrogen peroxide (H_2O_2), permanganate (MnO_4^-) and persulfate ($S_2O_8^{2-}$) (Krembs et al. 2010). Each chemical oxidant has advantages and disadvantages with respect to stability and reactivity as listed in Table 1.1.

1.2 Hydrogen Peroxide

Catalyzed H_2O_2 propagations (CHP) reactions which occur when elevated concentrations of peroxide are mixed with ferrous iron was the first ISCO process thoroughly studied and employed at the field scale. In a CHP system, the strong oxidant hydrogen peroxide is activated by a catalyst (e.g., soluble iron and iron oxide minerals) to generate free radicals (hydroxyl radical, $OH^{\cdot}$; and hydroperoxyl radical, $HO_2^{\cdot}$) and anions (hydroperoxide anion, HO_2^-; and superoxide radical anion $O_2^{\cdot -}$) (Mitchell et al. 2014) as given by:

$$H_2O_2 + Fe^{2+} \rightarrow OH^{\cdot} + OH^- + Fe^{3+} \qquad \text{(Eq 1.1)}$$

$$OH^{\cdot} + H_2O_2 \rightarrow HO_2^{\cdot} + H_2O \quad \text{(Eq 1.2)}$$

$$HO_2^{\cdot} \leftrightarrow O_2^{\cdot -} + H^+ \quad \text{(Eq 1.3)}$$

$$HO_2^{\cdot} + Fe^{2+} \leftrightarrow HO_2^- + Fe^{3+} \quad \text{(Eq 1.4)}$$

The generation of active radicals and reactive species enable the CHP system to have universal reactivity with a wide range of organic contaminants (Watts et al. 2007). The rapid degradation of aqueous phase organic contaminants adjacent to the NAPL-water phase increases the mass transfer of organic contaminants from the NAPL phase to aqueous phase, which can significantly enhance NAPL degradation rates in a CHP system (Petri et al. 2011). However, H_2O_2 is a short-lived oxidant with a half-life of several hours to days, which limits H_2O_2 travel to < 3 m from an injection well in some cases (Watts et al. 2007; Xu and Thomson 2007). This low persistence significantly reduces the effectiveness of the CHP system to interact with organic contaminants. To overcome this issue, stabilizers such as ethylenediamine tetraacetic acid (Xu and Thomson 2007) or a phosphate stabilizer (Baciocchi et al. 2004) have been used to stabilize H_2O_2.

1.3 Permanganate

Permanganate (MnO_4^-) is a strong transition metal oxidant with a high reduction potential of +1.68 volts (V) and is available as sodium permanganate ($NaMnO_4$) (a liquid) or potassium permanganate ($KMnO_4$) (a solid) (Huling et al. 2006; Petri et al. 2011). The form of permanganate has little impact on the reactivity with organics, and related consumption during the oxidation process (Petri et al. 2011; Siegrist et al. 2002). Permanganate mainly degrades organic compounds through direct electron transfer rather than a free radical process. The following half reactions show the electron transfer behavior of permanganate at different pH conditions (Petri et al. 2011):

$$MnO_4^- + 8H^+ + 5e^- \rightarrow Mn^{2+} + 4H_2O \quad pH < 3.5 \quad \text{(Eq 1.5)}$$

$$MnO_4^- + 2H_2O + 3e^- \rightarrow MnO_2(s) + 4OH^- \quad 3.5 < pH < 12 \quad \text{(Eq 1.6)}$$

$$MnO_4^- + 1e^- \rightarrow MnO_4^{2-} \quad pH > 12 \quad \text{(Eq 1.7)}$$

Three electrons are transferred in the half-reaction given by Eq 1.6, which is the dominant reaction in most natural groundwater systems. The non-toxic by-product (manganese dioxide solid) is inevitably generated when this dominant reaction occurs.

The use of permanganate in the field is well understood and there exists a substantial amount of supporting literature (Petri et al. 2011). Permanganate is very stable and can persist for months and travel considerable distances in the subsurface. The predictable chemical behavior and high stability makes permanganate the most often selected oxidant based on the statistics gathered by Krembs et al. (2010). The reaction between permanganate and TCE generates CO_2 and Cl^- from TCE, and $MnO_{2(s)}$ from MnO_4^- (Li & Schwartz 2004a):

$$C_2HCl_3(\text{TCE}) + 2MnO_4^- \rightarrow 2MnO_{2(s)} + 2CO_{2(g)} + 3Cl^- + H^+ \qquad \text{(Eq 1.8)}$$

Li and Schwartz (2004b) determined that the $MnO_{2(s)}$ generated from the oxidation of TCE by permanganate was semi-amorphous potassium-rich birnessite with a chemical formula of $K_{0.854}Mn_{1.786}O_4 \cdot 1.55\ H_2O$.

The by-product $MnO_{2(s)}$ can adversely affect the performance of permanganate for NAPL treatment (Heiderscheidt et al. 2008; Siegrist et al. 2002). Many studies have shown that the formation and deposition of $MnO_{2(s)}$ at the NAPL/water interface reduces NAPL/water mass transfer (Li and Schwartz 2004a; MacKinnon and Thomson 2002; Tunnicliffe and Thomson 2004). Li and Schwartz (2002) reported that $MnO_{2(s)}$ was rapidly formed as a precipitate rind above a NAPL pool once permanganate came in contact with NAPL, and further limited dissolution. In a two-dimension model sand aquifer, the $MnO_{2(s)}$ deposited from the reaction between PCE and permanganate directly limited water flow around a PCE pool and hence the PCE/water mass transfer rate (MacKinnon and Thomson 2002). The accumulation of $MnO_{2(s)}$ may also reduce the permeability of a porous medium (Huling et al. 2006; Petri et al. 2011; Schroth et al. 2001). Li and Schwartz (2004a) quantified a hydraulic conductivity reduction as high as 80 % in a series of column experiments. Huang et al. (2002) indicated that the $MnO_{2(s)}$ generated from the reaction between TCE and permanganate caused a 20 % reduction of pore space in a column test. Other stduies have shown that the $MnO_{2(s)}$ accumulated close to the oxidant injection point and reduced the local permeability of the porous medium (Huang et al. 2002; Li and Schwartz 2002), and then subsequent injections were limited (Heiderscheidt et al. 2008; Huling and Pivetz 2006; Petri et al. 2011). Tunnicliffe and Thomson (2004) observed that $MnO_{2(s)}$ formation appeared and behaved

like a flexible "membrane skin" that varied between 1 and 15 mm over a DNAPL. In an interfacial deposition experiment reported by Urynowicz and Siegrist (2005), $MnO_{2(s)}$ was observed to rapidly deposit as a film at a DNAPL interface.

The reduction of the NAPL dissolution rate and clogging of pore spaces may limit the oxidation rate and hence treatment performance using permanganate. Research efforts have focused on the development of approaches to eliminate the effects of the $MnO_{2(s)}$. Li and Schwartz (2004 b&c) proposed to use organic acids (citrate and oxalate) to dissolve and remove $MnO_{2(s)}$. Likewise, sodium hexametaphosphate (HMP) has been implemented to stabilize $MnO_{2(s)}$ during permanganate delivery in column studies (Crimi et al. 2009). Chokejaroenrat et al. (2014) recently found that sodium HMP was able to prevent the formation of a $MnO_{2(s)}$ crust and improve the treatment of TCE in a low permeability zone.

Permanganate is regarded as selective oxidant because its simple electron transfer scheme restricts its reactivity to a limited range of organic contaminants compared to other oxidants (Petri et al. 2011). Permanganate has a high reactivity with alkenes, chlorinated ethenes (e.g., TCE, PCE), phenols, and some PAHs, which are electron-rich (Table 1.1). Permanganate is ineffective in oxidizing saturated hydrocarbons without functional groups, such as alkane compounds, benzene, and chlorinated aromatics.

1.4 Persulfate

Compared to hydrogen peroxide and permanganate, persulfate ($S_2O_8^{2-}$) is the newest chemical oxidant. Persulfate can be activated by various means (e.g., transition metals, heat, alkaline substances, and UV) to form the sulfate radical $SO_4^{\cdot -}$ (Eq 1.9) (Wilson et al. 2013). The sulfate radical not only oxidizes organic compounds but also initiates the formation of other radicals (e.g., the hydroxyl radical $OH^{\cdot}$ and superoxide anion radical $O_2^{\cdot -}$) through a series of radical propagation chain reactions (Furman et al. 2010). The termination reactions consume these radicals to oxidize target organic compounds and form reaction products (Petri et al. 2011).

$$S_2O_8^{2-} + 2e^- \rightarrow SO_4^{2-} + SO_4^{\cdot -} \qquad \text{(Eq 1.9)}$$

$$SO_4^{\cdot -} + H_2O \rightarrow HSO_4^- + OH^{\cdot} \qquad \text{(Eq 1.10)}$$

The formation of these radicals enable persulfate to degrade a wider range of organic contaminants than permanganate (Huling et al. 2006; Petri et al. 2011; Watts et al. 2006). Sra (2010) showed that persulfate is effective to degrade gasoline compounds including benzene (C_6H_6; Eq 1.11) and 1-methylnaphthalene ($C_{11}H_{10}$; Eq 1.12).

$$C_6H_6 + 15S_2O_8^{2-} + 12H_2O \rightarrow 30SO_4^{2-} + 6CO_{2(g)} + 30H^+ \quad \text{(Eq 1.11)}$$

$$C_{11}H_{10} + 27S_2O_8^{2-} + 22H_2O \rightarrow 54SO_4^{2-} + 11CO_{2(g)} + 54H^+ \quad \text{(Eq 1.12)}$$

Persulfate persists longer in the subsurface than H_2O_2 (Huang et al. 2002; Sra et al. 2014). As a result, persulfate has the potential to be transported in porous media, and migrate into low-permeability zones through diffusion (Liu et al. 2014).

Ferrous iron (Fe (II)) is the most common activator mainly due to its easy accessibility and low environmental toxicity (Petri et al. 2011). When mixed with persulfate, ferrous iron donates an electron to generate a sulfate radical (Eq 1.13), which then can oxidize an organic compound or produce other radicals through propagation reactions (Liang et al. 2004a; Petri et al. 2011). A ferrous iron activated persulfate system can generate high degradation rates (Liang et al. 2004a); however, the transport distance and distribution of ferrous iron in the subsurface is limited by various reactions (Huling et al. 2006). Liang et al. (2004a) indicated that persulfate activation by Fe (II) was not efficient and large amounts of Fe (II) are required because Fe(II) was consumed and transformed to Fe(III), which is less efficient as a persulfate activator.

$$S_2O_8^{2-} + Fe^{2+} \rightarrow SO_4^{2-} + SO_4^{\cdot -} + Fe^{3+} \quad \text{(Eq 1.13)}$$

1.5 Research Needs and Objectives

Recently, the potential properties of $MnO_{2(s)}$ to activate persulfate have gained attention (Ahmad et al. 2010b; Jo et al. 2014). Manganese oxides have been identified as a common activator for H_2O_2. As an analogy to H_2O_2, it has been speculated that persulfate could potentially be activated by manganese dioxide (Petri et al. 2011). Ahmad et al. (2010) found that the mineral birnessite [δ-MnO_2] synthesized through permanganate oxidation of concentrated hydrochloric acid was the most effective persulfate activator among six subsurface minerals. Do et al. (2010)

revealed that pyrolusite [β-MnO_2] increased persulfate reactivity in a series of slurry batch reactors. However, the potential ability of $MnO_{2(s)}$ to activate persulfate is poorly understood, and the benefit of a combined permanganate and persulfate (PM/PS) system has not been demonstrated. The dual oxidant (PM/PS) system proposed in this research could potentially utilize the strong features of each oxidant and produce several attractive benefits. Figure 1.1 shows a schematic representation of the conceptual PM/PS system used to treat a residual NAPL source zone. In this conceptual model, a limited mass of permanganate is initially delivered into the source zone to generate $MnO_{2(s)}$ that precipitates in the vicinity of the NAPL/water interface. After an appropriate reaction period has passed, persulfate is then delivered into the source zone using the same infrastructure. The presence of the $MnO_{2(s)}$ will activate persulfate at the NAPL/water interface where dissolution occurs. In this PM/PS system the co-injection of an activator solution (e.g., ferrous iron) is not required and activator/persulfate reactions that occur away from the reaction zone or front are avoided. As long at the $MnO_{2(s)}$ remains unaltered *in situ*, multiple persulfate injection episodes are possible to ensure dosing requirements are reached. For a single component NAPL amenable to permanganate treatment this PM/PS system will minimize pore clogging and related hydraulic conductivity impacts, and maximize treatment efficiency. While for a multiple component NAPL containing a complex mixture of saturated hydrocarbons and chlorinated ethenes, this PM/PS system will use the permanganate to react with the chlorinated ethenes to generate $MnO_{2(s)}$ which can then be used to activate persulfate to treat the saturated hydrocarbons. This proposed PM/PS system limits the amount of permanganate and production of $MnO_{2(s)}$, minimizes the need for a separate persulfate activation system, and enhances the efficiency of persulfate to destroy NAPL mass.

The overall goal of this research is a proof-of-concept demonstration of the proposed PM/PS system. To achieve this goal, the following specific research objectives were established:

- Evaluate the ability of $MnO_{2(s)}$ formed separately with different types of organic compounds and permanganate to activate persulfate in aqueous batch experiments.
- Examine the PM/PS system in aqueous batch experiments.
- Execute a series of column experiments to evaluate the application of the PM/PS system in a simulated *in situ* condition.
- Provide initial guidance on permanganate and persulfate molar ratios.

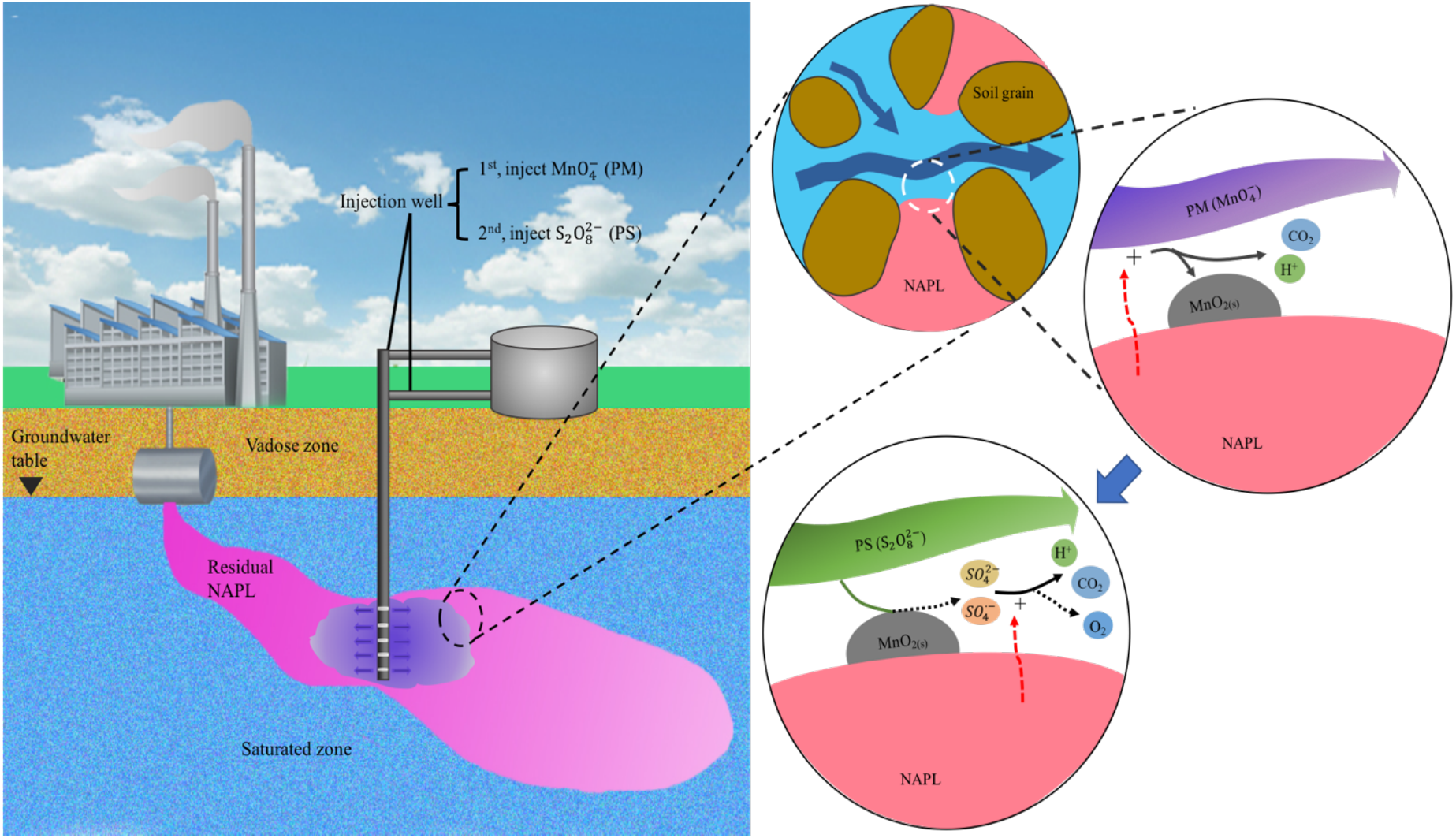

Figure 1.1 Conceptual model of the proposed PM/PS system to treat residual NAPL *in situ*.

Table 1.1 Characteristics of Common Chemical Oxidants for ISCO.

(adapted from Huling et al. 2006; Siegrist et al. 2011, 2001; Watts et al. 2006).

Oxidants	Hydrogen Peroxide	Permanganate	Persulfate
Reagent form	Liquid	Liquid or powder	Liquid or powder
Chemical formula	H_2O_2	$KMnO_4$ or $NaMnO_4$	$Na_2S_2O_8$
Reactive species	hydroxyl radical ($OH^{\cdot}$), superoxide radical ($O_2^{\cdot-}$), perhydroxyl radical ($HO_2^{\cdot}$), hydroperoxide anion (HO_2^-)	permanganate anion (MnO_4^-)	persulfate anion ($S_2O_8^{2-}$), sulfate radicals ($SO_4^{\cdot-}$), hydroxyl radical ($OH\cdot$) superoxide radical ($O_2^{\cdot-}$)
Activator	soluble iron, iron chelates, iron minerals, iron oxide minerals	None	Heat, alkaline substances, UV, transition metals, H_2O_2
Organics amenable to treat	BTEX, polyaromatic hydrocarbons (PAHs), chlorinated alkenes and alkanes, phenols, benzene derivatives	substituted aromatics (with ring activating groups), chlorinated alkenes, chlorinated aromatics, phenols, some PAHs	all aromatics and alkenes, halogenated aliphatics, nitroorganics, fuel hydrocarbons
Organics difficult to treat	some alkanes, PCBs	alkanes, benzene, chloroalkanes, polychlorinated biphenyls (PCBs), MTBE.	
Oxidant stability	Low: hours to days	High: > 3 months	Mid: hours to weeks
Limitations	Minimal persistence in subsurface limits transport and reaction time resulting in the insufficient removal of organics. Activation is required to generate radicals.	Applicable only to a narrow range of organic contaminants. The solid byproducts (MnO_2) have the potential to impede groundwater flow and reduce mass transfer from NAPL.	Activation mechanism is required to generate radical.

Chapter 2

Chapter 2
Methodology

2

2.1 Overview

Two series of batch experiments were performed to examine the ability of $MnO_{2(s)}$ to activate persulfate (PS). Based on the information generated from these batch experiments, a series of column experiments were executed to mimic *in situ* conditions.

In the first series of batch experiments, $MnO_{2(s)}$ solids were generated separately through oxidation of a PAH compound or a chlorinated ethene by permanganate (PM), and then mixed with PS and a dissolved phase model organic compound. The degradation kinetics of the model organic compound were used to evaluate the ability of $MnO_{2(s)}$ to activate PS. The role of the $MnO_{2(s)}$ to PS mass ratio was also investigated.

The second series of batch experiments focused on the production of $MnO_{2(s)}$ and subsequent treatment of a dissolved phase model organic compound in the same reactor. In this system, a limited mass of PM was first added to an aqueous system comprised of a chlorinated ethene and a model organic compound, and then PS was added. This approach closely mimics the sequential delivery of oxidants consistent with the conceptual model. The mass of PS added was controlled by the mass of $MnO_{2(s)}$ formed from PM reduction. The time interval between PM addition and PS addition was based on the visual disappearance of the deep purple PM color. The degradation kinetics of the chlorinated ethene and the model organic compound were used to evaluate treatment performance.

Extending from the results of the batch experiments, a series of column experiments were performed to closely simulate the application of this dual oxidant system *in situ*. Specifically, a two-component NAPL (chlorinated ethene + model organic compound) was placed within a saturated column. The column was then flushed sequentially with PM and PS. The PM/chlorinated ethene molar ratio, and $MnO_{2(s)}$/PS mass ratio determined from the batch experiments were used to prescribe the PM and PS mass loading. Evaluation of treatment

performance was based on changes in the system effluent concentration, and the mass of NAPL removed.

2.2 Materials

Potassium permanganate ($KMnO_4$, > 99 %), sodium persulfate ($Na_2S_2O_8$, ≥ 98%), calcium sulfate ($CaSO_4$, 98%) and 1-methylnaphthalene ($C_{11}H_{10}$, 95%) were purchased from Sigma-Aldrich, USA. Potassium iodide (KI, 99%), sodium bicarbonate ($NaHCO_3$, ACS), calcium carbonate ($CaCO_3$, ACS), sodium chloride (NaCl, 99%) were purchased from BDH, USA. Benzene (C_6H_6, 99.4 %) and trichloroethylene ($ClCHCCl_2$, 100%) were purchased from J.T. Baker, USA. Dichloromethane (CH_2Cl_2, ≥ 99.5%) and methanol (CH_3OH; ≥ 99.9%) were purchased from EMD Millipore, Germany, and Sudan III ($C_{22}H_{16}N_4O$, 86%) was purchased from Fisher Scientific, USA. All chemicals were reagent grade and used as received.

Milli-Q water or synthetic groundwater was used to prepare aqueous solutions. Synthetic groundwater was prepared by adding 100 mg/L calcium carbonate, and 50 mg/L calcium sulfate to Milli-Q water. Then purified CO_2 gas was bubbled until a pH of 4.5 was reached. Following 12 hours of vigorous mixing using a magnetic stirrer (IKA® C-MAG HS 7), purified N_2 gas was bubbled into the solution to adjust the pH to 7.

For the column experiments, a column was constructed from a 6-cm long section of 1.5 cm internal diameter glass tubing. One end of the column was open while the other end was rounded to meet a 2.5-cm long by 0.4-cm internal diameter glass tube (Figure 2.3). Barco silica sand (#71, Opta Minerals Inc.) was used as the porous medium in the columns. This sand was washed with 10 % nitric acid, left overnight, rinsed with Milli-Q water, and then oven dried at 50 ℃ for 24 hours.

2.3 Experimental Design

2.3.1 Batch tests

2.3.1.1 Pre-synthesized $MnO_{2(s)}$ system

2.3.1.1.1 Synthesis of manganese oxide solids

Four different types of manganese oxide solids were investigated for their potential ability to activate PS: birnessite, $MnO_{2(s)}$ generated from the oxidation of a chlorinated ethene by PM in Milli-Q water (Sample #1), and in synthetic groundwater (Sample #2), and $MnO_{2(s)}$ formed by the oxidation of a PAH compound by PM in Milli-Q water (Sample #3).

Birnessite $[\delta - MnO_2]$ was synthesized in accordance with the Method(a) described by McKenzie (1971). Concentrated hydrochloric acid (0.8 M) was dropwise added to a boiling PM (0.4 M) solution with vigorous stirring, and boiled for an additional 10 minutes with a magnetic stirrer (IKA® C-MAG HS 7). After cooling, the solution was vacuum filtered (2.5-µm, Grade 42, Whatman®), and then the precipitate was rinsed with Milli-Q water to remove residual salts and then oven-dried at 50 ℃ for 28 hours. The mass of the birnessite precipitate produced was 22 g/L of the mixture.

$MnO_{2(s)}$ Sample #1 or Sample #2 was prepared by adding the pure phase chlorinated ethene (trichloroethylene, TCE; 0.07 M) and potassium PM (0.125 M) in Milli-Q water or synthetic groundwater and vigorous stirring for 24 hours. The solution was then vacuum filtered (2.5-µm, Grade 42, Whatman®), and the precipitate was rinsed with Milli-Q water or synthetic groundwater and then oven-dried at 50 ℃ for 28 hours. The generated mass of $MnO_{2(s)}$ Sample #1 was 9.5 g/L of the mixture, and the mass of $MnO_{2(s)}$ Sample #2 was 11.6 g/L of the mixture. $MnO_{2(s)}$ Sample #3 were prepared by reacting a pure phase PAH (1-methylnaphthalene; 0.01 M) and potassium PM (0.125 M) in Milli-Q water. The solution and the precipitate were treated as stated above. The mass of produced $MnO_{2(s)}$ Sample #3 was 9.08 g/L of the mixture.

2.3.1.1.2 Experiment setup

Batch experiments were conducted to estimate the potential for the pre-synthesized $MnO_{2(s)}$ to activate PS. As a model PAH organic compound, 1-methylnaphthalene was selected since it is a representative compound in PAH mixtures and is present at numerous contaminated sites (USEPA 2013). The degradation kinetics of 1-methylnaphthalene were used as an indicator to evaluate the efficiency of $MnO_{2(s)}$ to activate PS. For comparison purposes, birnessite which has been shown to activate PS (Ahmad et al. 2010; Do et al. 2010) was also used.

All experiments were performed in 40 mL batch reactors (borosilicate glass vials fitted with 22 mm open cap and Teflon/silicone septa). Details of the experimental conditions are provided in Table 2.1. The stock solution of $Na_2S_2O_8$ (PS) and 1-methylnaphthalene were prepared by mixing the desired quantity of the reagent-grade chemicals with Milli-Q water or synthetic groundwater. The initial 1-methylnaphthalene concentration was 5 mg/L due to its low aqueous solubility (25 mg/L), and the PS concentration was chosen to be 0.5 g/L in order to allow sufficient temporal data to be collected over a reasonable timeframe. A prescribed mass of birnessite or $MnO_{2(s)}$ were loaded into a reactor, then Milli-Q water or synthetic groundwater was added, then the 1-methylnaphthalene and PS stock solutions were added simultaneously (Figure 2.1). Approximately 2 mL of headspace was purposely left in the reactor to allow potential pressure buildup due to gas production (likely O_2, CO_2).

Negative experimental controls consisted of 1-methylnaphthalene and Milli-Q water (Ctrl-MQ), and 1-methylnaphthalene and synthetic groundwater (Ctrl-GW). A positive experimental control consisted of 1-methylnaphthalene and PS only in Milli-Q water (Ctrl-PS). Birnessite was employed at a mass ratio of 5 g birnessite /g persulfate (PS-Birnessite (1:5)) based on a series of preliminary experiments (not discussed) and the findings from Ahmad et al. (2010). For $MnO_{2(s)}$ Sample #1 and Sample #3, the following three mass ratios were explored with Milli-Q water: 5, 10 and 20 g $MnO_{2(s)}$ /g PS (denoted as PS-MnO_2 (1:5), PS-MnO_2 (1:10), and PS-MnO_2 (1:20)). Finally, for the highest mass ratio, the role of synthetic groundwater instead of Milli-Q water was investigated with $MnO_{2(s)}$ Sample #2 (PS-MnO_2 (1:20) /GW).

All experimental series were prepared in triplicate with sacrificial reactors. At least 25 mL of supernatant was extracted from each reactor with a glass syringe (Micro-Mate®) and used to quantify pH and the concentration of PS and 1-methylnaphthalene. The pH and PS concentration

were determined daily. The concentration of 1-methylnaphthalene was determined at Day 0, 1, 2, 4, 6, 8 and 10 for pre-synthesized $MnO_{2(s)}$ Sample #1 and Sample #2 systems, and at Day 0, 1, 2, 4, and 7 for the pre-synthesized $MnO_{2(s)}$ Sample #3 system. All reactors were kept in the dark at a temperature of ~20 ℃ and manually shaken daily.

2.3.1.2 PM/PS system

The focus of these batch experiments was to investigate elements of the PM/PS system where $MnO_{2(s)}$ solids are produced by the initial addition of PM and then PS is added and activated by the generated $MnO_{2(s)}$. Preliminary trials were conducted with an aqueous combination of TCE and 1-methylnaphthalene; however, the relatively high concentration of TCE interfered with the analytical method used to determine the concentration of 1-methylnaphthalene. To avoid this complication, benzene was employed as the model organic compound in place of 1-methylnaphthalene. Benzene is unreactive to PM but reacts with PS (Petri et al. 2011). A series of experiments similar in principal to those discussed in Section 2.3.1.1 was conducted to demonstrate that benzene can be degraded by PS activated by $MnO_{2(s)}$ (see Appendix).

These experiments were performed in 40 mL reactors (borosilicate glass vials fitted with 22 mm open cap and Teflon/silicone septa) with synthetic groundwater. The detailed experimental conditions are listed in Table 2.2. The stock solution of PS and PM were prepared separately by mixing the required quantity of chemicals with synthetic groundwater. The organic compound stock solution was prepared by mixing pure phase benzene (0.2 mL) and TCE (8 mL) with 1L of synthetic groundwater. This mixture was placed on a stirrer (IKA® C-MAG HS7) in the dark for 24 hours and then left undisturbed for > 48 hours to allow equilibrium to be established. Each reactor was filled with 37 mL of the mixed organic compound solution, followed by 2 mL of the PM stock solution. After a predetermined time interval for the PM to be completely consumed by the TCE, 1 mL of the PS stock solution was added (Figure 2.2). Headspace was intentionally left to accommodate pressure buildup due to gas production (likely O_2, CO_2).

The treatment of benzene and TCE by the PM/PS system was examined in the series identified as PM/PS. The initial benzene and TCE concentrations were 18 and 750 mg/L, respectively, and the initial concentration of PM was 1.6 g/L. The PM to TCE molar ratio was 1.77, which was less than the theoretical stoichiometric ratio of 2.0 required for complete oxidation of TCE. The mass

of PM was selected to produce the desired mass of $MnO_{2(s)}$ (estimated to be 35.2 mg). To achieve a high $MnO_{2(s)}$ to PS mass ratio, a low PS concentration was used (0.5 g/L). One negative control experiment was conducted with the mixed organic compound solution and synthetic groundwater in place of the oxidant(s) (Ctrl-GW), and two positive experimental controls were conducted with the mixed organic compound solution and a single oxidant PM or PS (Ctrl-PM, and Ctrl-PS).

All experimental series were prepared in triplicate using sacrificed reactors. An aliquot of the supernatant (30 mL) was extracted from each reactor with a glass syringe (Micro-Mate®) and used to quantify pH and the concentration of TCE, benzene, PS and PM. The pH, and PS and PM concentrations were analyzed daily. The concentrations of TCE and benzene were determined at Day 0, 1, 2, 3, 5, 7, 9, and 11. All reactors were kept in the dark at a temperature of ~20 ℃ and manually shaken daily.

2.3.2 Column experiments

To verify and complement the findings from the batch experiments, column experiments were executed to evaluate the performance of the proposed PM/PS system in a situation that closely mimics *in situ* conditions. The design was consistent with the conceptual model of the PM/PS system (Figure 1.1) where PM is delivered to the treatment zone to generate $MnO_{2(s)}$ and then PS is subsequently delivered and activated at the NAPL/water interface by $MnO_{2(s)}$. The experimental design of this bench-scale stop-flow column system is shown in Figure 2.3.

The glass tube at the bottom of the column was filled with Pyrex® fiber glass wool (8 μm) to ensure the column contents remained intact. The bottom glass tube was fitted with 316 stainless steel tubing fittings (Swagelok®, reducing union, 1/4 in.×1/8 in.) to facilitate connection with Teflon tubing. Each column was packed in the following order: (1) the bottom 1.5 cm of the column was filled under saturated conditions with sand (Zone 1), (2) the next 1.5 cm was the source zone and consisted of saturated sand mixed with 50 μL pure TCE and 50 μL pure 1-methylnaphthalene dyed red (Sudan III, Fisher Scientific) (Zone 2 or the source zone), and (3) the top 3 cm was filled under saturated conditions with sand and then topped with a 0.15 × 0.15 mm stainless steel mesh (Zone 3). The NAPL saturation in the source zone was approximately 10%. The weight difference between the saturated and unsaturated column was used to determine the pore volume. After packing, the top of the column was fitted with a 316-stainless steel Swagelok®

tube fitting (Swagelok®, bored-through reducing union, 3/4 in.×1/4 in.) and then connected to Teflon tubing. A seal was maintained between the fitting and the column with a Teflon O-ring. The top outlet tubing was connected to a stainless steel three-way ball valve (1/8 inch, SS-41GXS2 series, Swagelok, USA). The effluent sample was collected by a 5-mL borosilicate glass syringe equipped with Luer locks, interchangeable barrels, and plungers (Chemglass®), which was connected to the three-way ball valve through a stainless-steel syringe needle. This column outlet-valve-syringe system ensured that the column was sealed at all times and minimized volatilization of TCE and 1-methylnaphthalene (Figure 2.4). A peristaltic pump (Cole-Parmer) was used to control the flow rate. The influent was either synthetic groundwater supplied from an Erlenmeyer flask or PM/PS supplied from a glass pipette.

Each column was initially flushed with synthetic groundwater for 3 PVs prior to the injection of an oxidant. The flow rate of synthetic groundwater was set at 0.003 mL/min (pore velocity of 2.4 cm/day) to closely mimic a natural groundwater flow system. The PM or PS solution was then subsequently flushed into the column. The flow rate of an oxidant injection episode was increased to 0.03 mL/min (pore velocity of 24 cm/day). The effluent sample associated with each system PV was collected for analysis of TCE and 1-methylnaphthalene. The injection concentration of PM was determined by the PM/TCE molar ratio of 0.8: 1. The mass of TCE in the system was estimated as the difference between the mass emplaced and mass removed by the 3 PVs of synthetic groundwater. The PS concentration was controlled by the mass of $MnO_{2(s)}$ generated. The target PS to $MnO_{2(s)}$ mass ratio was 1:5 based on the results from the batch experiments.

Replicated column trials (PM/PS-1 and PM/PS-2) were performed to examine the performance of the PM/PS system to treat the TCE/1-methylnaphthalene source zone. Following the flush of synthetic groundwater, 0.25 PV of the PM solution was injected followed by the injection of 0.25 PV of synthetic groundwater to transport the PM solution into the source zone. The flow was then stopped to allow the PM to be reduced to $MnO_{2(s)}$. After a 1- day reaction period, 1 PV of the PS solution was injected and then the flow was stopped for 5 days. Following this 5-day reaction period, 1 PV of synthetic groundwater was flushed through the PM/PS-1 column to capture aqueous rebound conditions immediately post treatment. One negative control column was operated with synthetic groundwater used in place of the oxidant(s) (Ctrl-GW). Two positive control columns were conducted using a single oxidant followed by a 5-day reaction period. At the conclusion of each column experiment, the columns were opened and the complete source zone

and Zone 3 were removed and analyzed for remaining TCE and 1-methylnaphthalene mass. The detailed column operating conditions are provided in Table 2.3.

2.4 Analytic Methods

PS concentration was determined by the spectrophotometric method developed by Liang et al. (2008). In this method, 0.2 g of sodium bicarbonate ($NaHCO_3$) and 4 g of potassium iodine (KI) are added into the PS measurement vial (40 mL, EPA glass vial) followed by 10 mL of Milli-Q water. Then 0.1 mL of the sample or diluted sample (if required) was added to the PS measurement vial. After mixing for at least 15 minutes, the absorbance of the solution was determined spectrophotometrically (wavelength of 352 nm) using a UV spectrophotometer (Genesys^{TM} 10S UV-Vis, Thermo Fisher Scientific, Inc). Eight standards (0.1 to 2 g/L) were prepared by diluting a fresh sodium PS stock solution (10 g/L) with Milli-Q water in a series of 100 mL volumetric flasks. Based on the standards an absorbance calibration curve ($r^2 > 99\%$) was developed from 0.1 to 2 g/L. All PS concentrations reported are in g of $Na_2S_2O_8$/L. PM concentration was also measured spectrophotometrically at a wavelength of 525 nm with a UV spectrophotometer (Genesys^{TM} 10S UV-Vis, Thermo Fisher Scientific, Inc). A fresh stock solution of potassium PM was prepared at 1 g/L and then diluted with Milli-Q water to a concentration between 0.005 and 0.2 g/L in seven 100 mL volumetric flasks. An absorbance calibration curve ($r^2 > 99\%$) was developed for the range from 0.005 to 0.2 g/L. All PM concentrations reported are in g of $KMnO_4$/L.

The quantification of TCE was accomplished by a head-space solid phase micro-extraction (HS-SPME) method (ASTM-D6520-06, 2012) using an HP 6890 series GC coupled with a Varian 8200 series autosampler. The GC was equipped with a flame ionization detector (FID), a 30 m × 0.53 m column length with a 3 µm film (Supelco®), and an SPME absorbing fiber 100 µm coated by PDMS (Supelco®). A spilt/spiltless injector equipped with SPME injection sleeve (0.75 mm, Hewlett-Packard® 26375) was used. The injector temperature was 200 ℃. The column was monitored with helium flowing at 4.5 mL/min under a pressure of 24 kPa. The detector temperature was 280 ℃ with hydrogen flowing 35 mL/min. The extraction time was 2 minutes and the desorbing time was 2 minutes. A fresh methanolic stock solution of TCE was prepared by injecting 0.3 mL of pure phase TCE through a septum into 20 mL aliquot of methanol. TCE standards (10

to 1000 mg/L) were prepared by spiking Milli-Q water with aliquots of the fresh stock solution. A sample of 0.7 mL was extracted by a gas-tight syringe (1 mL, 1001 Hamilton syringe series, Sigma-Aldrich, USA). A calibration curve with a linear slope (>99%) was constructed by plotting the concentration of standards versus their GC responses. The MDL for TCE was 1.6 μg/L.

The aqueous concentration of 1-methylnaphthalene and benzene was determined using a micro-extraction GC technique. The GC (Agilent 7890 A) was equipped with a splitless injection port, a 30 m × 0.25 mm DB5 capillary column with a film thickness of 0.25 μm and a flame ionization detector. The injection port temperature was 275 ℃. The initial column temperature was 35 ℃ followed by a heating rate of 15℃/min to reach a final temperature of 300 ℃ with helium flowing 5 mL/min. The detector temperature was 325 ℃. A fresh methanolic stock solution of 1-methylnapthalene or benzene was prepared by injecting 0.3 mL of the pure compound into a 60 mL aliquot of methanol. The calibration standards covering the expected sample range were prepared by spiking Milli-Q water with a concentrated methanolic stock solution. The aqueous standard or sample was placed in a 20-mL vial (borosilicate glass vials fitted with 22 mm open cap & Teflon/silicone septa) followed by the addition of 1 mL of dichloromethane. The vial was quickly sealed and agitated at 350 rpm on a platform shaker (Thermolyne) for 20 minutes. After shaking, the vial was inverted and left to stand for > 30 minutes to allow for phase separation. An aliquot of the solvent phase (~ 0.5 mL) was removed through the septa using a 1 mL gas-tight syringe (1001 Hamilton syringe series, Sigma-Aldrich, USA) and then placed in a 2 mL Teflon-sealed autosampler vial (VWR) for GC measurement. A calibration curve with a linear slope (>99%) was developed for benzene or 1-methylnaphthalene. The method detection limit ranged from 2-5 μg/L.

To determine the bulk soil concentration of TCE and 1-methylnaphthalene present in the porous medium used in the column experiments, the material collected from a column was placed in a 40 mL Teflon-septa glass vial previously filling 20 mL dichloromethane. The vial was then quickly sealed and placed on a platform shaker (Thermolyne) and shaken at 50 rpm for at least one day. After shaking, the solvent phase was allowed to separate and extracted with a 1 mL gas-tight syringe for TCE and 1-methylnaphthalene analyses as described above.

The pH of aqueous samples was measured by an Orion pH meter (Model A324, ThermoScientific).

The surface morphology and chemical composition of the synthesized manganese oxides were characterized by environmental scanning electron microscopy (ESEM) (Quanta 250 FEG, FEI) coupling with energy dispersive X-ray spectroscopy (EDX) (Oxford INCA). The dried synthesized manganese oxides were crushed into powder size and placed on a silicon wafer (one side, polished, Sigma-Aldrich, USA) in small chambers for SEM and EDX analyses with an acceleration voltage of 20 kV.

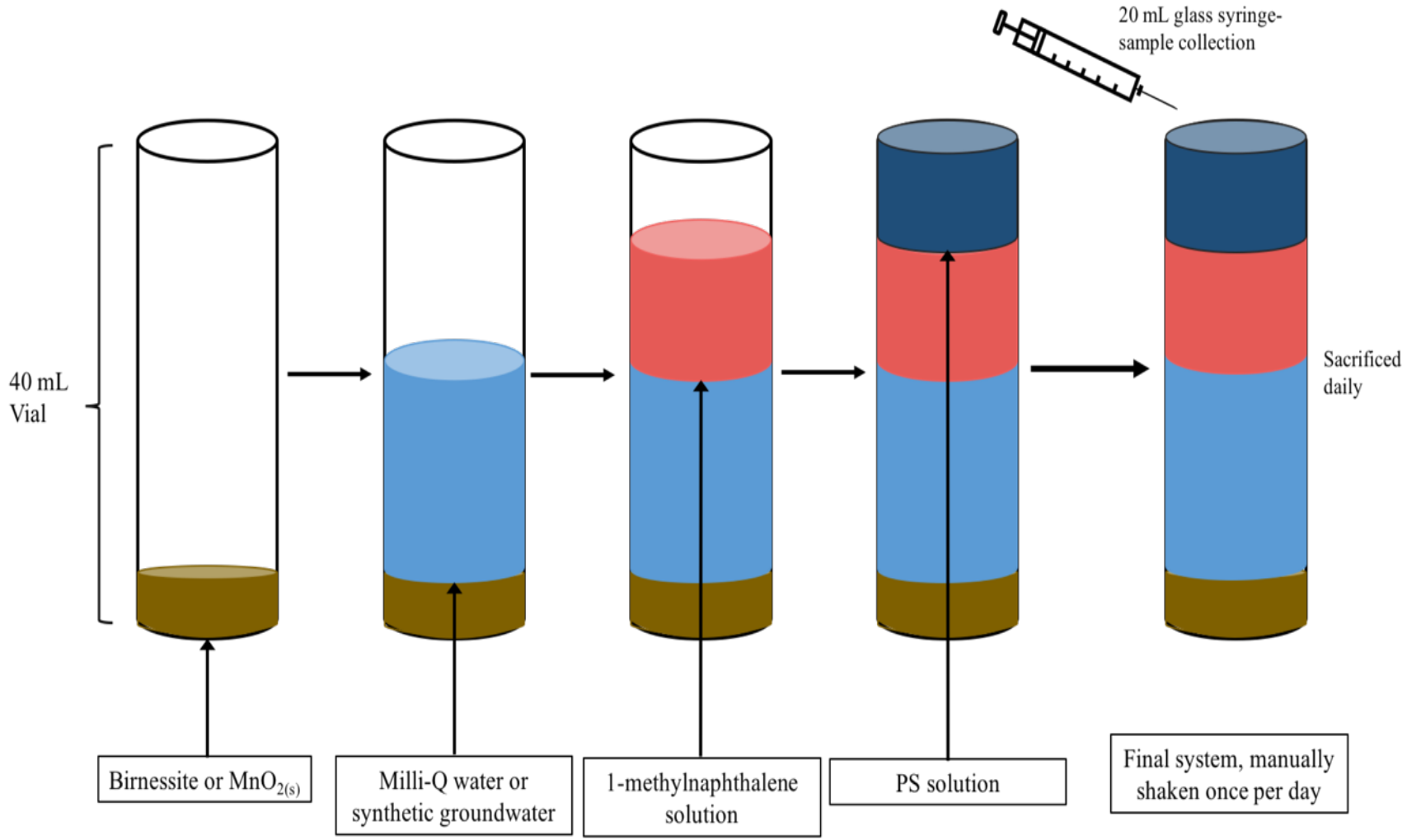

Figure 2.1 Schematic of the pre-synthesized $MnO_{2(s)}$ system batch reactors.

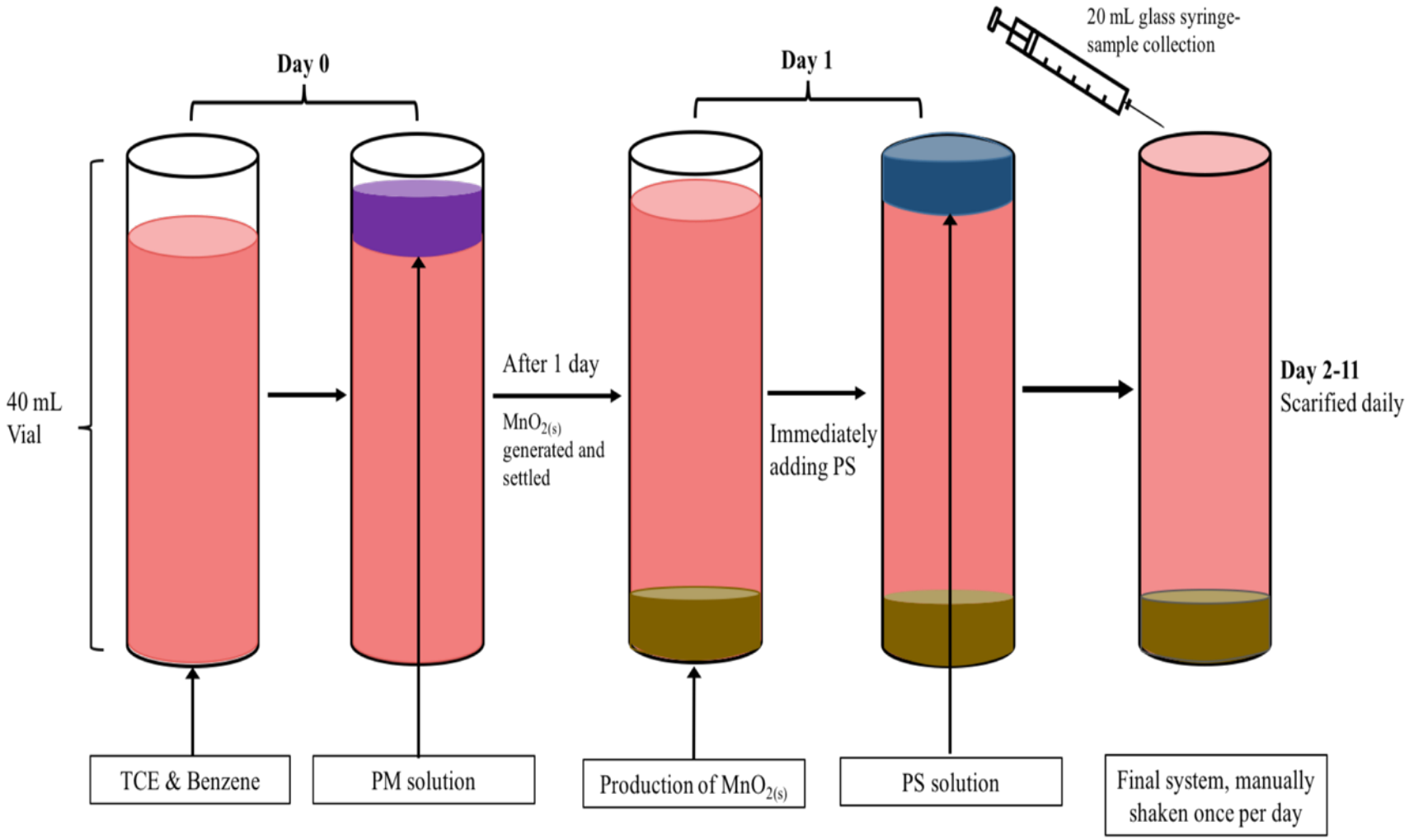

Figure 2.2 Schematic of PM/PS system batch reactors.

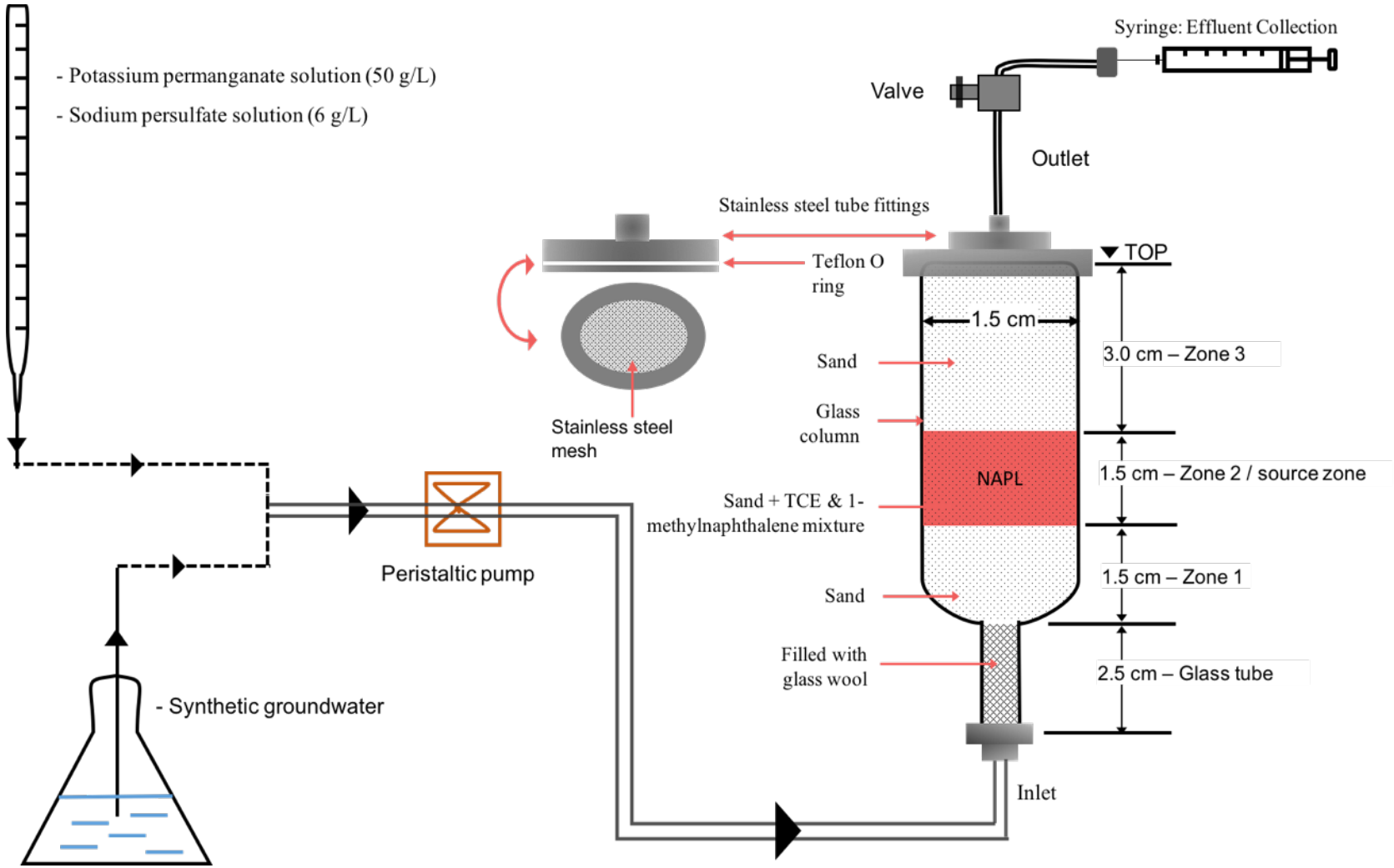

Figure 2.3 Schematic of the set-up of bench-scale column experiment.

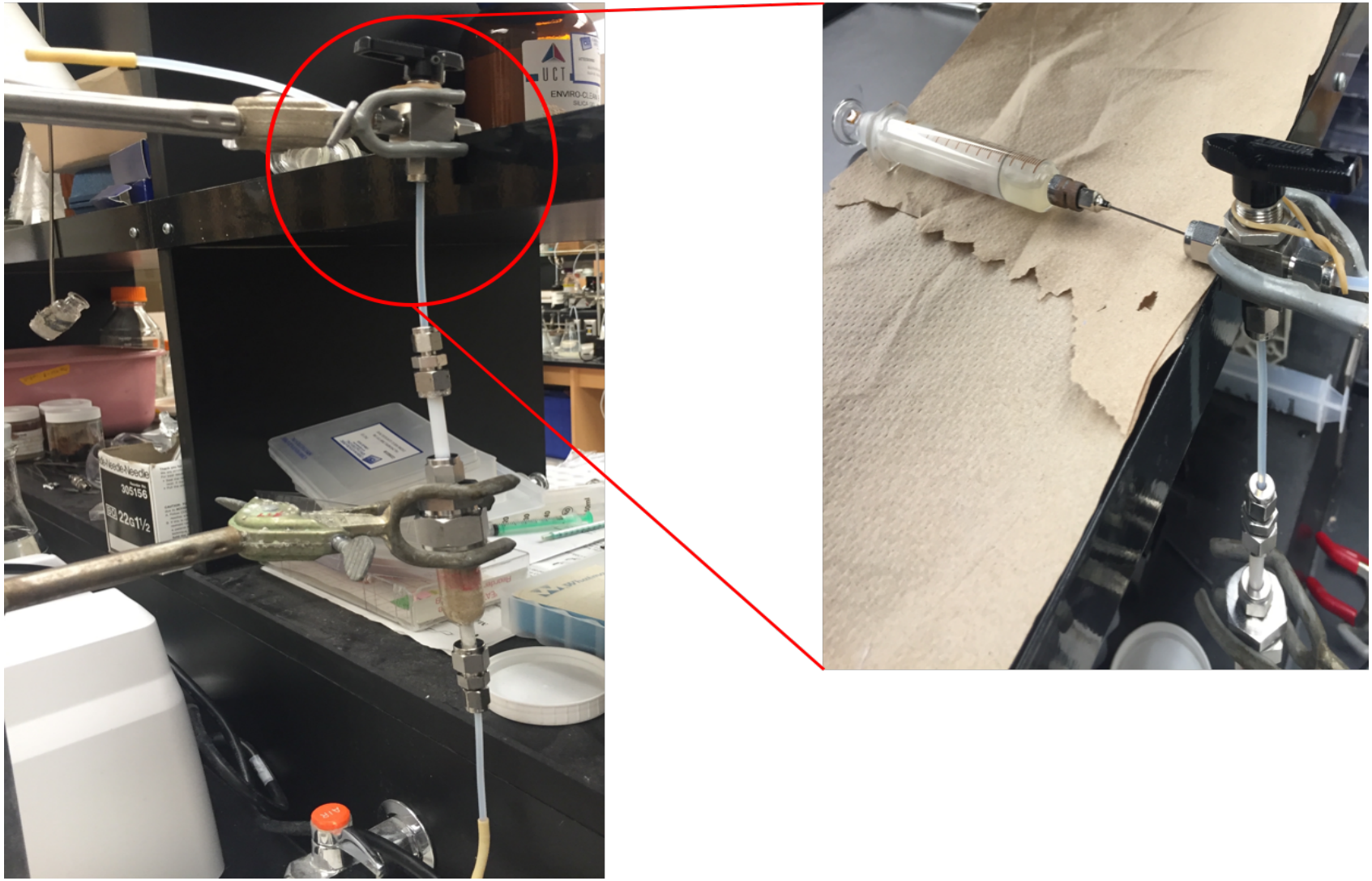

Figure 2.4 The out-valve-syringe system in the column experiments.

Table 2.1 Summary of experimental conditions for batch experiments using the pre-synthesized $MnO_{2(s)}$.

Series identifier [a]	Initial concentrations		
	1-methylnaphthalene concentration (mg/L)	PS concentration (g/L)	Mass of $MnO_{2(s)}$ (g)
Ctrl-MQ	5.5	-	-
Ctrl-GW	5.3	-	-
Ctrl-PS	5.4	0.56	-
PS-Birnessite (1:5 [a])	5.1	0.57	0.1 [b]
PS-MnO_2 (1:5)	5.3	0.54	0.1 [c]
PS-MnO_2 (1:10)	5.3	0.56	0.2 [c]
PS-MnO_2 (1:20)	5.3	0.58	0.4 [c]
PS-MnO_2 (1:20) /GW	5.5	0.58	0.4 [d]

Notes:

a. mass ratio of PS to $MnO_{2(s)}$.
b. Pre-synthesized birnessite.
c. Pre-synthesized $MnO_{2(s)}$ Sample #1 or $MnO_{2(s)}$ Sample #3.
d. Pre-synthesized $MnO_{2(s)}$ Sample #2.

Table 2.2 Summary of experimental conditions for batch experiments using the PM/PS system.

Series identifier	Initial concentration			
	Benzene concentration (mg/L)	TCE concentration (mg/L)	PM concentration (g/L)	PS concentration (g/L)
Ctrl-GW	17.5	723	-	-
Ctrl-PM	16.0	742	1.6	-
Ctrl-PS	16.8	735	-	0.5
PM/PS [a]	16.4	747 [b]	1.6	0.5 [c]

Notes:

a. The time interval between the addition of PM and PS was 1 day.
b. The molar ratio of TCE and PM was 1:1.77.
c. The mass ratio of PS and $MnO_{2(s)}$ was 1:1.76.

Table 2.3 Column operating conditions.

Ctrl-GW	Ctrl-PM	Ctrl-PS	PM/PS-1	PM/PS-2
GW (3 PVs) [a]	GW (3 PVs)	GW (3 PVs)	GW (3 PVs)	GW (3 PVs)
GW (1 PV)	PM (1 PV) [b]	PS (1 PV) [c]	PM (0.25 PV) + GW (0.25 PV) [d]	PM (0.25 PV) + GW (0.25 PV)
Stop-flow-1 (1 day) [e]	Stop-flow (5 days) [f]	Stop-flow (5 days)	Stop-flow-1 (1 day)	Stop-flow-1 (1 day)
GW (1 PV) [g]	Open Column [h]	Open Column	PS (1 PV) [i]	PS (1 PV)
Stop-flow-2 (5 days)			Stop-flow-2 (5 days)	Stop-flow-2 (5 days)
Open Column			GW (1 PV)	Open Column
			Open Column	

Notes:

a. Synthetic groundwater was flushed through column for 3 pore volumes (PVs) at flow rate of 0.003 mL/min.
b. PM was flushed through column for 1 PV at flow rate of 0.03 mL/min.
c. PS was flushed through column for 1 PV at flow rate of 0.03 mL/min.
d. PM was flushed through column for 0.25 PV at flow rate of 0.03 mL/min, and synthetic groundwater was flushed through column for 0.75 PV at flow rate of 0.03 mL/min.
e. Stop flow for 1 day.
f. Stop flow for 5 days.
g. Synthetic groundwater was flushed though column at flow rate of 0.05 mL/min.
h. Column was open and the complete source zone and Zone 3 were removed.
i. PS was flushed through column at flow rate 0.05 mL/min.

Chapter 3

Chapter 3
Result & Discussion

3

3.1 Batch Experiments

3.1.1 Pre-synthesized $MnO_{2(s)}$ system

PS activation was investigated in the presence of four types of manganese oxide solids: the synthesized birnessite, and $MnO_{2(s)}$ Sample #1, Sample #2 and Sample #3. The degradation kinetics of 1-methylnaphthalene were used to evaluate the ability of these manganese oxide solids to activate PS.

3.1.1.1 Characterization of the pre-synthesized manganese oxide solids

The elemental composition and the micromorphology of the four manganese oxide solids were determined by EDX and SEM, respectively. The synthesized birnessite was reddish-brown and lumpy, while the $MnO_{2(s)}$ Sample #1, Sample #2 and Sample #3 were darker and finer (Figure S3.1). The synthesized birnessite contained 4.89% potassium (K), 55.95% manganese (Mn), 38.47% oxygen (O), and 0.7% chloride (Cl) (Figure 3.1; Table 3.1). This composition was consistent with the elemental composition of birnessite reported by others (Händel et al. 2013; Table S3.1). According to McKenzie (1971), birnessite ($\delta - MnO_2$) contained less than the stoichiometric proportion of oxygen, and thus the oxygen to manganese ratio should be < 1.9. Based on the elemental analysis, the molecular formula of the birnessite produced in this study could be expressed as $K_{0.25}Cl_{0.04}Mn_2O_{4.73}$. The oxygen to manganese ratio of 2.37 was not consistent with the ratio reported by McKenzie (1971). The micromorphology images (Figure S3.2) showed that the crystalline structure of the synthesized birnessite contained clusters of needles which was similar to the crystalline structure of cryptomelane ($\alpha - MnO_2$) reported by McKenzie (1971) and Mn oxide powder reported by Li and Schwartz (2004a). Hence the generated birnessite is likely cryptomelane.

The element weight fractions indicated that $MnO_{2(s)}$ Samples #1, Sample #2 and Sample #3 contained a K content of 5.16, 3.83 and 14.03 %, respectively (Table 3.1). McKenzie (1971) indicated that the K content of cryptomelane was < 7% (wt), which suggested that Sample #3 was not cryptomelane. Based on the expected ratio of oxygen to manganese, Sample #1 and Sample #2 could be either birnessite or cryptomelane. The molecular formula of Sample #1, Sample #2 and Sample #3 could be represented as, $K_{0.23}Mn_2O_{3.48}$, $K_{0.17}Mn_2O_{3.66}$, and $K_{0.77}Mn_2O_{4.71}$ respectively. The crystalline structure of Sample #1 and Sample #2 appeared as rounded aggregates (Figure S3.3 and S3.4). Sample #3 had a cloudy and spherical microstructure (Figure S3.5).

3.1.1.2 Results and discussion

The normalized 1-methylnaphthalene profiles for the $MnO_{2(s)}$ systems are shown in Figure 3.2 and Figure S3.6. Each data point is the average from the triplicate reactors, and the standard deviation was < 8.5 %. Data from the two negative controls series (Ctrl-MQ and Ctrl-GW) show that 1-methylnaphthalene was stable in Milli-Q water and synthetic groundwater, suggesting that no significant loss of 1-methylnaphthalene occurred during the experimental period.

The degradation of 1-methylnaphthalene in the presence of $MnO_{2(s)}$ Sample #3 at the different mass ratios explored was less than Ctrl-PS suggesting that $MnO_{2(s)}$ Sample #3 was not able to significantly activate PS (Figure S3.6 and Figure S3.7).

The Ctrl-PS series resulted in 50 % degradation of 1-methylnaphthalene over the 10-day reaction period. According to the direct 1-methylnaphthalene oxidation by unactivated PS (Eq 1.12), the complete oxidation of 0.2 mg of 1-methylnaphthalene required at least 9 mg of PS, suggesting that sufficient PS was available at the beginning of the reaction (20 mg) to degrade 1-methylnaphthalene through direct oxidation. McIsaac (2013) observed almost completed degradation of 1-methylnaphthalene in an aqueous system using 20 g/L of unactivated PS.

The highest 1-methylnaphthalene degradation (99.6 %) was achieved by $MnO_{2(s)}$ Sample #2 at a mass ratio of 20:1 (g $MnO_{2(s)}$: g PS) using synthetic groundwater. Birnessite at a mass ratio of 5:1 (g birnessite: g persulfate) using Milli-Q water was able to degrade 94.8 % of 1-methylnaphthalene. The 1-methylnaphthalene removal percentages achieved by $MnO_{2(s)}$ Sample #1 at a mass ratio 5:1, 10:1 and 20:1 (g $MnO_{2(s)}$: g PS) with Milli-Q water were 65.1, 73.6, and

87.2 %, respectively (Figure 3.3). It is clear that the degradation of 1-methylnaphthalene increased with an increase in the mass of $MnO_{2(s)}$ present in the system.

At the same mass ratio of 5:1, the 1-methylnaphthalene degradation in the birnessite system was 30% higher than that in the $MnO_{2(s)}$ Sample #1 system, suggesting that the birnessite system was more efficient to degrade 1-methylnaphthalene.

The degradation of 1-methylnaphthalene was accompanied by the consumption of PS. The PS consumption over 10 days in the presence of $MnO_{2(s)}$ Sample #1 and Sample #2 is shown in Figure 3.4. Less than 30% PS consumption was observed in all systems. The greatest PS consumption (27% over 10 days) occurred in the presence of $MnO_{2(s)}$ Sample #2 at a mass ratio of 20:1 (g $MnO_{2(s)}$: g PS) with synthetic groundwater, followed by birnessite (26 %). PS consumption was between 16 to 21 % in the presence of $MnO_{2(s)}$ Sample #1 with Milli-Q water. Approximately 13 % PS was consumed in the Ctrl-PS series. The stoichiometry mass ratio of PS to 1-methylnaphthalene (Table 3.2) ranged from 26 to 30 g-PS /g-1-methylnaphthalene for the reactors containing manganese oxide solids (birnessite, $MnO_{2(s)}$ Sample #1 and Sample #2). The stoichiometric mass ratio in the presence of $MnO_{2(s)}$ was higher than for the Ctrl-PS series reflective of the interaction between PS and $MnO_{2(s)}$.The overall kinetic rate law for the oxidation of 1-methylnaphthalene by PS can be written as:

$$r = \frac{\mathrm{d}[\mathrm{C_{11}H_{10}}]}{\mathrm{dt}} = -k_{1-methylnaphthalene}[\mathrm{S_2O_8^{2-}}][\mathrm{C_{11}H_{10}}] \qquad \text{(Eq 3.1)}$$

The initial molar ratio of PS:1-methylnaphthalene was approximately 60:1 and hence PS was in excess and Eq 3.1 can be simplified to:

$$r = \frac{\mathrm{d}[\mathrm{C_{11}H_{10}}]}{\mathrm{dt}} = -k_{obs}[\mathrm{C_{11}H_{10}}] \qquad \text{(Eq 3.2)}$$

where $k_{obs} = k_{1-methylnaphthalene}[\mathrm{S_2O_8^{2-}}]$ is the observed 1st-order reaction rate coefficient. Applying the integrated form of Eq 3.2, k_{obs} can be determined with Eq 3.2, where C_0 is the initial concentration of 1-methylnaphthalene, and C_t is the concentration of 1-methylnaphthalene at time t. k_{obs} was determined by linear least square regression analysis of $\ln(C/C_0)$ versus reaction time (t).

$$\ln\left(\frac{C_t}{C_0}\right) = -k_{obs} * t \qquad \text{(Eq 3.3)}$$

The best-fit observed reaction rate coefficient for all systems varied from 10^{-2} to 10^{-1} day^{-1} with $r^2 > 0.96$ (Table 3.2) indicating that the pseudo first-order rate law could represent the degradation of 1-methylnaphthalene. The reaction rate coefficient for the Ctrl-PS series was 7.78×10^{-2} ($r^2 > 0.96$), which is similar to the reaction coefficient reported by McIsaac (2013).

The reaction rates for the birnessite or $MnO_{2(s)}$ (Sample #1 and Sample #2) systems were one-order of magnitude higher than for the Ctrl-PS series, and followed the order of Sample #2 > birnessite > Sample #1. A higher dose of $MnO_{2(s)}$ resulted in a higher 1-methylnaphthalene reaction rate coefficient and produced a linear relationship ($r^2 = 0.99$) (Figure 3.5). For the same PS to $MnO_{2(s)}$ mass ratio (1:20), the reaction rate coefficient for the system containing synthetic groundwater was 2.6 times greater than the system containing Milli-Q water. A higher PS consumption was also observed in the presence of synthetic groundwater (PS-MnO_2 (1:20)/GW), implying that synthetic groundwater enhanced the interaction between PS and $MnO_{2(s)}$ and the degradation of 1-methylnaphthalene. This observation is consistent with the findings reported by Li et al. (2017) that the presence of ions in groundwater will impact PS activation and therefore the treatment of organic compounds.

Figure 3.6 shows the pH profile for each system. The pH of the two negative controls (Ctrl-MQ and Ctrl-GW) was neutral (6 and 7.3, respectively). The pH of birnessite and Sample #1 systems with Milli-Q water were between 4 and 5 (Figure 3.6, Table S3.4). The pH in the Sample #2 system using synthetic groundwater was below 4.

PS oxidation reactions mainly involves two pathways: (a) a kinetically slower direct reaction between PS and target organic; and (b) the decomposition of PS to form highly reactive free intermediate radicals that can rapidly degrade target organics (Petri et al. 2011). It is speculated that the 1-methylnaphthalene degradation by unactivated PS in the Ctrl-PS system was mainly through direct oxidation involving electron transfer. In the $MnO_{2(s)}$ (Sample #1 and Sample #2) systems, the greater removal of 1-methylnaphthalene, the higher loss of PS, and the acceleration of 1-methylnaphthalene reaction rate kinetics may be attributed to $MnO_{2(s)}$ activated PS, which produces highly reactive radicals (e.g., $SO_4^{\cdot-}$) (Liu et al. 2016; Liu et al. 2014; Petri et al. 2011). More PS was converted in the presence of $MnO_{2(s)}$ (Sample #1 and Sample #2); however, the pH difference between the $MnO_{2(s)}$ system and Ctrl-PS system was insignificant, which indirectly demonstrates that a portion of consumed PS likely formed intermediate species through a series of chain reactions rather than protons through direct oxidation. Liang et al. (2007) stated that the

sulfate radical ($SO_4^{\cdot-}$) predominated under acidic conditions. Combined with the findings from Liu et al. (2014), the following $MnO_{2(s)}$ (Sample #1 and Sample #2) catalyzed decomposition reaction of PS is proposed:

$$2S_2O_8^{2-} \xrightarrow{MnO_{2(s)}} SO_4^{2-} + SO_4^{\cdot-} + S_2O_8^{\cdot-} \quad \text{(Eq 3.4)}$$

No significant color change of $MnO_{2(s)}$ solids was observed during the experiment period (Figure S3.8), suggesting that the $MnO_{2(s)}$ surface remained unaltered. A similar result was reported by Do et al. (2010) that manganese oxide (pyrolusite) did not transform when used to activate persulfate.

The data assembled show that $MnO_{2(s)}$ (Sample #1 and Sample #2) is able to activate PS, and that the higher mass of $MnO_{2(s)}$ present in the system the greater 1-methylnaphthalene degradation and reaction kinetics. The lowest reaction rate coefficient was achieved at the mass ratio of 5:1 (g $MnO_{2(s)}$: g PS) with Milli-Q water, and the difference between the performance of this system and the Ctrl-PS system was minimal (Figure 3.2). This suggests that the mass ratio of $MnO_{2(s)}$ to PS should be > 5 to impact treatment. Ahmad et al. (2010) demonstrated that for PS to be activated by birnessite the mass ratio of birnessite to PS must be > 0.084. The difference in the minimum dosage required for PS activation between $MnO_{2(s)}$ and birnessite is related to the greater effectiveness of birnessite compared to $MnO_{2(s)}$ solids.

$MnO_{2(s)}$ Sample #1 and Sample #2 were able to activate PS, while $MnO_{2(s)}$ Sample #3 was not able to activate PS at observable rates. Extending from the EDX and SEM results, the potassium (K) content might be a key factor in determining the capability of $MnO_{2(s)}$ to activate PS. Based on the limited data collected in this study, $MnO_{2(s)}$ with a K content < 7% appears to be required.

3.1.2 PM/PS system

The potential for the PM/PS system to degrade a benzene and TCE mixture in synthetic groundwater was investigated. The Ctrl-PM and PM/PS system at 0, 2 and 20 hrs are shown in Figure 3.7. The purple color of the mixed solution faded over time and by 20 hrs the color was clear and the precipitated brown-black $MnO_{2(s)}$ solids settled at the bottom of reactor. In the PM/PS system, the amount of $MnO_{2(s)}$ was estimated ~0.88 g/L based on the consumed mass of PM.

The percent TCE and benzene removed at Day 11 are shown in Figure 3.8. Approximately 10 % TCE and 1.45 % benzene were removed in the Ctrl-GW system likely due to volatilization. A rapid degradation of TCE was observed in the Ctrl-PM and PM/PS systems over the first 24 hrs (Figure S3.9) due to the presence of PM which was completely consumed (Table S3.5). Approximately 91 % removal of TCE was observed in the Ctrl-PM system (Figure 3.8). Based on the reaction between TCE and PM (Eq 1.8), the applied PM mass (64 mg) should have been sufficient to oxidize 26.6 mg of TCE (91 % of the initial TCE mass in a reactor), which was observed in Ctrl-PM system. TCE was less than MDL in the PM/PS system after Day 9 indicating that continuous removal of TCE was accomplished by PS after PM had disappeared from this system.

Approximately 20 % of TCE and 9 % of benzene was degraded in the Ctrl-PS system, and ~15 % of benzene was degraded in the PM/PS system. About 13 and 15 % of the initial PS mass was consumed in the Ctrl-PS and PM/PS systems, respectively (Table S3.5). A slightly higher mass of benzene was degraded in the PM/PS system with the same mass of PS consumed as the Ctrl-PS system suggesting that the use of PS was more efficient in the PM/PS system. The low benzene removal was attributed to the low PS concentration. According to the direct oxidation of benzene by PS (Eq 1.11), the oxidation of benzene (0.72 mg) requires at least 32 mg of PS, which was higher than the initial PS concentration. The mass ratio of $MnO_{2(s)}$ to PS used was 1.76:1, which was much lower than the mass ratio used in the pre-synthesized $MnO_{2(s)}$ systems. The low mass ratio of $MnO_{2(s)}$ to PS might also have contributed to the low benzene degradation and PS decomposition in the PM/PS system. Ahmad et al. (2010) also only observed 15 % PS decomposition at a mass ratio of 1.68:1 (g birnessite: g PS). However, a low mass ratio of $MnO_{2(s)}$ to PS still resulted in a higher mass of benzene removed (15 %) in the PM/PS system compared to the 9 % achieved in the Ctrl-PS system.

The results from the PM/PS system showed enhanced reactivity of PS without the co-addition of an activator solution. It was concluded that the sequential injection of PM and persulfate (dual oxidant system) leads to persulfate activation and effective treatment particularly for some organic compounds that are not reactive with PM (i.e., benzene).

3.2 Column Experiments

The column experiments were designed to examine the capability of the PM/PS system, outlined in the conceptual model, to degrade a simulated NAPL mixture (pure phase TCE and 1-methylnaphthalene).

The weight difference between the saturated and unsaturated column was used to determine the column pore volume (PV; 4.0 to 4.3 mL).

After the injection of the PM solution into the PM/PS-1 and PM/PS-2 columns (Figure 3.9), a pressure build-up was observed at the inlet of column resulting presumably from a decrease of hydraulic conductivity due to $MnO_{2(s)}$ precipitates (Huang et al. 2002b; MacKinnon and Thomson, 2002). To overcome this pressure build-up, the flow rate for the PS injection phase was increased from 0.03 to 0.05 mL/min for PM/PS-1 and PM/PS-2.

Based on the findings from the batch experiments and a host of preliminary column experiments, the PM dosage was estimated based on the remaining TCE mass in the source zone after flushing with 3 PVs of synthetic groundwater, and a PM to TCE molar ratio of < 2. The remaining TCE mass was estimated by subtracting the aqueous effluent TCE mass from the initial loading of TCE mass (73 mg or 50 μL). Limited by the PM solubility (63 g/L) and using a PM to TCE molar ratio of 0.8:1, the concentration of the PM injection solution was determined as 50 g/L. Thus, the PM mass dosage delivered into the source zone was ~65 mg. Theoretically this PM mass is reduced to ~35.8 mg of $MnO_{2(s)}$ with the majority remaining within the source zone. The PS concentration was constrained by the need to satisfy the $MnO_{2(s)}$ to PS mass ratio of 5:1 (from the Pre-synthesized $MnO_{2(s)}$ Sample #1 batch experiment). As a result, the PS injection concentration was 6 g/L, and a PS dosage delivered into the source zone was 7.5 mg.

Images of the columns are shown in Figures S3.11-S3.15. In the PM/PS columns, the color of the source zone changed from red (dyed NAPL) to black after the exposure to PM, confirming $MnO_{2(s)}$ formation (Figures 3.9 (a)&(d)). After the injection of PS, the dark color in the source zone did not change.

3.2.1 Effluent concentrations

For the Ctrl-GW column, the TCE effluent concentration increased from 687 to 950 mg/L during the first 3 PVs of synthetic groundwater injection. As dissolution proceeded, TCE concentration gradually increased to ~1000 mg/L before Stop-flow-2 (Figure 3.10; Table S3.6). The 1-methylnaphthalene concentration also gradually increased from 4.4 mg/L to about 8.5 mg/L during the first 3 PVs of synthetic groundwater injection, and then to 9 mg/L before Stop-flow-2 (Figure 3.11; Table S3.6). The increasing trend of TCE and 1-methylnaphthalene concentration in the other columns was consistent with these data during the first 3 PVs of synthetic groundwater injection (Figures 3.10 and 3.11). A baseline concentration of TCE (935 mg/L) and 1-methylnaphthalene (9.25 mg/L) was established and used for the comparison to the treatment systems.

Following PM injection into Ctrl-PM, the TCE and 1-methylnaphthalene aqueous effluent concentrations decreased by about 75% and 11% compared to the baseline concentrations, respectively (Figure 3.10 and 3.11; Table S3.7). The rapid decrease in the aqueous effluent concentration for TCE is likely due to its high solubility (Thomson et al. 2008). Following PS injection into Ctrl-PS, the TCE effluent concentration decreased by about 55%, but the 1-methylnaphthalene effluent concentration increased by 10% (Figures 3.10 and 3.11; Table S3.8).

After the addition of PM into the PM/PS columns ('Before treatment'), the effluent TCE concentration decreased by 73 %, and after the addition of PS ('After treatment'), the TCE effluent concentration reduced to less than MDL. In the PM/PS-2 column, the effluent 1-methylnaphthalene concentration increased by ~12 % after PM addition, and then reduced by ~11 % after PS addition compared to the baseline concentration (Figures 3.10 and 3.11). The rebound of the 1-methylnaphthalene effluent concentration before treatment can be explained by Raoult's law given by

$$S_i^E = X_i \times S_i \qquad \text{(Eq 3.5)}$$

where S_i^E was the effective solubility of compound i, X_i was the molar fraction of compound i, and S_i was the solubility of compound i. The decline of TCE concentration decreased the molar fraction of TCE from 99 to 95%, and increased the molar fraction of 1-methylnaphthalene from 1 to 5% in NAPL. Based on Raoult's law (Eq 3.5), the effective solubility of 1-methylnaphthalene was expected to increase which was consistent with the slight increase of the 1-methylnaphthalene

concentration following PM injection. This rebound has also been reported by Thomson et al. (2008) after source zone treatment with PM during a pilot scale field trial. The decrease of the effluent 1-methylnaphthalene concentration after the addition of PS implies that the 1-methylnaphthalene degradation was enhanced in the presence of PS in the PM/PS systems.

The slight change in the 1-methylnaphthalene concentration compared to the significant decline in the TCE concentration for the Ctrl-PM and PM/PS columns indicated that TCE degradation was preferred to 1-methylnaphthalene in the presence of PM. This is consistent with the findings from Waldemer and Tratnyek (2006) that the reaction rate coefficient for TCE was one-order-of-magnitude higher than for 1-methylnaphthalene.

After PS addition in PM/PS-1, the 1-methylnaphthalene aqueous effluent concentration decreased by about 25% compared to the baseline concentration; after 1 PV of synthetic groundwater injection following the 5-day reaction period, the 1-methylnaphthalene concentration decreased by about 50 %.

The decrease of the effluent TCE and 1-methylnaphthalene concentration is consistent with the PM/PS aqueous batch experiments that the PM/PS system could improve the treatment of aqueous-phase organics.

3.2.2 Residual mass

Residual mass is defined as the mass of aqueous and non-aqueous organic compounds remaining in the column at the termination of the experiment. Residual mass was estimated by the analysis of the remaining aqueous and non-aqueous phase TCE and 1-methylnaphthalene mass in the source zone and Zone 3.

In the Ctrl-GW column, about 70 % of the initial TCE mass and 80 % of the initial 1-methylnaphthalene mass remained in the source zone (Table 3.3). Approximately 14 and 74 % of initial TCE and 1-methylnaphthalene mass remained in the source zone of the Ctrl-PM column. The TCE mass remaining in the source zone indicated that the PM dosage delivered into the source zone was insufficient to completely degrade all the TCE. About 57% and 70% of initial TCE and 1-methylnaphthalene mass remained in the source zone of the Ctrl-PS column.

The TCE residual mass was less than MDL in the PM/PS columns. It was suspected that any TCE mass remained after PM injection was removed by the PS. About 50 % of the initial 1-

methylnaphthalene mass remained in the PM/PS system. This is 24% less than the mass remaining in the Ctrl-PM column and 20% less than the mass remaining in the Ctrl-PS column. Based on these data, the PM/PS system was more effective in removing TCE and 1-methylnaphthalene mass compared to the control systems.

3.2.3 Mass balance

To investigate the mass degraded, the following mass balance model was applied:

$$M_{IN} = M_{EFF} + M_{RES} + M_{OX} \quad \text{(Eq 3.6)}$$

where M_{IN} was the initial mass of TCE or 1-methylnaphthalene placed in the source zone at the beginning of the experiment, M_{EFF} was the mass of aqueous phase TCE or 1-methylnaphthalene collected in the effluent, M_{RES} was the residual mass of aqueous phase or non-aqueous phase TCE or 1-methylnaphthalene collected from the soil remaining in the column at the end of the experiment, and M_{OX} was the mass of oxidized TCE or 1-methylnaphthalene degraded by PM and/or PS. Eq 3.5 was established by assuming that: (a) during the experiment period, TCE and 1-methylnaphthalene dissolved into aqueous phase, (b) the oxidation of TCE and 1-methylnaphthalene by PM and PS occurred in the aqueous phase, (c) the effluent only contained aqueous phase TCE and 1-methylnaphthalene, (d) the residue in the column captured all the remaining aqueous and non-aqueous phase TCE and 1-methylnaphthalene, and (e) organic compound removal was accomplished by oxidation. Table 3.3 shows the details of the mass balance calculations for the different column systems.

The Ctrl-GW column was used to ascertain if Eq 3.5 is viable since no mass degradation was expected. Comparing to the initial mass of TCE (73 mg) and 1-methylnaphthalene (50 mg) emplaced in the column to the sum of M_{EFF} and M_{RES} indicated a mass balance error of 5 % for TCE, and 19 % for 1-methylnaphthalene.

The results from the PM/PS-1 and PM/PS-2 columns were averaged and the final result (PM/PS) was used. Eq 3.5 was applied to determine of M_{OX} by subtracting M_{EFF} and M_{RES} from M_{IN}. The percent of oxidized organics in each column was calculated by dividing M_{OX} by M_{IN}. Figure 3.12 shows the percent of oxidized TCE and 1-methylnaphthalene by PM and/or PS. For the Ctrl-PM column, the percent of oxidized TCE and 1-methylnaphthalene was 73 and 26 %,

respectively. The high TCE oxidation by PM was likely due to the high dissolved TCE concentration (~1000 mg/L). When PS was used alone (Ctrl-PS column), the percent of oxidized TCE and 1-methylnaphthalene was 26 and 30 %, respectively. The percent of oxidized organics achieved in the PM and PS treatment columns were both higher than the mass balance error associated with the Ctrl-GW column.

The PM/PS system oxidized 84 % of the initial TCE mass, which was 11 % higher than that achieved by Ctrl-PM column. Approximately 50 % of initial 1-methylnaphthalene mass was oxidized in PM/PS columns, which was 25 % higher than observed in Ctrl-PS column. The higher organic mass oxidized in the PM/PS system demonstrated that oxidation was the main mechanism for mass removal in the PM/PS system.

3.2.4 TCE and 1-methylnaphthalene mass removal rate

The mass removal rate was estimated by:

$$\text{mass removal rate } \left(\frac{\text{mg}}{\text{day}}\right) = \frac{\text{removed organic(s) mass (mg)}}{\text{reaction time (days)}} \qquad \text{(Eq 3.7)}$$

where organic mass removed was M_{OX}, and the reaction time was 5 days, except that the TCE reaction time in the PM/PS systems was 7 days:

$$\text{mass removal rate } \left(\frac{\text{mg}}{\text{day}}\right) = \frac{M_{ox}}{\text{5 days or 7 days}} \qquad \text{(Eq 3.8)}$$

The TCE and 1-methylnaphthalene mass removal rates are shown in Table 3.4. In the PM/PS systems, the TCE and 1-methylnaphthalene mass removal rate was 8.7 mg/day and 5 mg/day. The 1-methylnaphthalene mass removal rate achieved in the PM/PS system was 1.6 times higher than that by the Ctrl-PS system.

In the PM/PS (Table 3.4), the ratio between oxidized TCE mass ($M_{OX\text{-}TCE}$) and consumed PM mass was 1.13: 1. This observed stoichiometric ratio (1.13) was less than the theoretical ratio (2) for complete oxidation (Eq 1.8). Kim and Gurol (2005) also reported a lower ratio (1.56 to 1.78) of oxidized TCE and consumed PM in their study. Yan and Schwartz (2000) proposed a three-step reaction between TCE and PM: the first step involves the oxidation of 1 mole TCE by 1 mole PM and the production of cyclic hypomanganate ester, which is then transformed to carboxylic acids

in the second step and, in the final step, the oxidation of carboxylic acids to CO_2 through the consumption of the second mole of PM. The observed stoichiometric ratio of less than 2 indicates incomplete oxidation of TCE, and the stoichiometric ratio close to 1 suggests that TCE was oxidized to cyclic hypomanganate ester or carboxylic acids.

The minimum mass ratio of $MnO_{2(s)}$ to PS used in the Pre-synthesized $MnO_{2(s)}$ experiments was 5:1, and the equivalent molar ratio of PM and PS was 13.7:1. In the column experiments, the applied molar ratio of PM and PS was 13.1:1. Based on these data, the PM to PS molar ratio should be at least 13: 1.

Based on the findings from the Pre-synthesized $MnO_{2(s)}$ experiments, PM was able to oxidize 1-methylnaphthalene and produce $MnO_{2(s)}$, which was not able to activate PS. As a result, the produced $MnO_{2(s)}$ in PM/PS system would contain some "ineffective" $MnO_{2(s)}$. Thus, the mass ratio of effective $MnO_{2(s)}$ to PS might be less than 5, while an obvious improvement in mass removal was still observed. It is speculated that the underlying mechanisms in the PM/PS system might also involve a synergistic effect of the combined use of PS and PM (Cui et al. 2017).

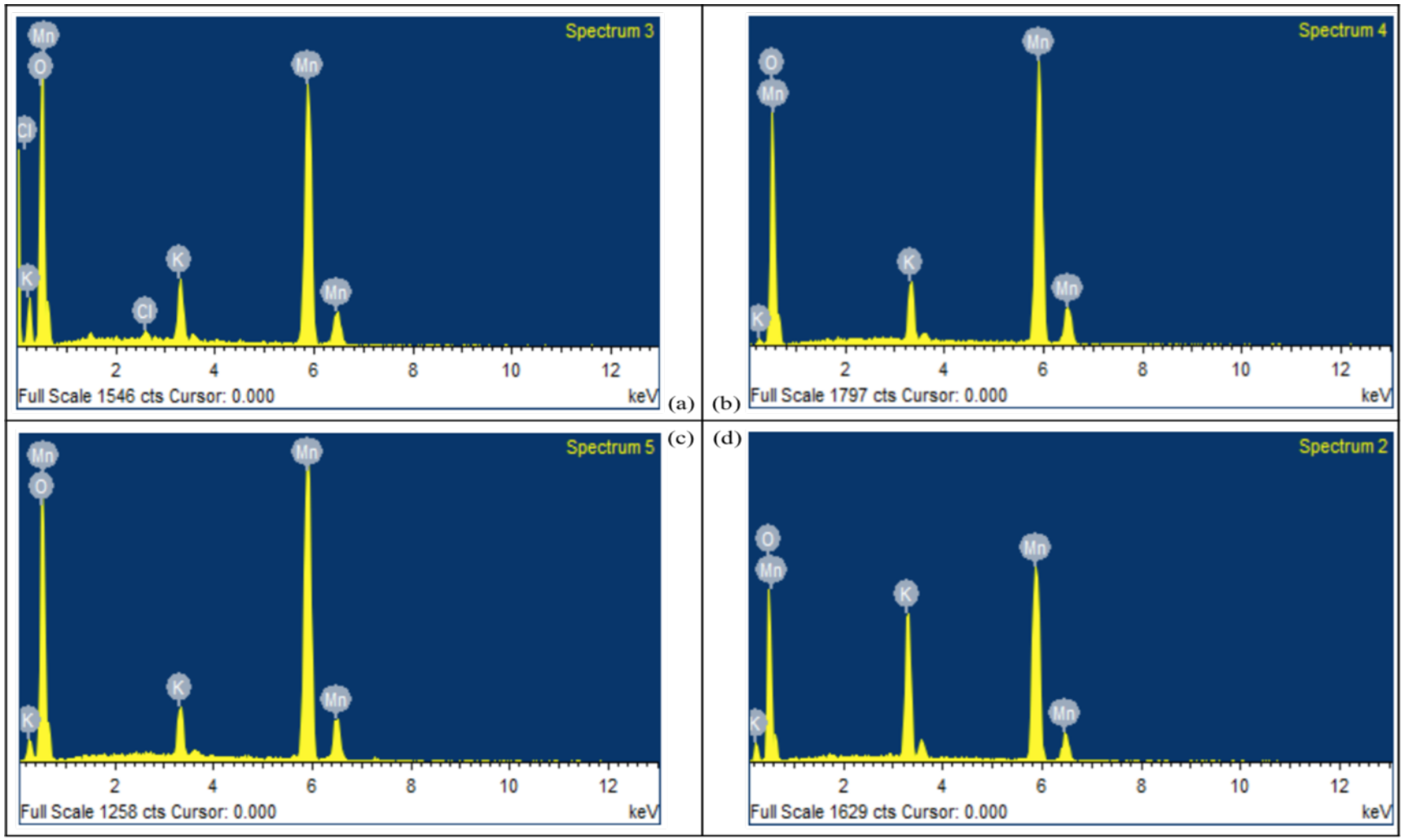

Figure 3.1 Element analysis of manganese oxide solids by EDX generated in pre-synthesized $MnO_{2(s)}$ systems. (a) Synthesized birnessite; (b) $MnO_{2(s)}$ Sample #1; (c) $MnO_{2(s)}$ Sample #2; (d) $MnO_{2(s)}$ Sample #3.

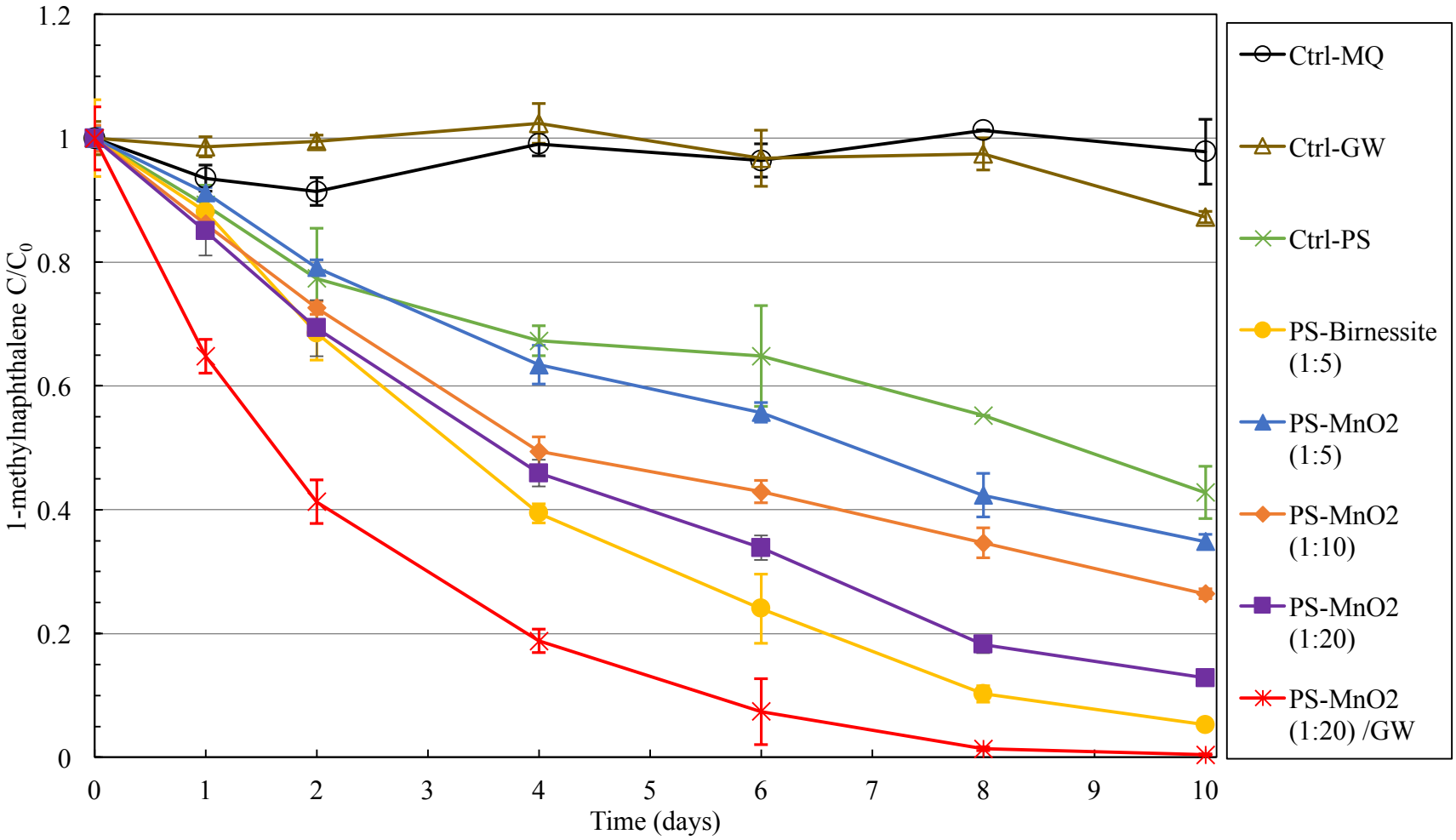

Figure 3.2 Normalized 1-methylnaphthalene temporal profiles in pre-synthesized birnessite and $MnO_{2(s)}$ Sample #1 and Sample #2 systems. The error bars represent the standard deviation from triplicate reactors.

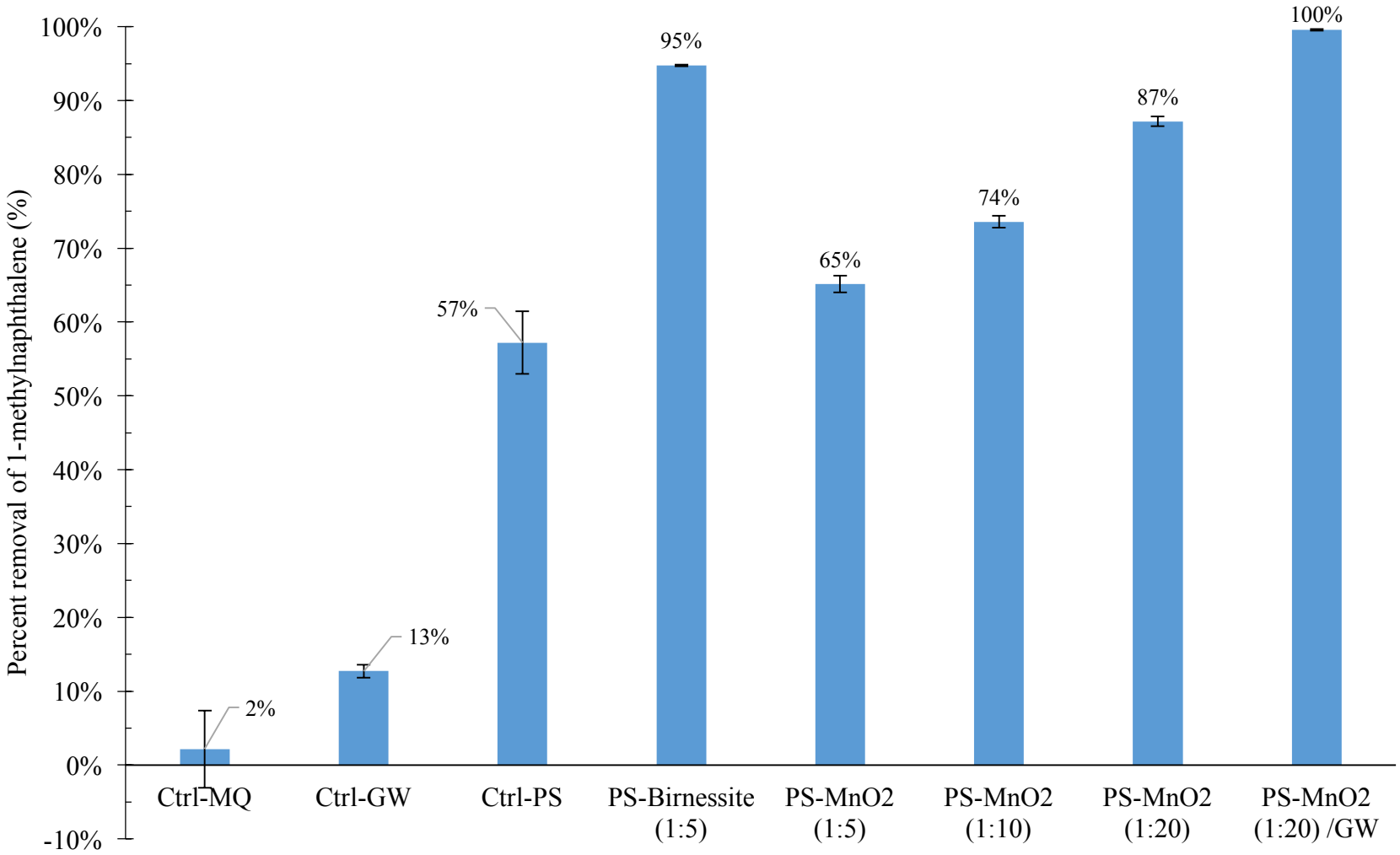

Figure 3.3 Percent removal of 1-methylnaphthalene in pre-synthesized birnessite and $MnO_{2(s)}$ Sample #1 and Sample #2 systems. The error bars represent the standard deviation from triplicate reactors.

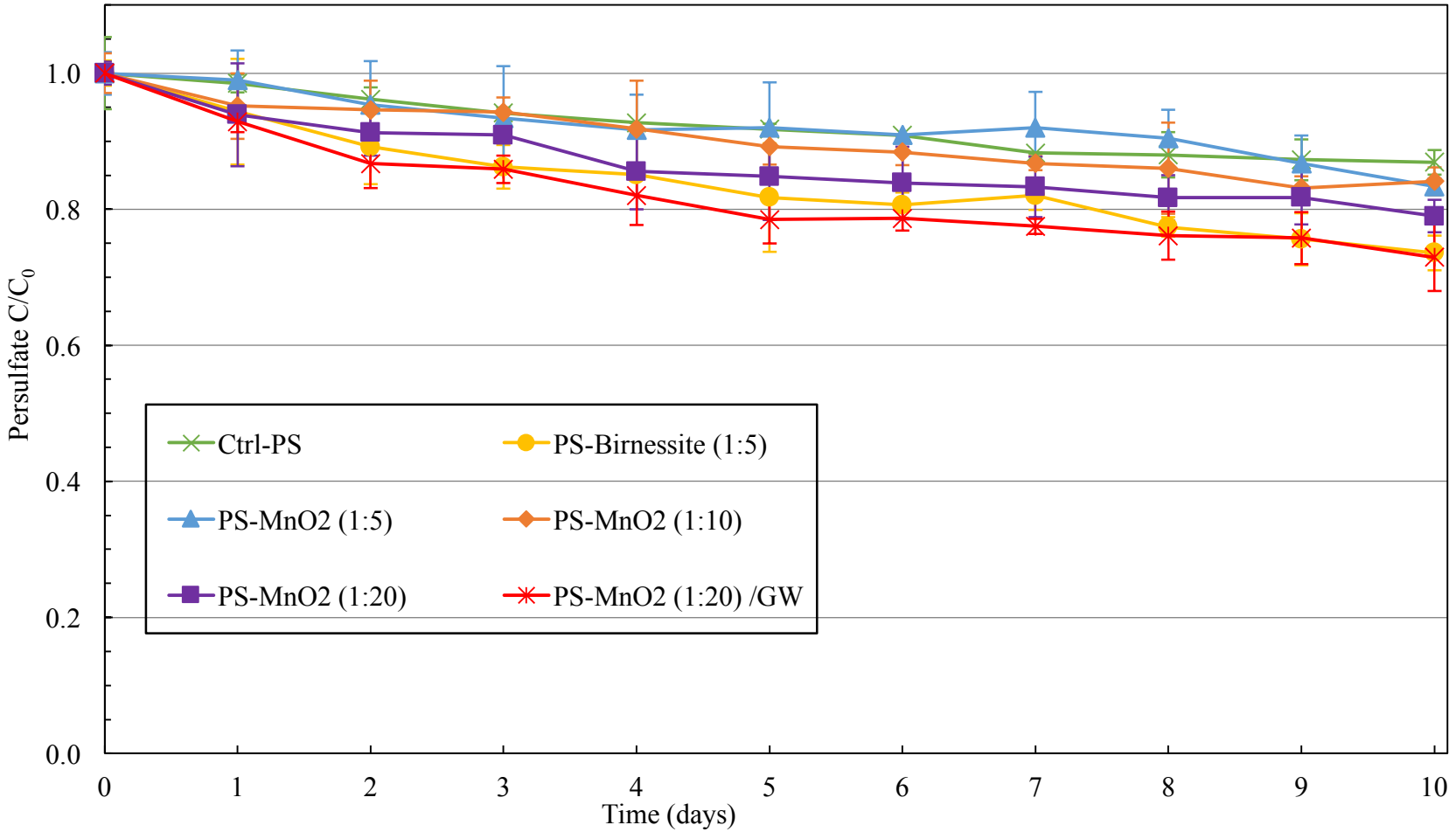

Figure 3.4 Normalized persulfate temporal profiles in pre-synthesized birnessite and $MnO_{2(s)}$ Sample #1 and Sample #2 systems. The error bars represent the standard deviation from triplicate reactors.

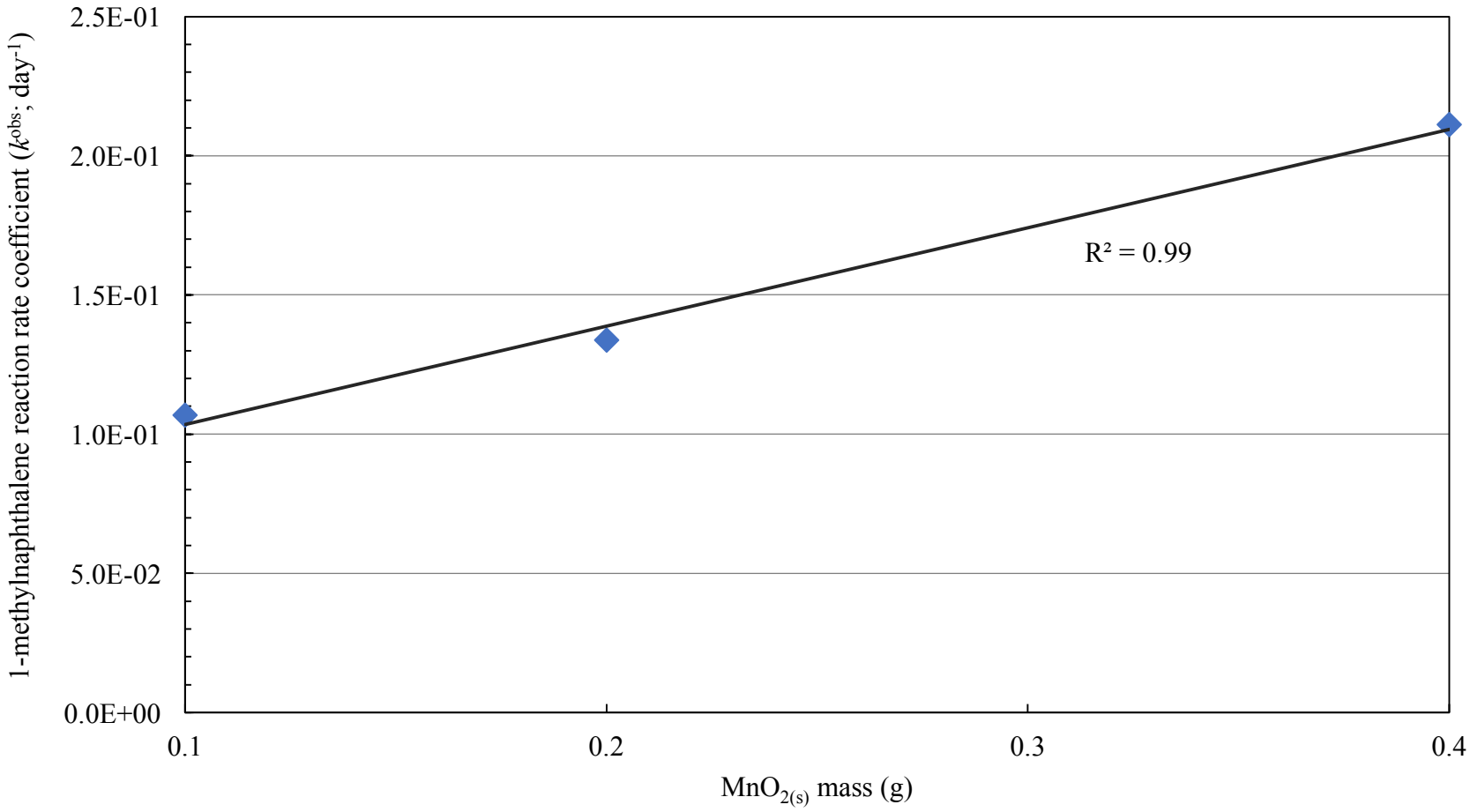

Figure 3.5 The linear relationship between 1-methylnaphthalene reaction rate coefficients and $MnO_{2(s)}$ mass (g) in pre-synthesized $MnO_{2(s)}$ Sample #1 system.

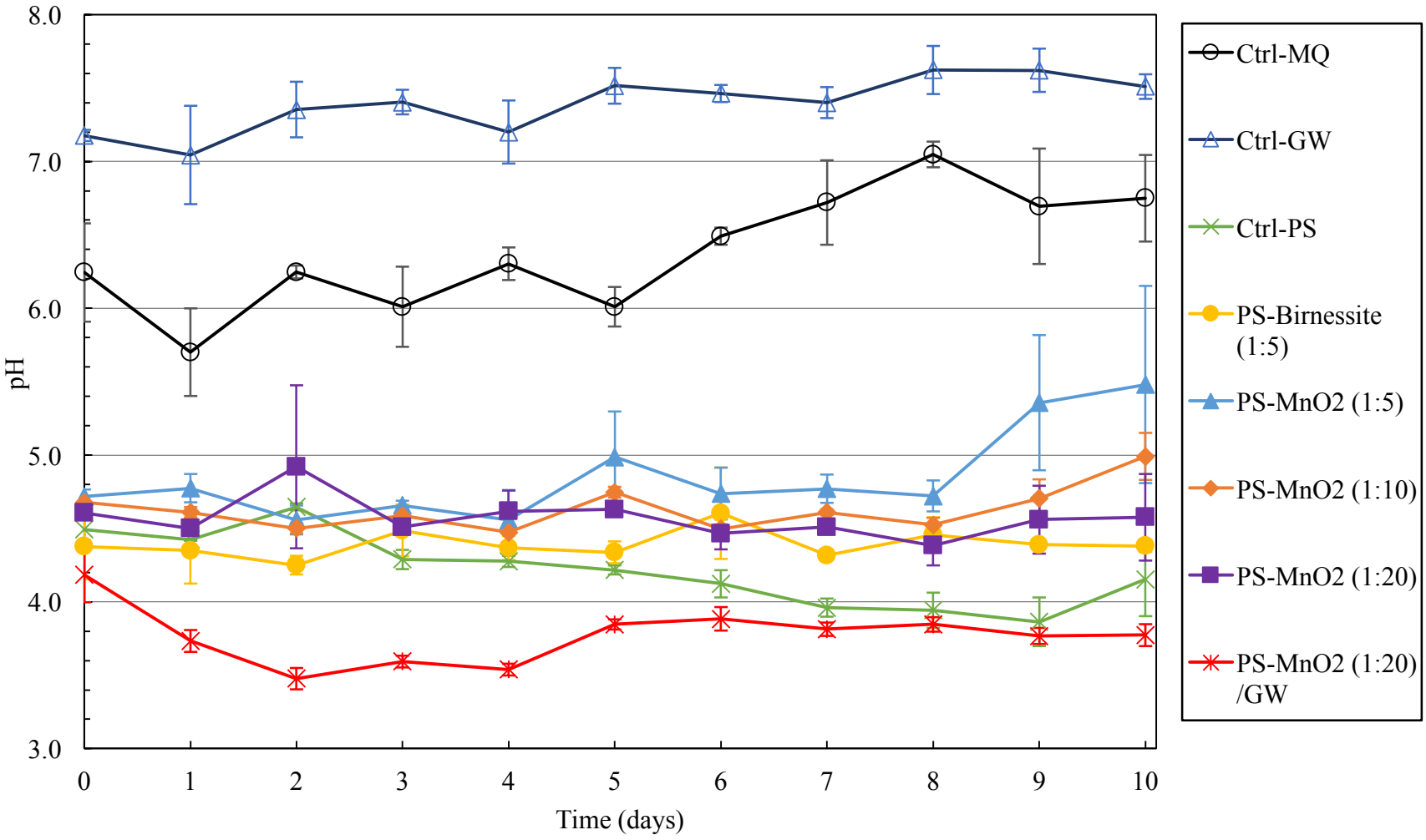

Figure 3.6 pH temporal profiles in pre-synthesized birnessite and $MnO_{2(s)}$ Sample #1 and Sample #2 systems. The error bars represent the standard deviation from triplicate reactors.

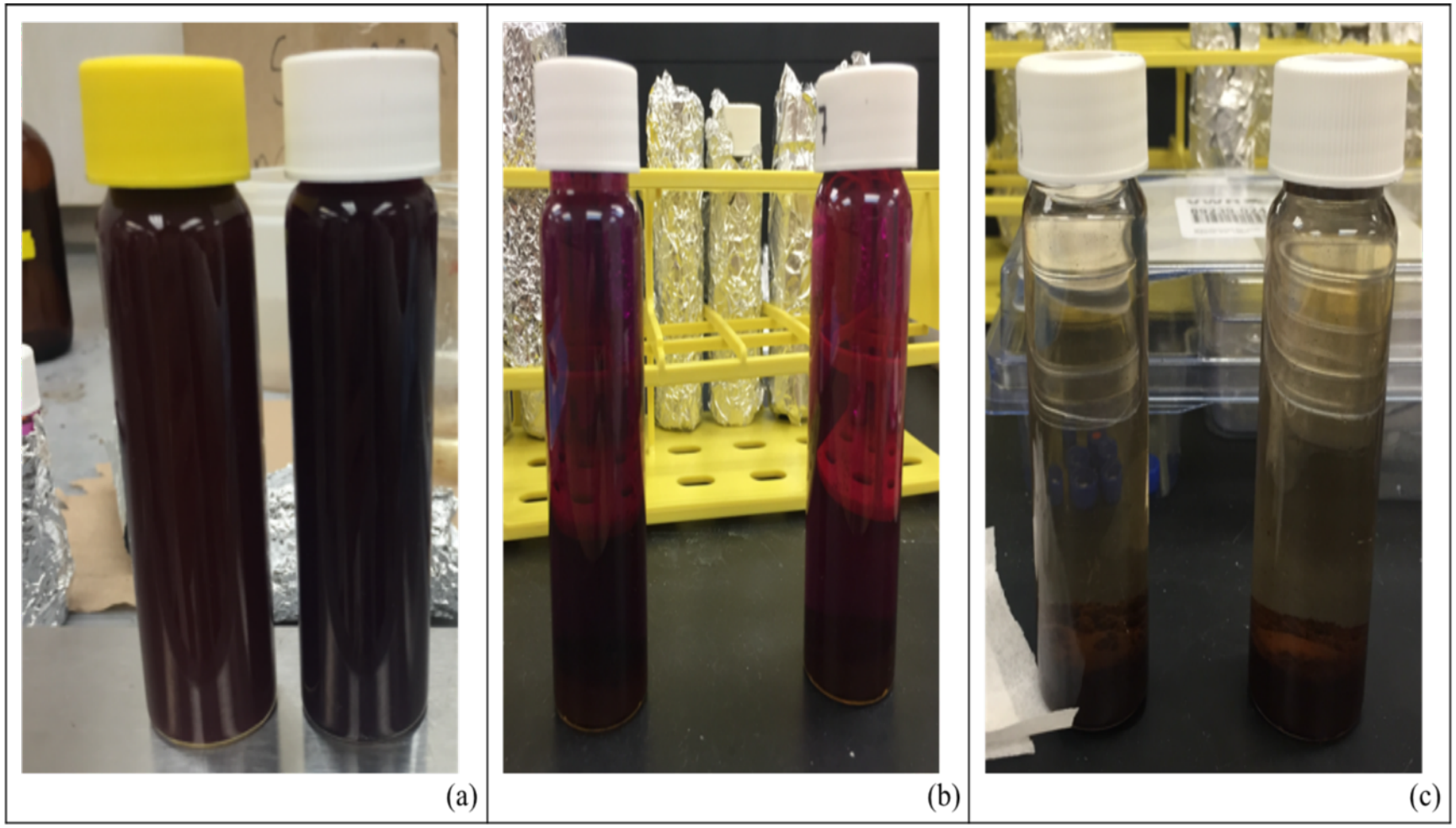

Figure 3.7 Each image shows two reactors (Ctrl-PM on the left, and PM/PS on the right) in the PM/PS system for: (a) start, (b) after 2 hrs, and (c) after 20 hrs.

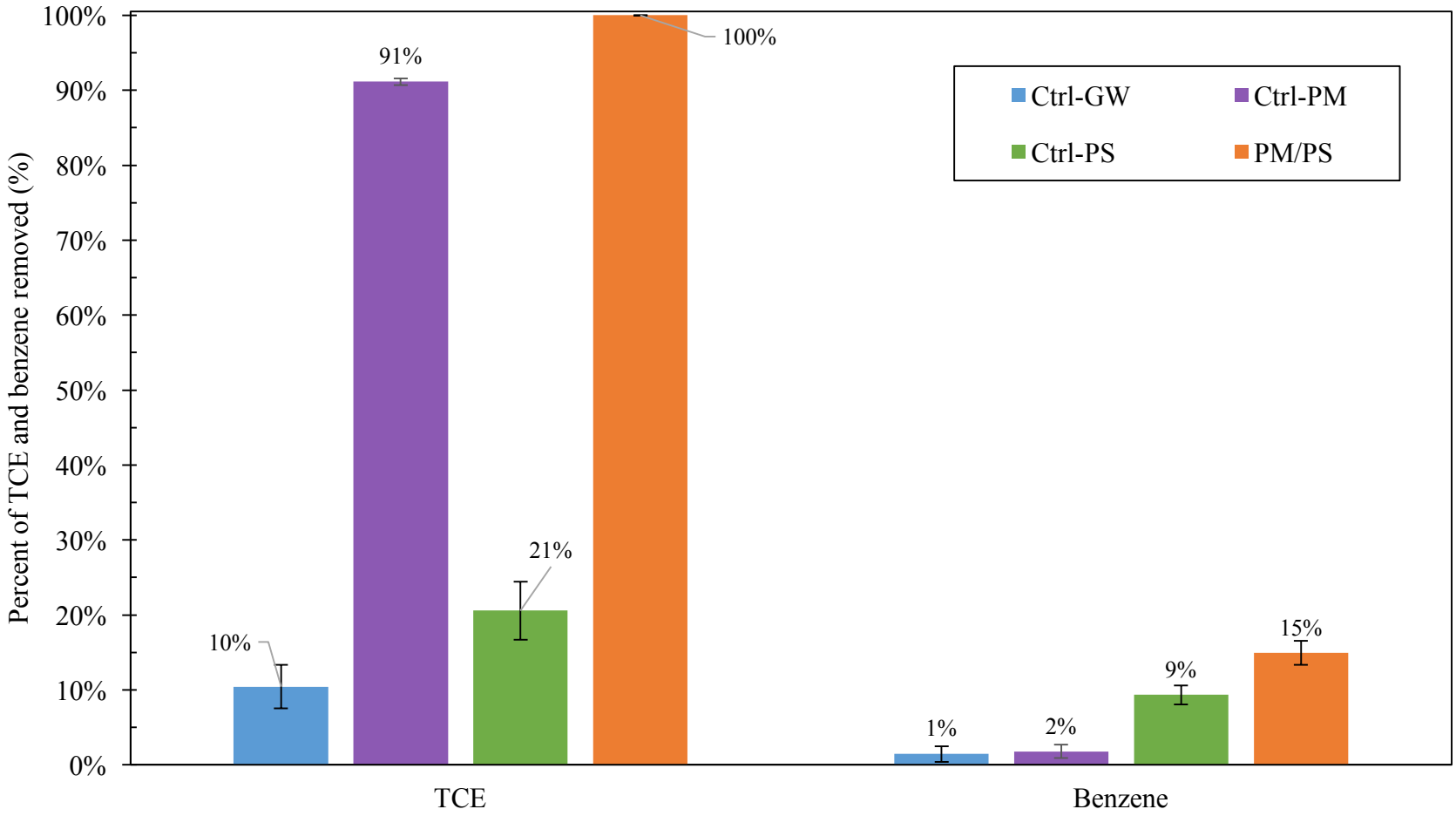

Figure 3.8 Percent TCE and benzene removed in the PM/PS system. The error bars represent the standard deviation from triplicate reactors.

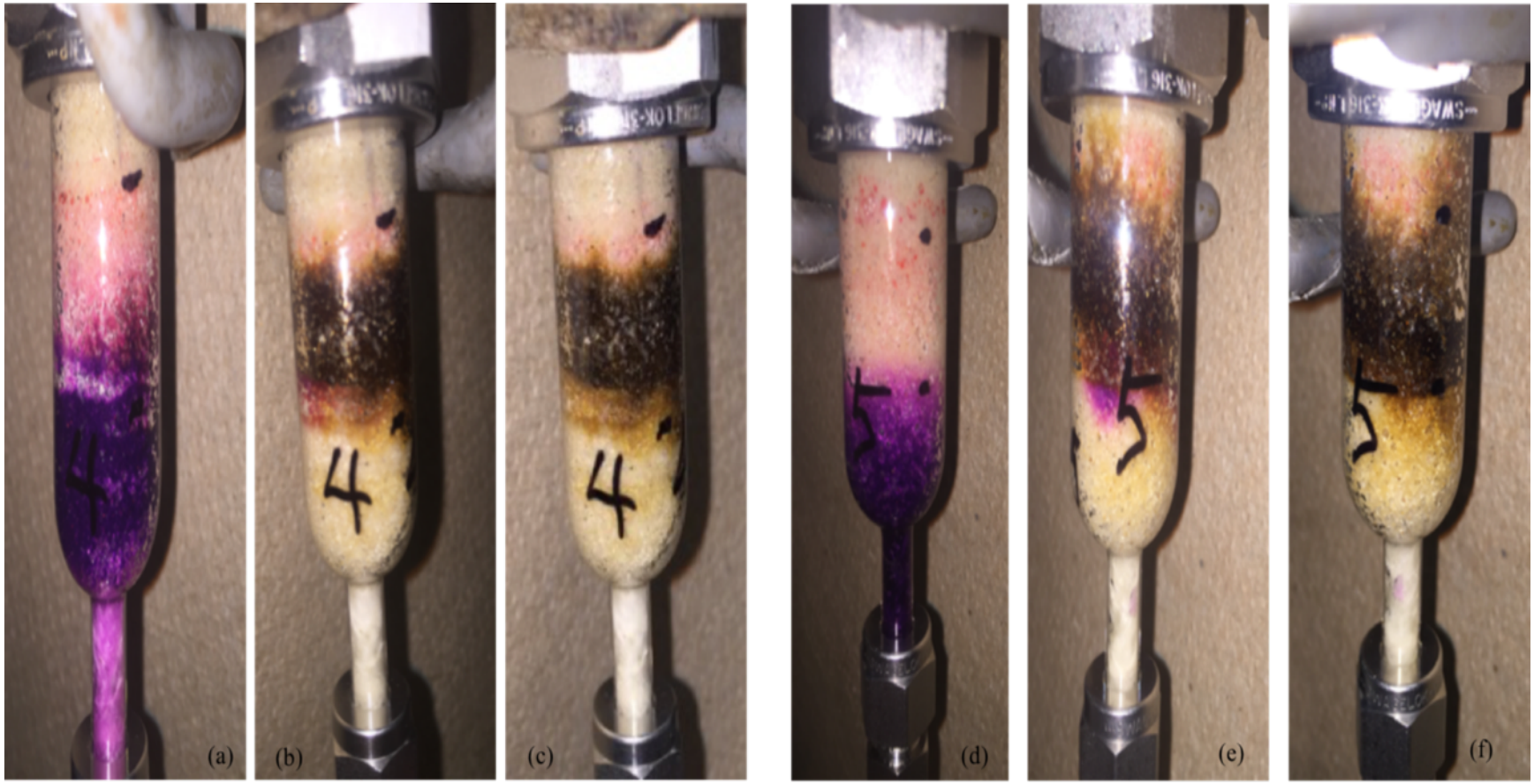

Figure 3.9 Images of column PM/PS-1 and PM/PS-2 during and after PM injection in the column experiments. (a, d) during the PM injection, (b, e) after PM injection, (c, f) during the 1-day stop-flow period.

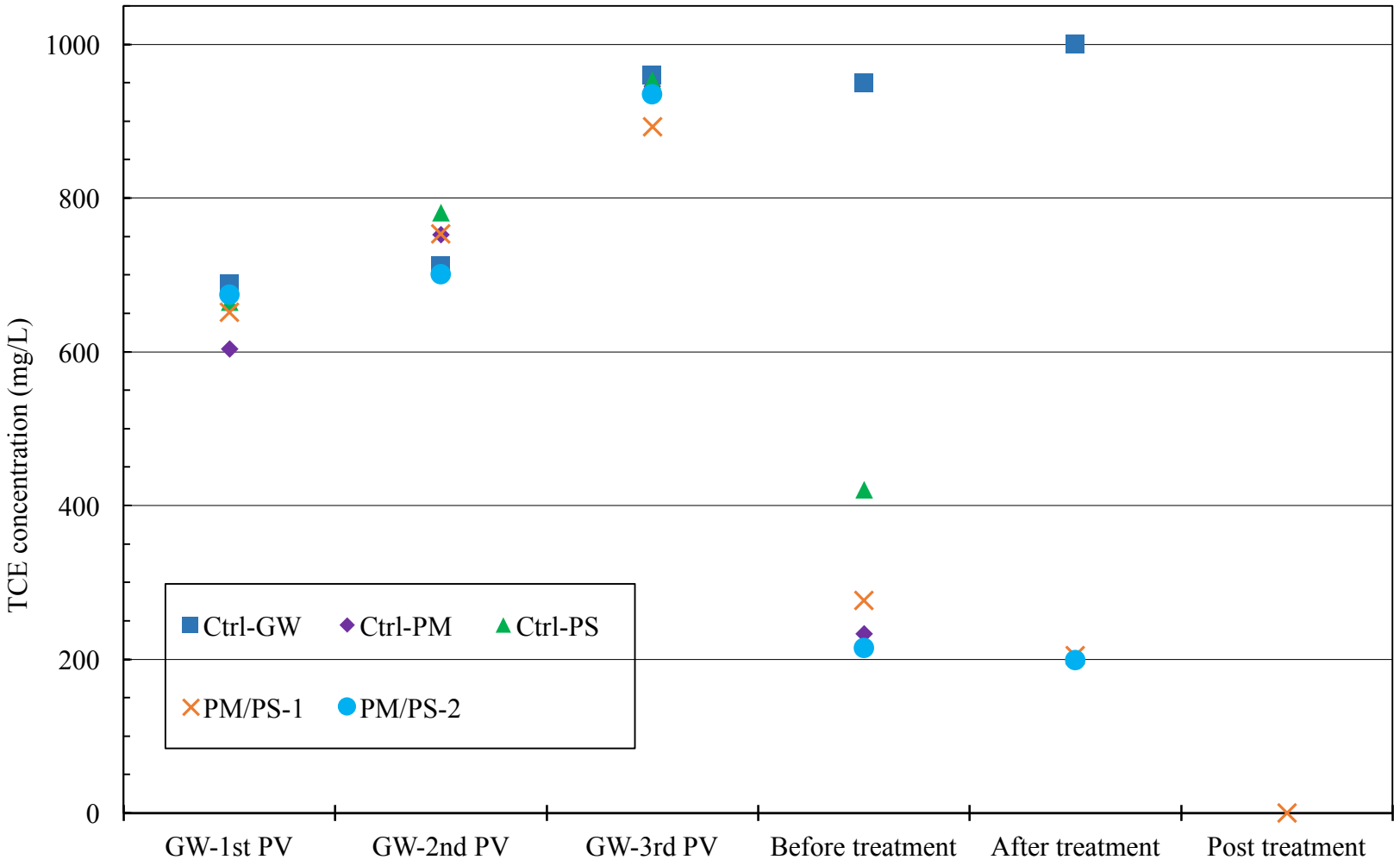

Figure 3.10 TCE effluent concentration of the column experiments.

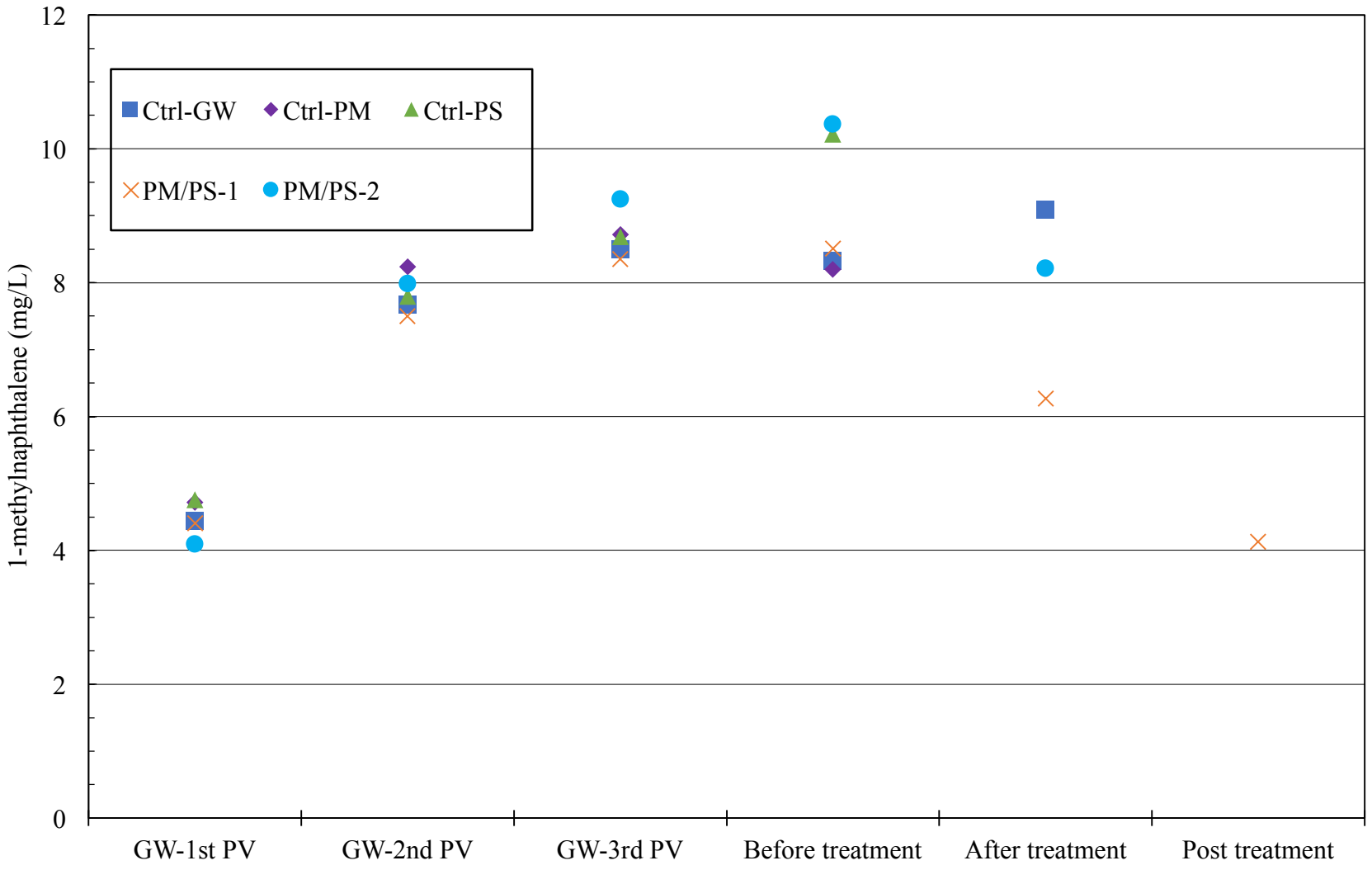

Figure 3.11 1-methylnaphthalene effluent concentration of the column experiments.

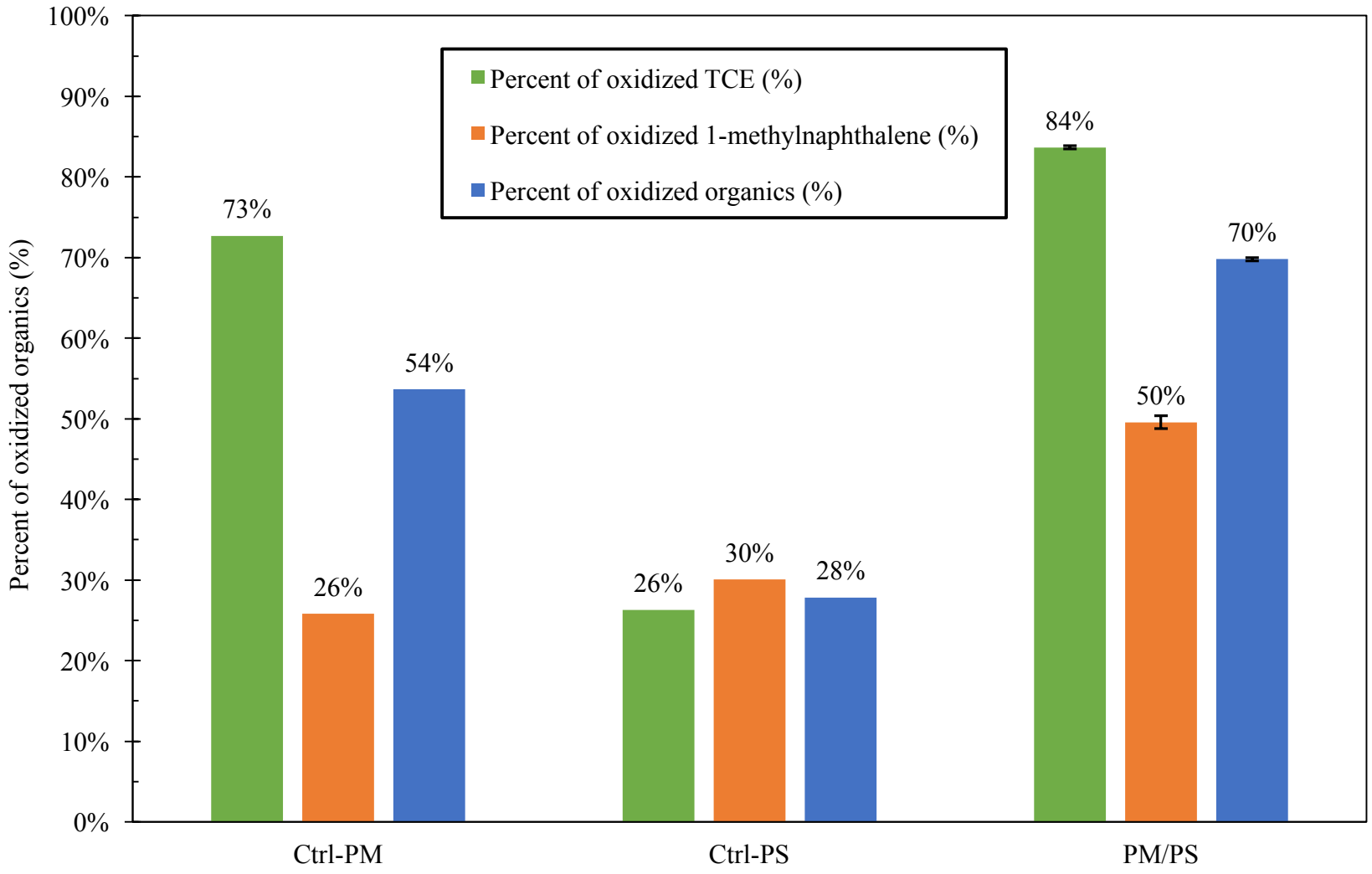

Figure 3.12 Percent of oxidized TCE and 1-methylnaphthalene in each column of the column experiments. The error bar in PM/PS is the deviation from duplicated column PM/PS-1 and PM/PS-2.

Table 3.1 Element weight fraction of manganese oxide solids of pre-synthesized $MnO_{2(s)}$ systems.

	Element Weight Fraction			
Sample indicator	Mn (wt.%)	K (wt.%)	O (wt.%)	Cl (wt. %)
Synthesized birnessite	56.0	4.9	38.5	0.7
$MnO_{2(s)}$ Sample #1[a]	63.0	5.2	31.9	-
$MnO_{2(s)}$ Sample #2[b]	62.8	3.8	33.4	-
$MnO_{2(s)}$ sample #3[c]	51.0	14.0	34.9	-

Note:

a. $MnO_{2(s)}$ Sample #1 generated from TCE and potassium PM in Milli-Q water.
b. $MnO_{2(s)}$ Sample #2 generated from TCE and potassium PM in synthetic groundwater.
c. $MnO_{2(s)}$ Sample #3 generated from 1-methylnaphthalene and potassium PM in Milli-Q water.

Table 3.2 Observed reaction rate coefficient and bulk stoichiometry of pre-synthesized $MnO_{2(s)}$ Sample #1 and Sample #2 systems.

Batch reactor indicator	k_{obs}[a] [10^{-2} day^{-1}]	r^2 [b]	PS / 1-methylnaphthalene (g/g)
Ctrl-MQ	-	-	-
Ctrl-GW	-	-	-
Ctrl-PS	7.8 ± 1.4	0.97	24
PS-Birnessite (1:5)	30 ± 2.3	0.99	31
PS-MnO_2 (1:5)	10.7 ± 0.8	0.99	26
PS-MnO2 (1:10)	13.4 ± 1.7	0.98	23
PS-MnO_2 (1:20)	21.1 ± 1.7	0.99	27
PS-MnO_2 (1:20) /GW	55.5 ± 9.2	0.98	29

Note:

a. k_{obs} is observed first-order reaction rate constant (d^{-1}) calculated from the data of Figure 3.2. The error based on $\pm$95% confidence interval for linear regression.
b. r^2 is the coefficient of determination; the values shown in the table are at 95% confidence interval.

Table 3.3 Mass balance estimates of the column experiments.

Column	Organic	M_{IN} [a] (mg)	M_{EFF} [b] (mg)	M_{RES} [c] (mg)	M_{OX} [d] (mg)
Ctrl-GW	TCE	73.0	18.2	51.1	0.0
	1Mn	50.1	0.16	40.2	0.0
	Total	123.1	18.4	91.4	0.0
Ctrl-PM	TCE	73.0	9.8	10.1	53.1
	1Mn	50.1	0.12	37.0	12.9
	Total	123.1	9.9	47.1	66.0
Ctrl-PM	TCE	73.0	11.9	41.9	19.2
	1Mn	50.1	0.13	34.9	15.0
	Total	123.1	12.1	76.7	34.2
PM/PS [e]	TCE	73.0	11.9	0.0	61.1
	1Mn	50.1	0.17	25.1	24.8
	Total	123.1	12.1	25.1	85.9

Note:

a. M_{IN} is the initial loading mass of TCE and 1-methylnaphthalene.
b. M_{EFF} is the mass of TCE and 1-methylnaphthalene in the aqueous effluent.
c. M_{RES} is the residual mass of non-aqueous phase and aqueous phase TCE and 1-methylnaphthalene remaining in the column at the termination of the experiment.
d. M_{OX} is the mass of oxidized TCE and 1-methylnaphthalene by PM and PS as calculated from Eq 3.5.
e. The data for PM/PS was the average of PM/PS-1 and PM/PS-2.

Table 3.4 The TCE and 1-methylnaphthalene oxidation rates of the column experiments.

Column	$M_{OX\text{-}TCE}$ (mg)	TCE oxidation rate (mg/day)	$M_{OX\text{-}1Mn}$ [a] (mg)	1-methylnaphthalene oxidation rate (mg/day)
Ctrl-PM	53.1	10.6	12.6	2.6
Ctrl-PS	19.2	3.8	15.0	3.0
PM/PS [b]	61.1	8.7	24.8	5.0

Note:

a. 1Mn represents 1-methylnaphthalene.

b. The data for PM/PS was the average of PM/PS-1 and PM/PS-2.

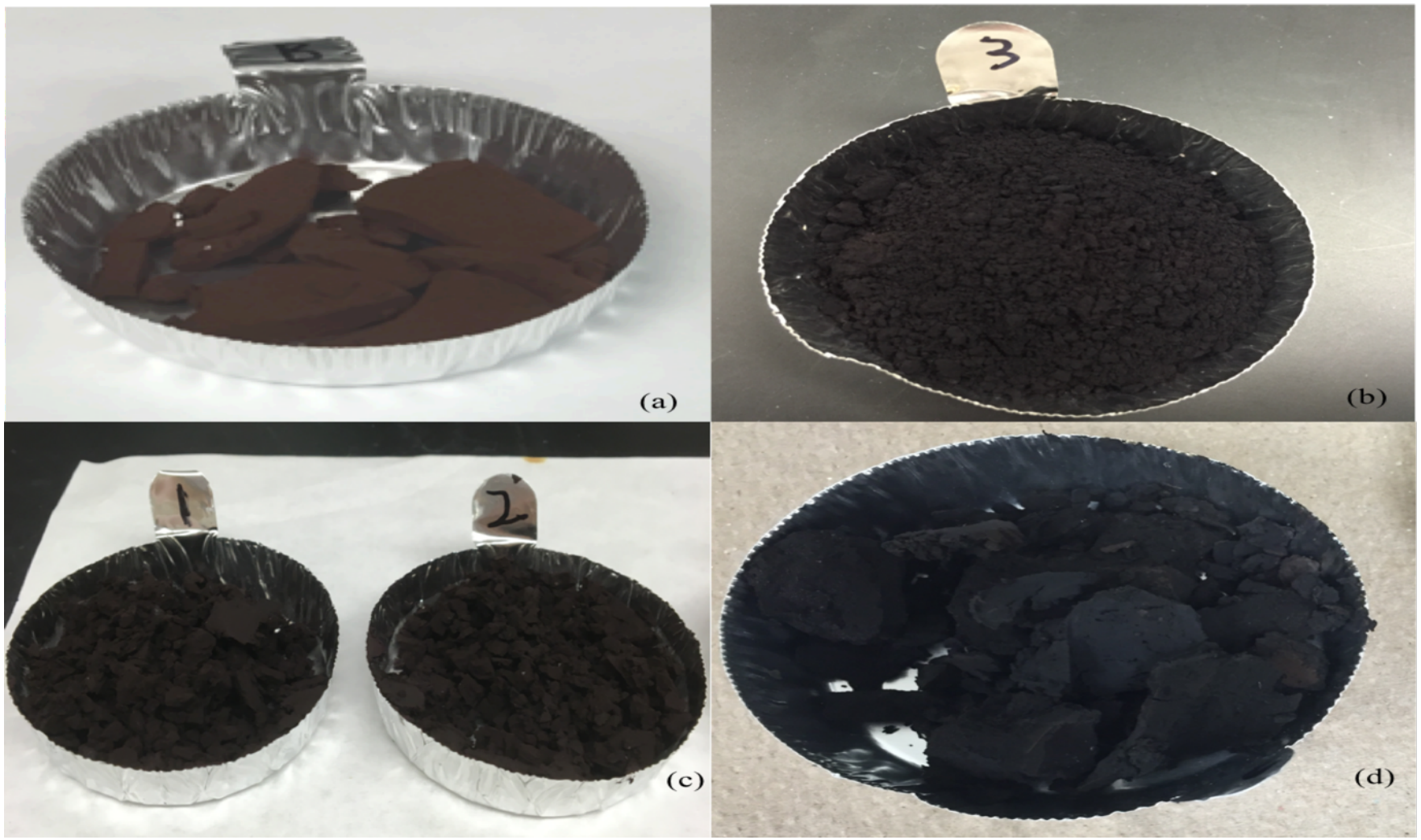

Figure S3.1 Photos of generated manganese oxide solids in the pre-synthesized $MnO_{2(s)}$ systems. (a) Synthesized birnessite, (b) $MnO_{2(s)}$ Sample #1, (c) $MnO_{2(s)}$ Sample #2, (d) $MnO_{2(s)}$ Sample #3.

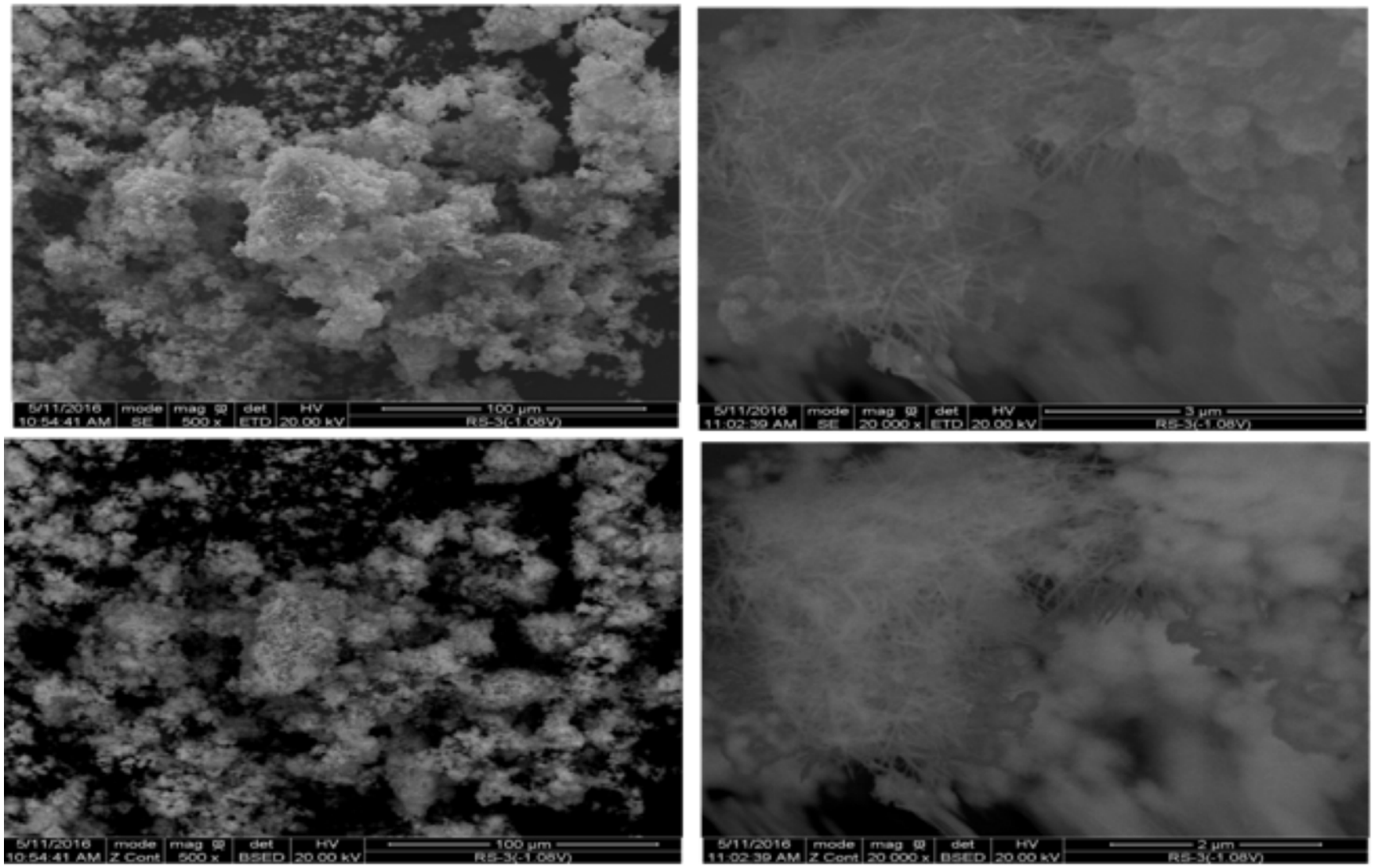

Figure S3.2 Selected SEM images for the synthesized birnessite in the pre-synthesized $MnO_{2(s)}$ systems.

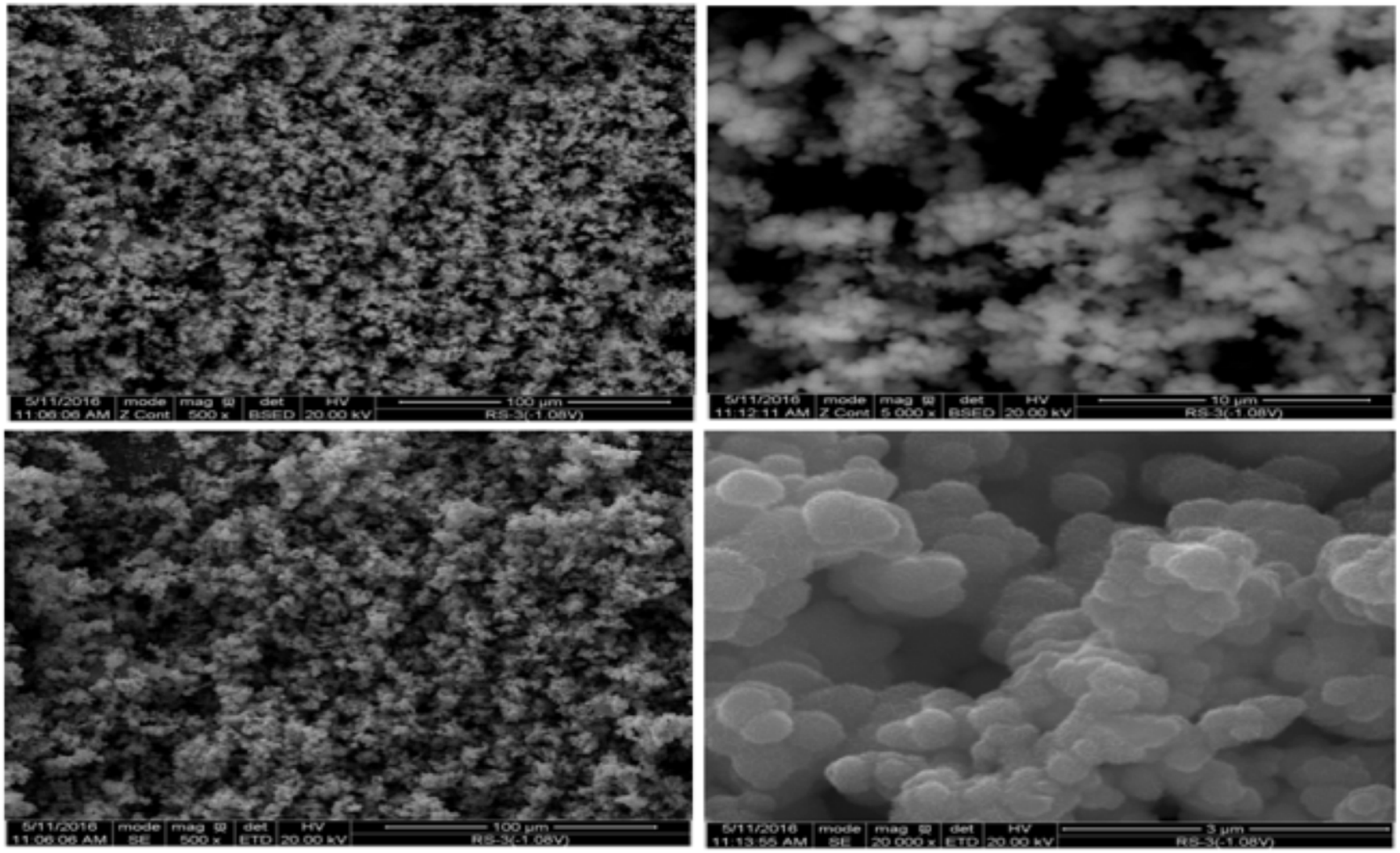

Figure S3.3 Selected SEM images for $MnO_{2(s)}$ Sample #1 in the pre-synthesized $MnO_{2(s)}$ systems.

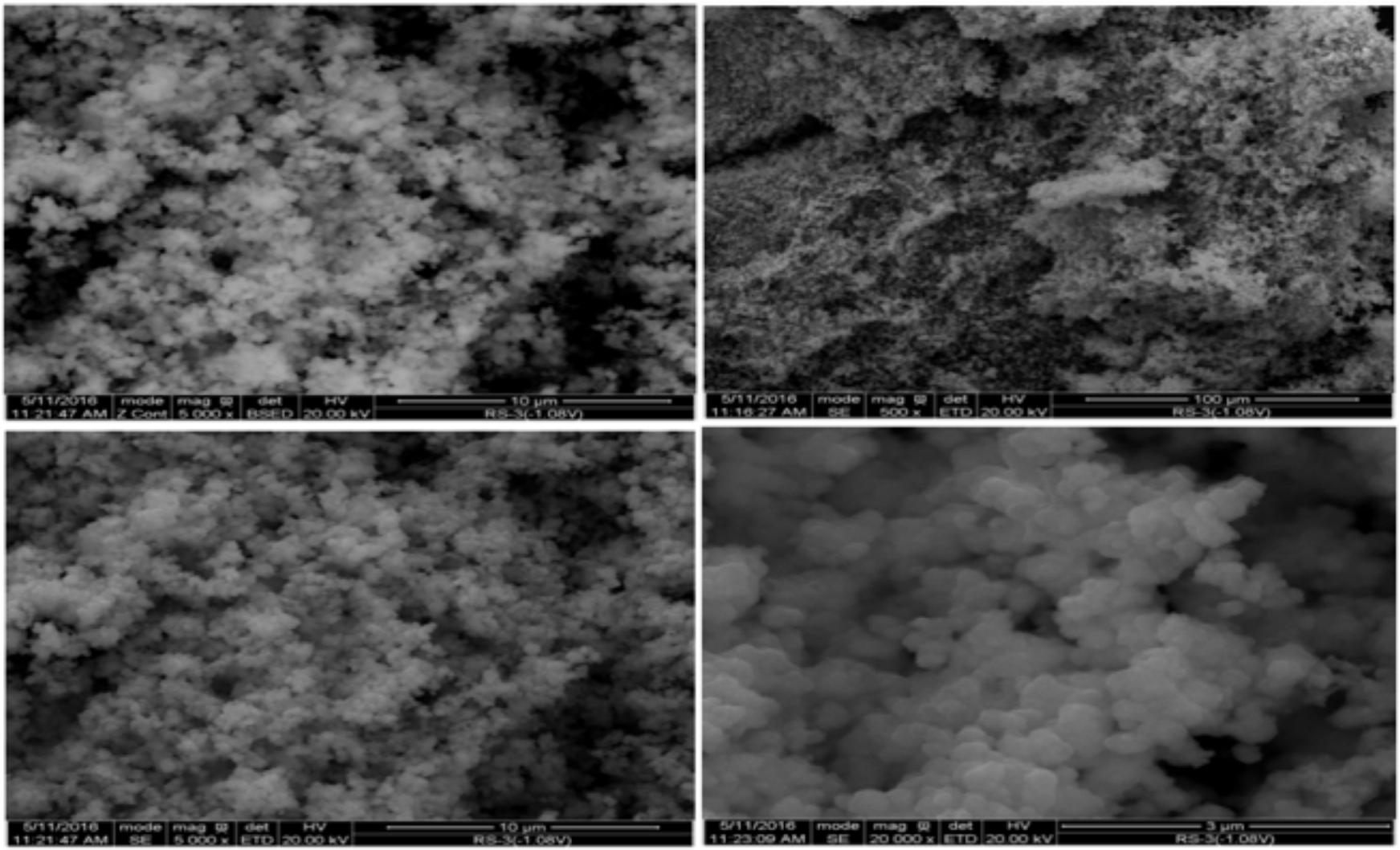

Figure S3.4 Selected SEM images for $MnO_{2(s)}$ Sample #2 in the pre-synthesized $MnO_{2(s)}$ systems.

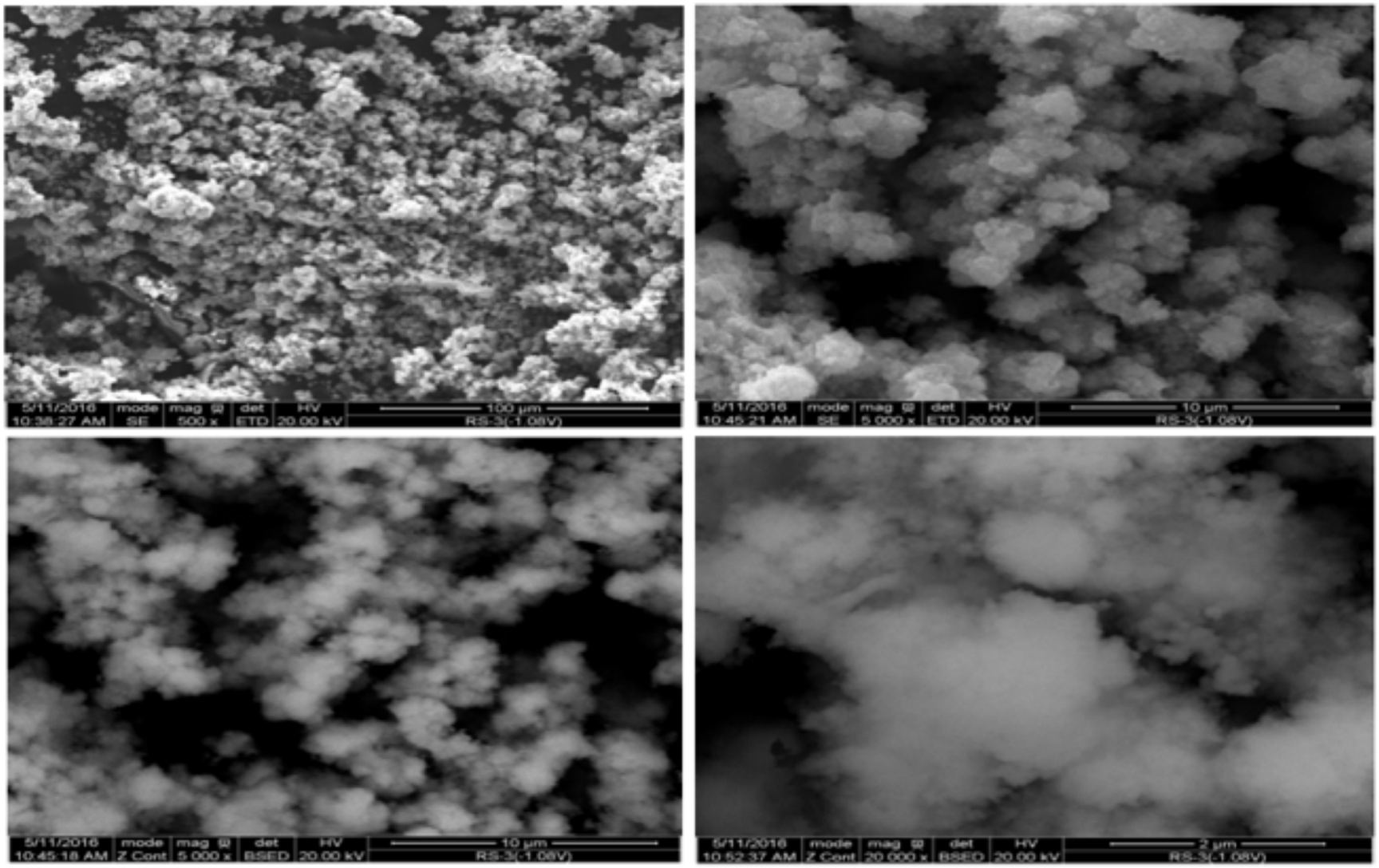

Figure S3.5 Selected SEM images for $MnO_{2(s)}$ Sample #3 in the pre-synthesized $MnO_{2(s)}$ systems.

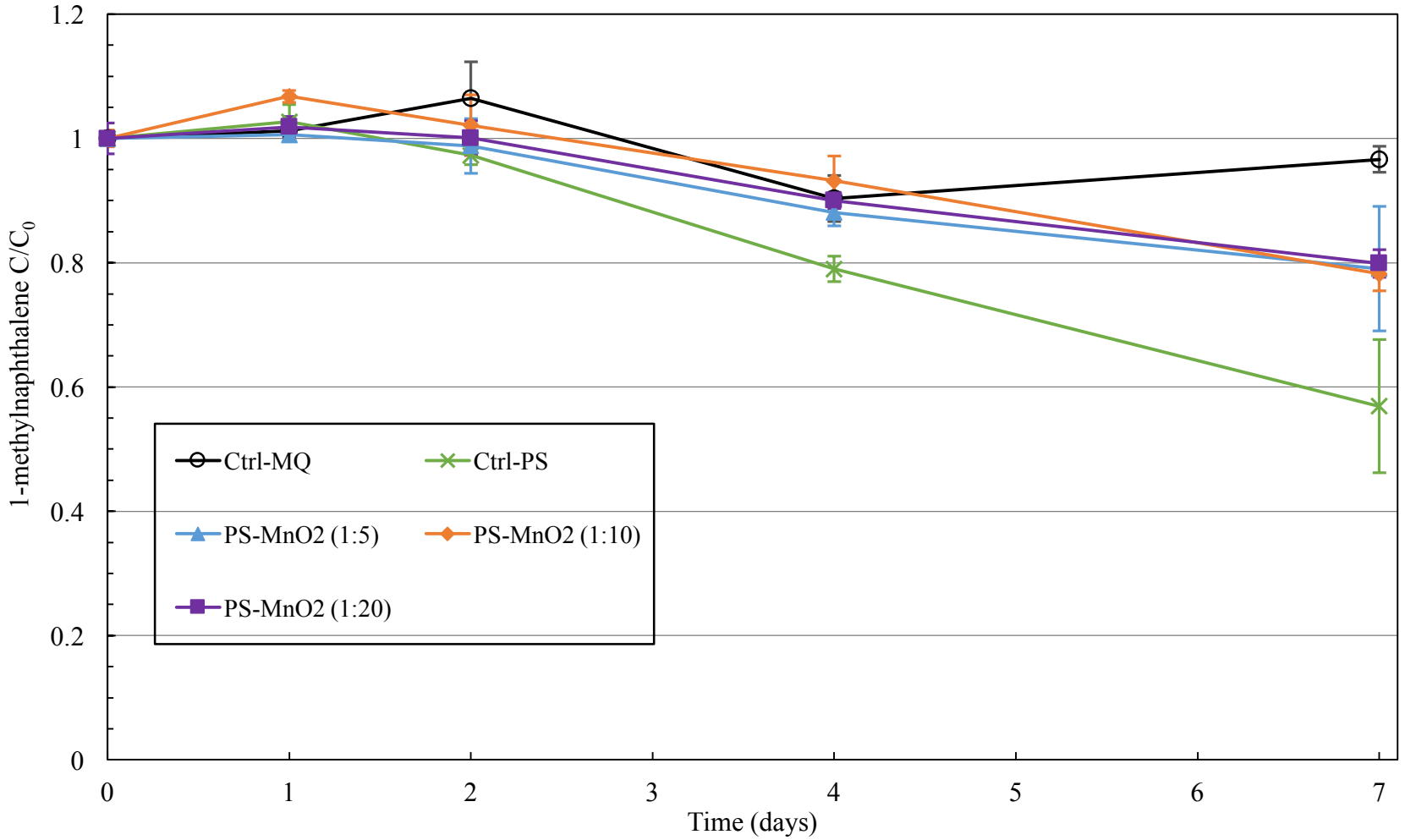

Figure S3.6 Normalized 1-methylnaphthalene temporal profiles in pre-synthesized $MnO_{2(s)}$ Sample #3 system. The error bars represent the standard deviation from triplicate reactors.

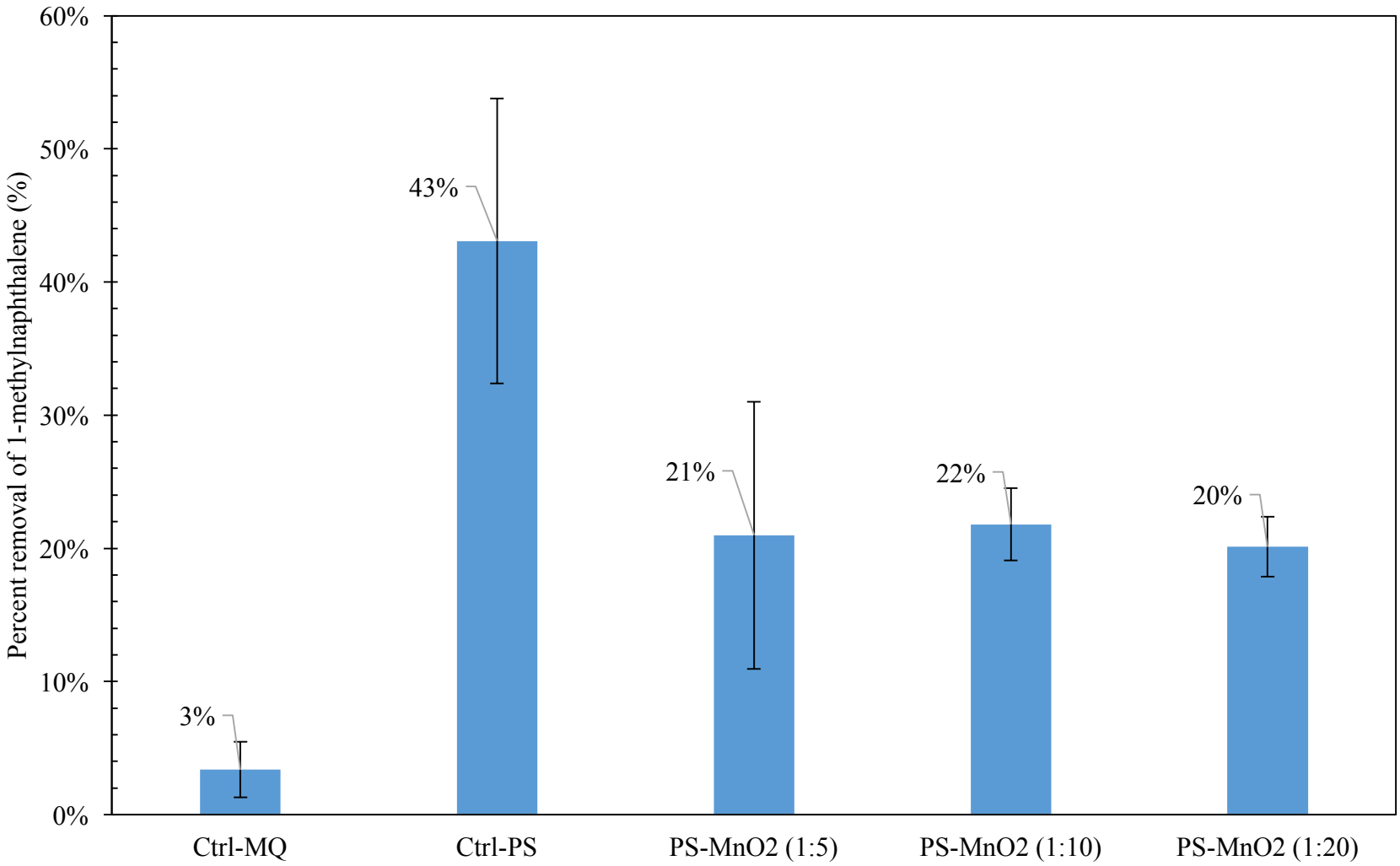

Figure S3.7 Percent removal of 1-methylnaphthalene in pre-synthesized $MnO_{2(s)}$ Sample #3 system. The error bars represent the standard deviation from triplicate reactors.

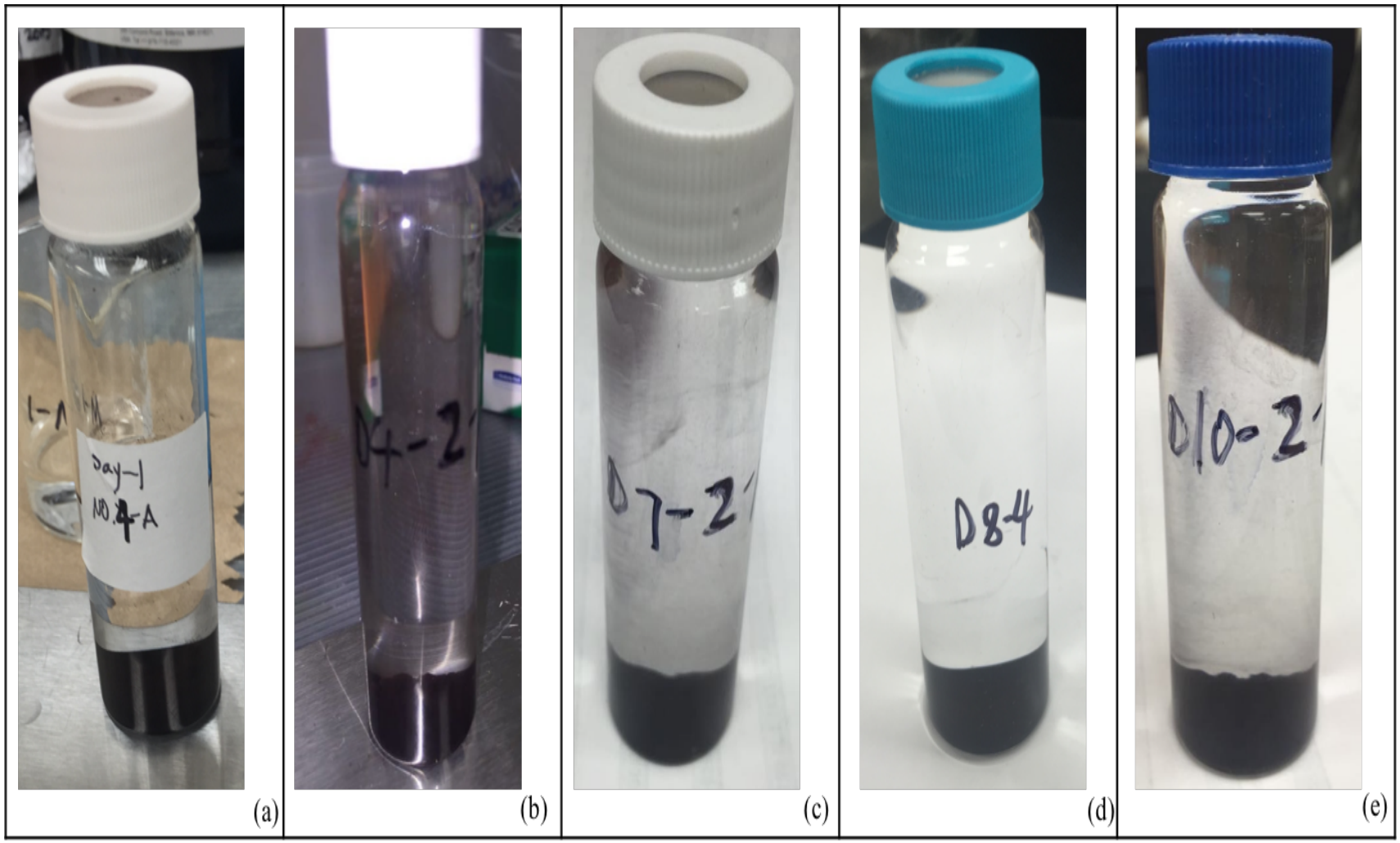

Figure S3.8 The visual observation of the reactors in pre-synthesized $MnO_{2(s)}$ Sample #1 system. (a) at Day 1, (b) at Day 4, (c) at Day 7), (d) at Day 8, (e) at Day 10.

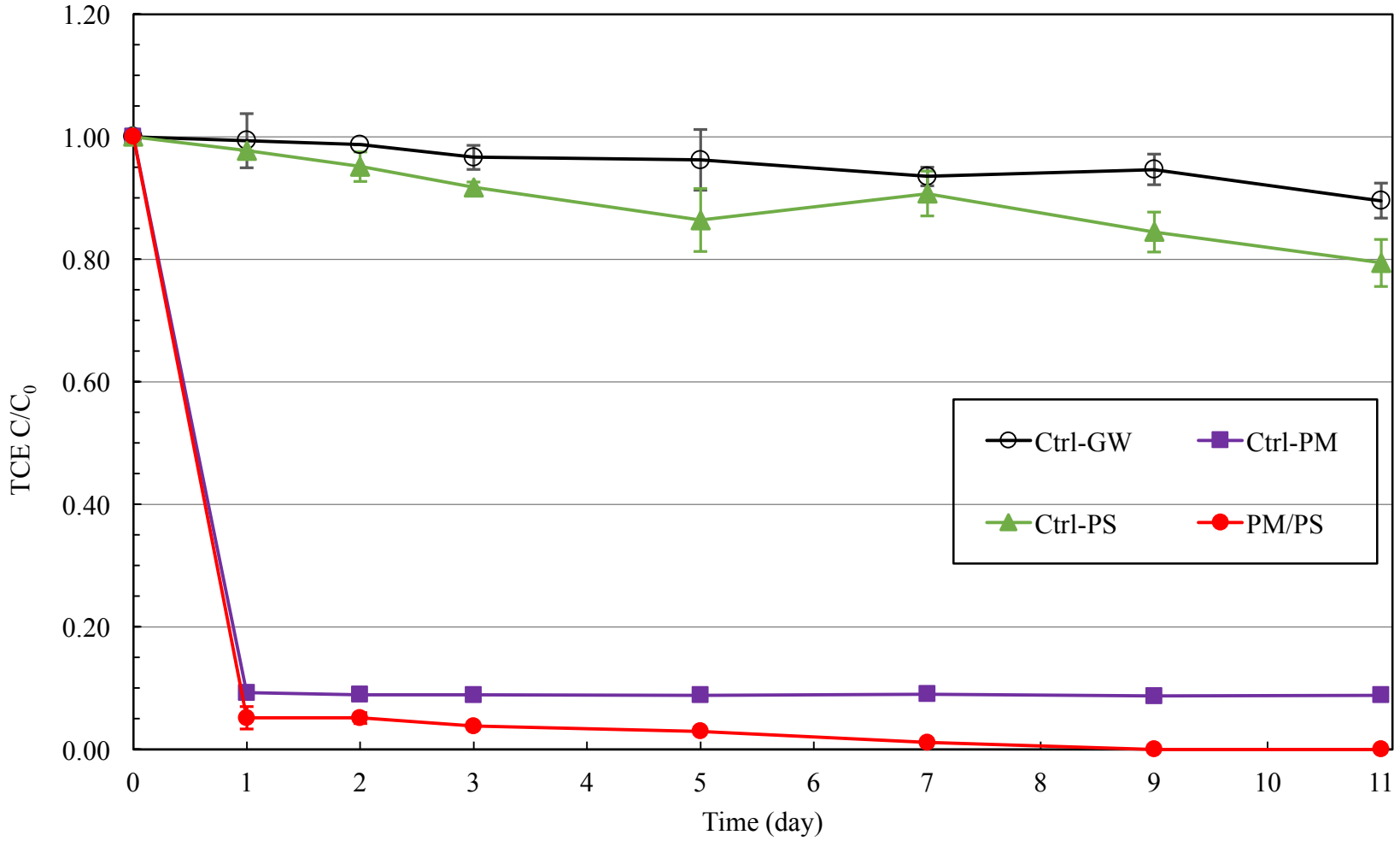

Figure S3.9 Normalized TCE temporal profiles in PM/PS system. The error bars represent the standard deviation from triplicate reactors.

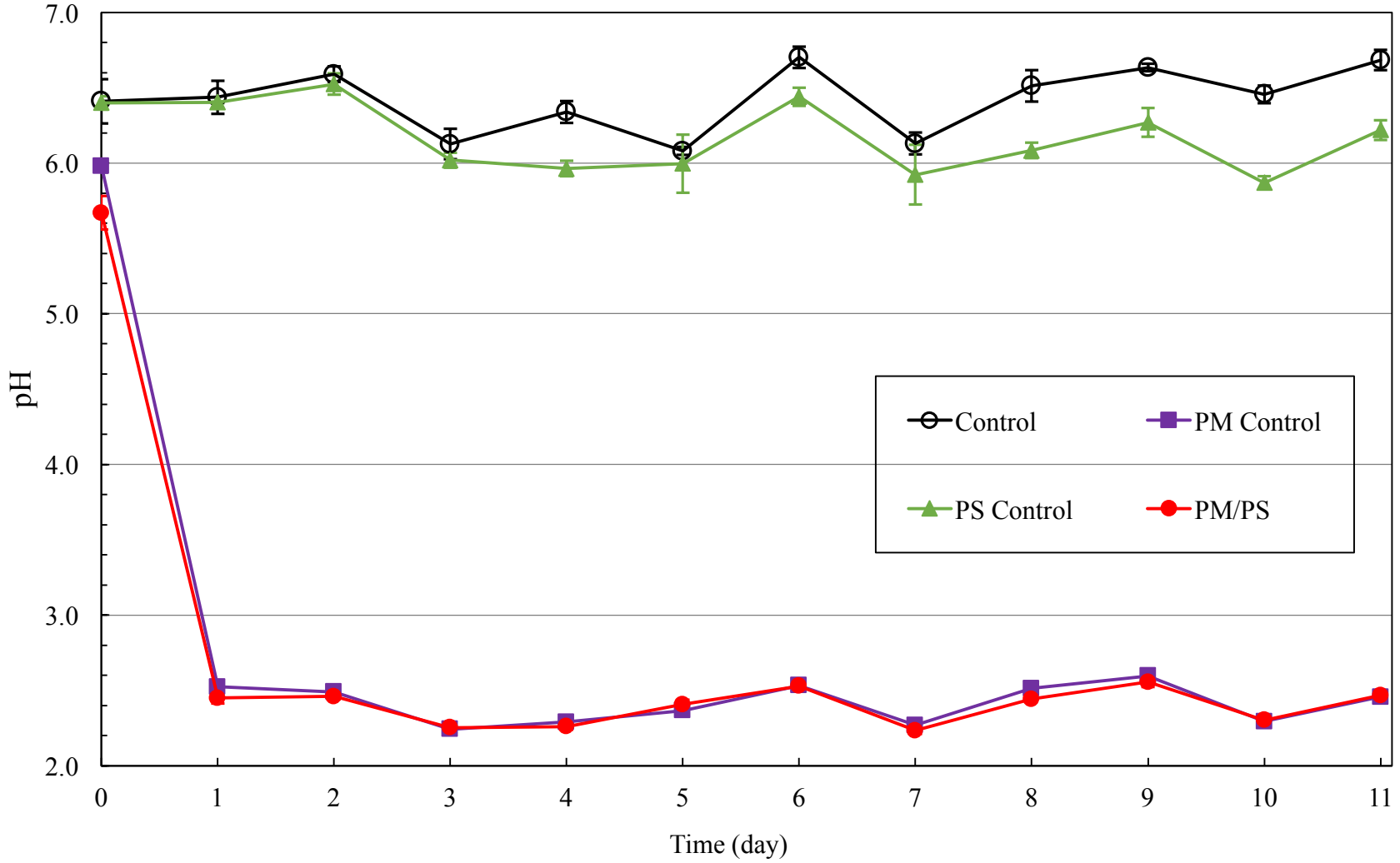

Figure S3.10 pH temporal profiles in PM/PS system. The error bars represent the standard deviation from triplicate reactors.

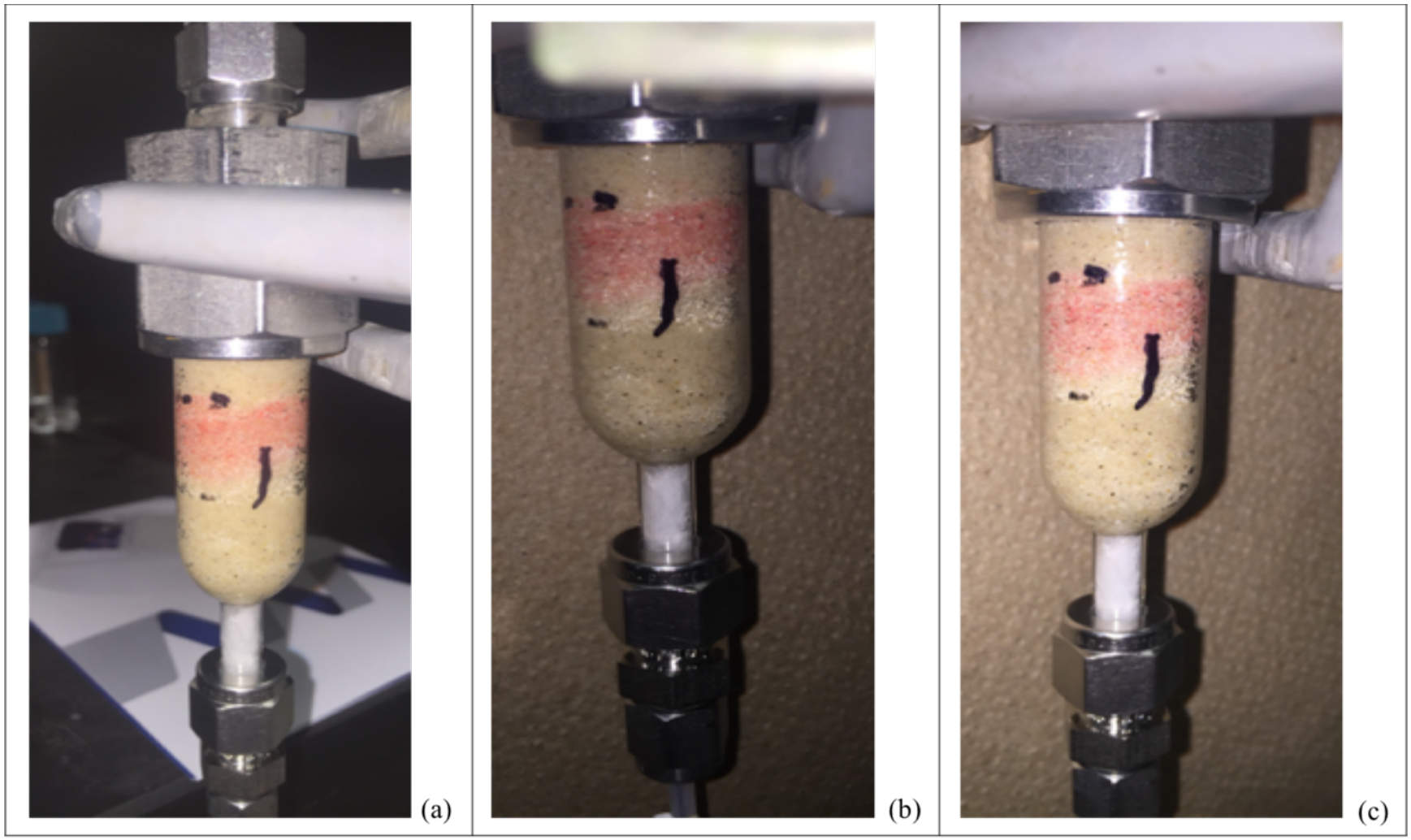

Figure S3.11 The images of the Ctrl-GW column. (a) at initial period, (b) during the synthetic groundwater injection, (c) at the end of experiment.

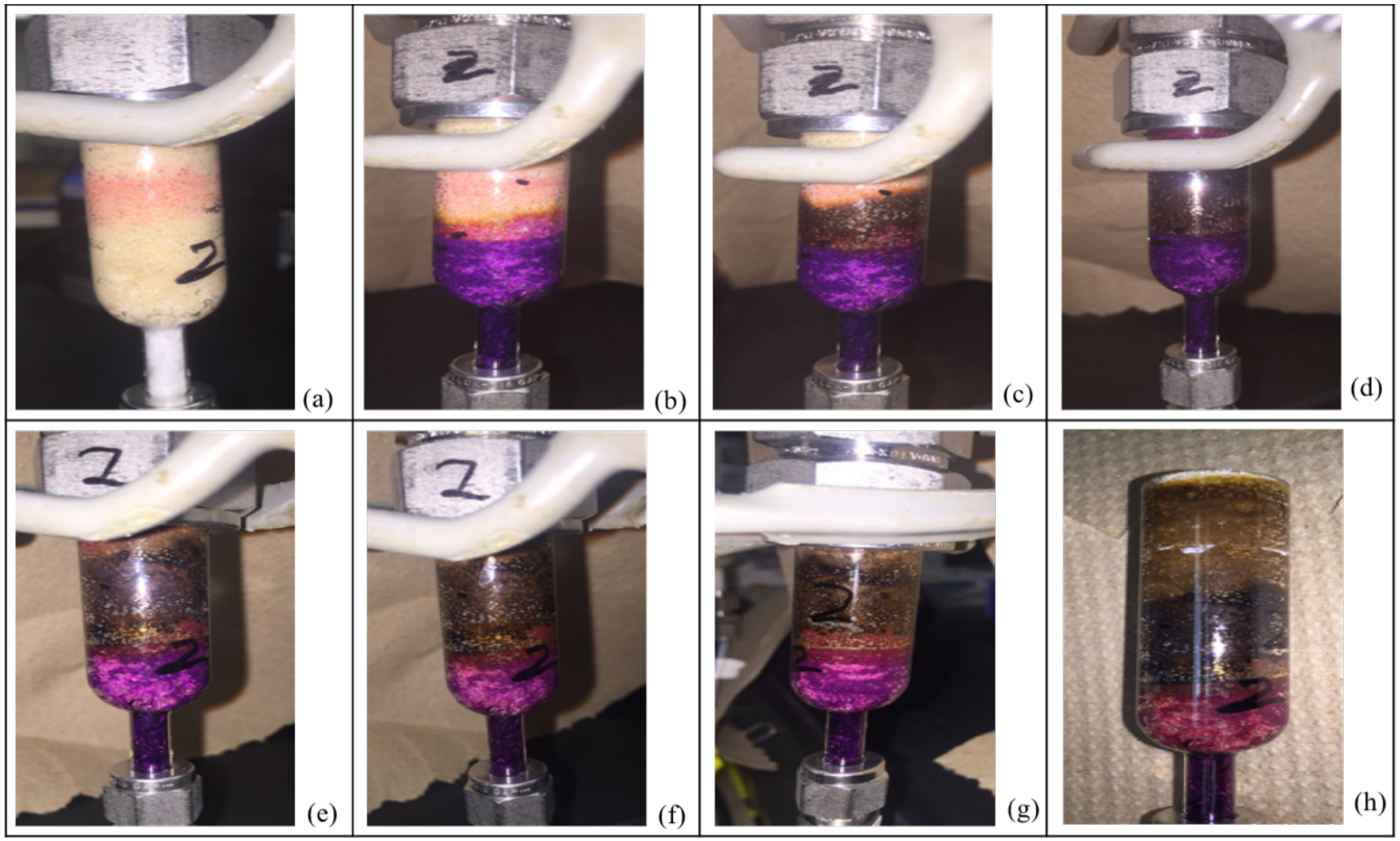

Figure S3.12 The images of the Ctrl-PM column. (a) at initial period, (b, c) during the PM injection, (d) after the PM injection, (e, f, g, h) during the 5-day stop-flow period, (h) open the column.

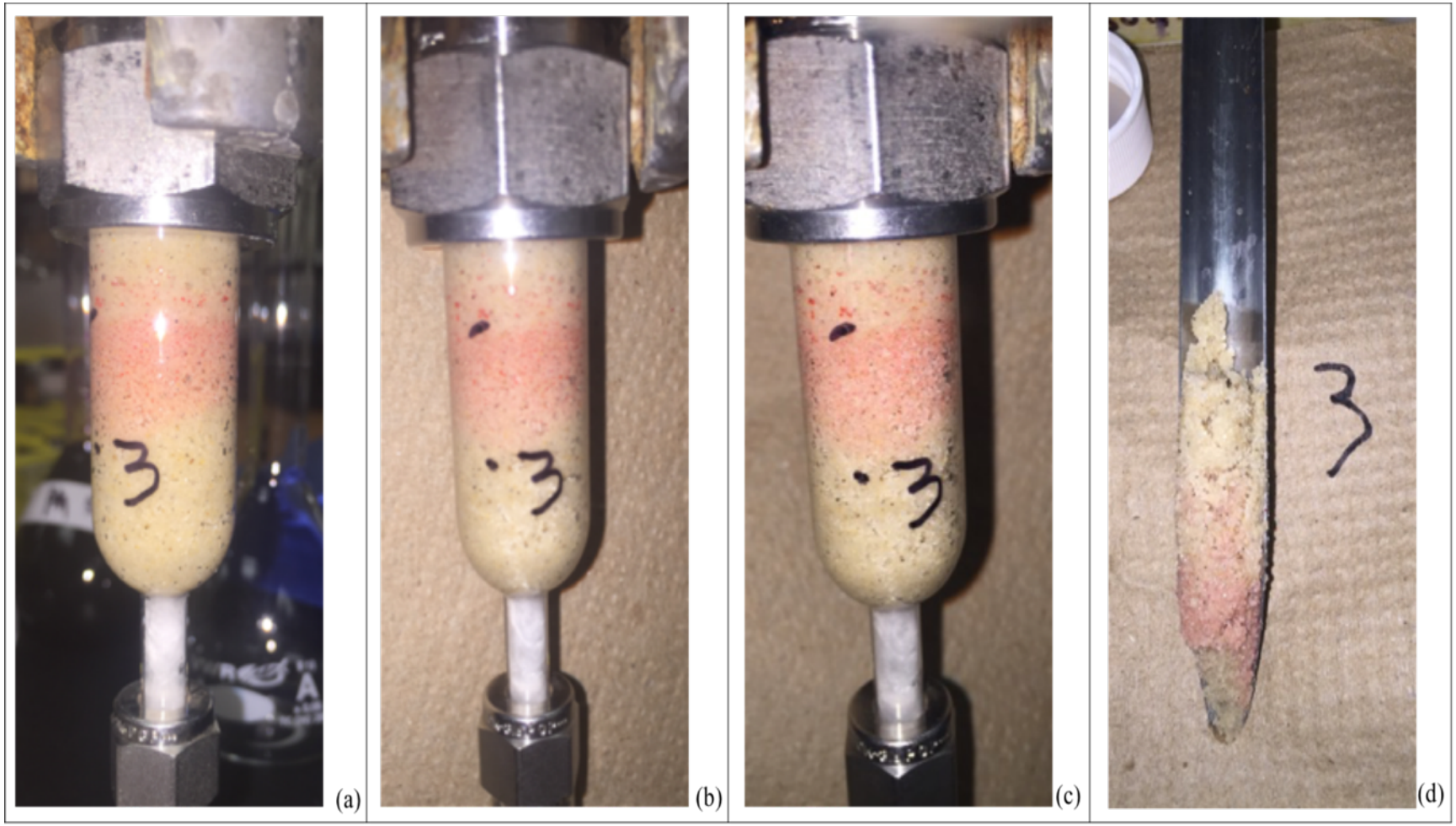

Figure S3.13 The images of the Ctrl-PS column. (a) at initial period, (b) during the PS injection, (c) during the 5-day stop-flow period, (h) treated soil in the Zone 3 and source zone.

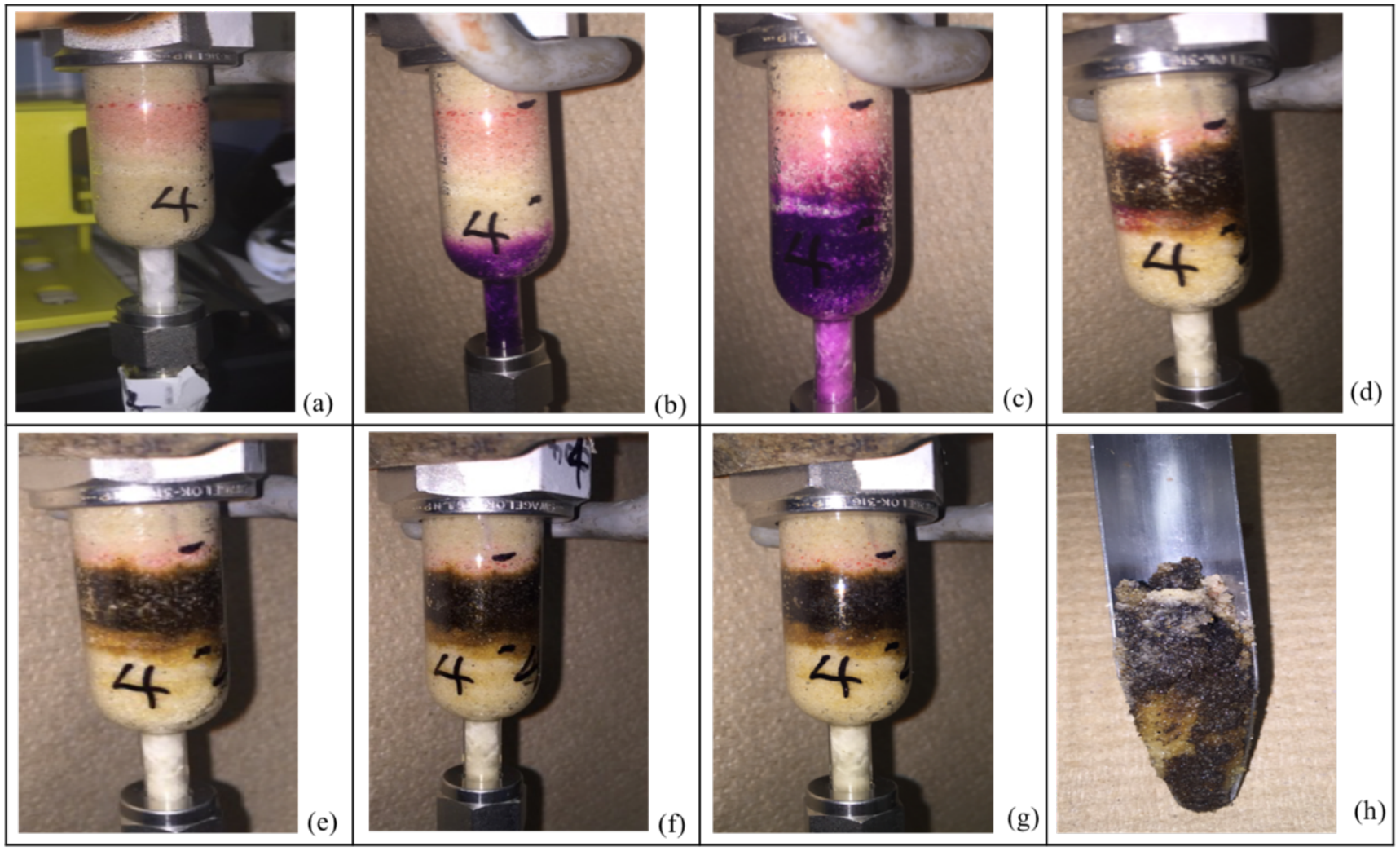

Figure S3.14 The images of the PM/PS-1 column. (a) at initial period, (b) during the PM injection, (c, d) during the synthetic groundwater injection, (e) during the 1-day stop-flow-1, (f) during the PS injection, (g) during 5-day stop-flow-2, (h) treated soil in the Zone 3 and source zone.

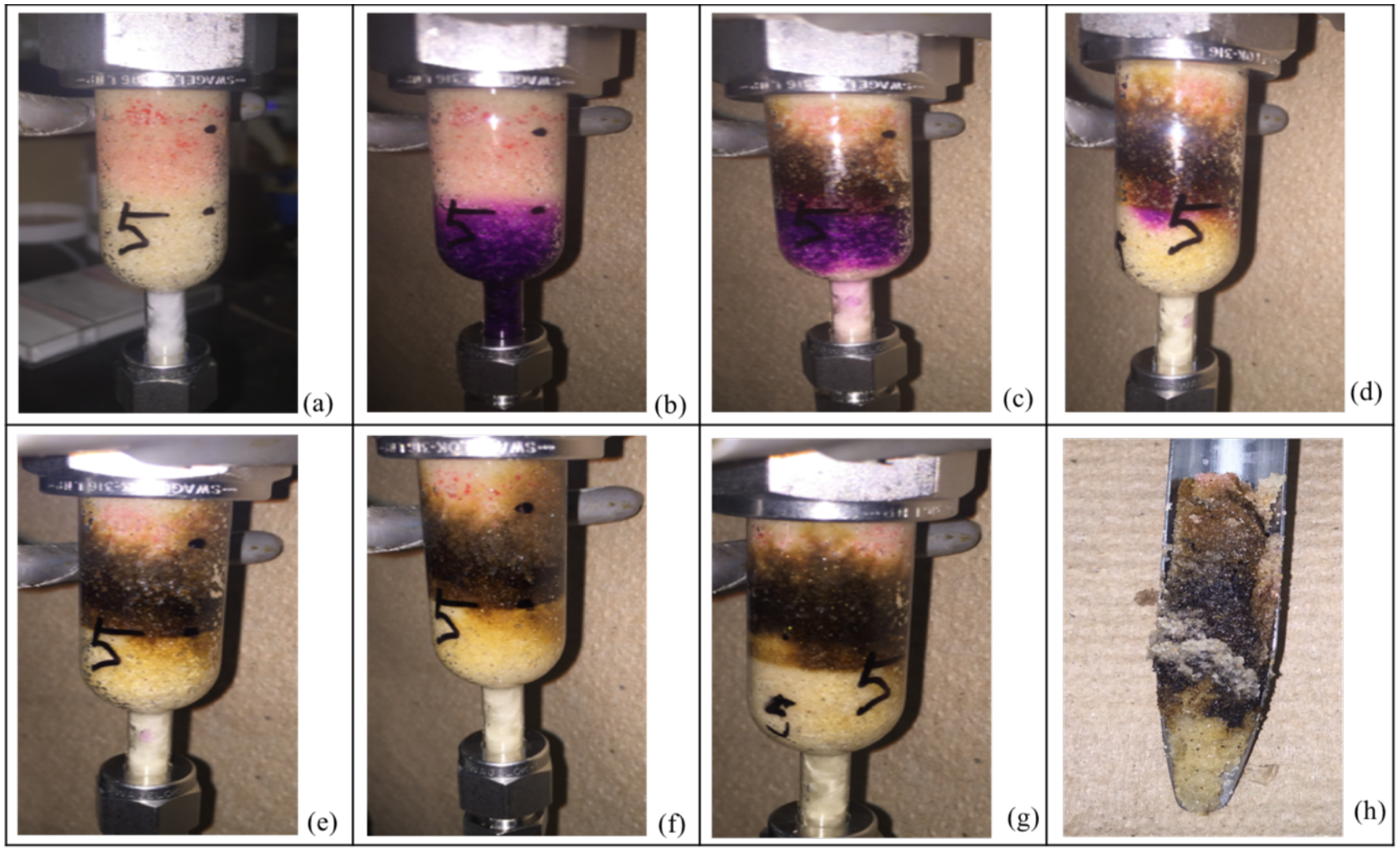

Figure S3.15 The images of the PM/PS-2 column. (a) at initial period, (b) during the PM injection, (c, d) during the synthetic groundwater injection, (e) during the 1-day stop-flow-1, (f) during the PS injection, (g) during 5-day stop-flow-2, (h) treated soil in the Zone 3 and source zone.

Table S3.1 Elemental composition of birnessite from different work (after Händel et al. 2013).

Sample source	Mn (wt.%)	K (wt.%)	Na (wt.%)	O+H (wt.%)	Cl (wt. %)
our birnessite	56.0	4.9	-	38.5	0.7
Händel et al. (2013)	55.5	5.1	0.9	38.5	-
(Händel et al., 2013) after McKenzie's method	55.7	4.8	<0.02	39.5	-
Gaines et al. (1997)	52.9	-	6.3	40.8	-
Ching et al. (1997)	54.9	10.9	-	38.2	-
Ma et al. (1999)	50.8	11.9	-	37.3	-

Table S3.2 1-methylnaphthalene concentration(mg/L) from pre-synthesized $MnO_{2(s)}$ Sample #1 and Sample #2 systems.

Time	Ctrl-MQ	Ctrl-GW	Ctrl-PS	PS-Birnessite (1:5)	PS-MnO_2 (1:5)	PS-MnO_2 (1:10)	PS-MnO_2 (1:20)	PS-MnO_2 (1:20)/GW
Day 0	5.5	5.3	5.4	5.1	5.3	5.3	5.3	5.5
Day 1	5.1	5.3	4.9	4.5	4.8	4.5	4.4	3.6
Day 2	5.0	5.3	4.2	3.5	4.2	3.8	3.7	2.3
Day 4	5.4	5.4	3.7	2.0	3.4	2.6	2.5	1.0
Day 6	5.3	5.1	3.5	1.2	3.0	2.3	1.8	0.4
Day 8	5.5	5.2	3.0	0.5	2.3	1.8	0.9	0.08
Day 10	5.4	4.6	2.3	0.3	1.9	1.4	0.7	0.02
Reduction (%)	2%	13%	57%	95%	65%	74%	87%	100%

Table S3.3 PS concentration (g/L) from pre-synthesized $MnO_{2(s)}$ Sample #1 and Sample #2 systems.

Time	Ctrl-MQ	Ctrl-GW	Ctrl-PS	PS-Birnessite (1:5)	PS-MnO_2 (1:5)	PS-MnO_2 (1:10)	PS-MnO_2 (1:20)	PS-MnO_2 (1:20)/GW
Day 0	-	-	0.56	0.57	0.54	0.56	0.58	0.58
Day 1	-	-	0.55	0.54	0.54	0.53	0.55	0.54
Day 2	-	-	0.54	0.51	0.52	0.53	0.53	0.50
Day 3	-	-	0.53	0.49	0.51	0.53	0.53	0.50
Day 4	-	-	0.52	0.49	0.50	0.51	0.50	0.47
Day 5	-	-	0.51	0.47	0.50	0.50	0.49	0.45
Day 6	-	-	0.51	0.46	0.49	0.49	0.49	0.45
Day 7	-	-	0.50	0.47	0.50	0.48	0.49	0.45
Day 8	-	-	0.49	0.44	0.49	0.48	0.48	0.44
Day 9	-	-	0.49	0.43	0.47	0.46	0.48	0.44
Day 10	-	-	0.49	0.42	0.45	0.47	0.46	0.42
Reduction (%)	-	-	13%	26%	17%	16%	21%	27%

Table S3.4 pH change in the reactors from pre-synthesized $MnO_{2(s)}$ Sample #1 and Sample #2 systems.

Time	Ctrl-MQ	Ctrl-GW	Ctrl-PS	PS-Birnessite (1:5)	PS-MnO_2 (1:5)	PS-MnO_2 (1:10)	PS-MnO_2 (1:20)	PS-MnO_2 (1:20)/GW
Day 0	6.2	7.2	4.5	4.4	4.7	4.7	4.6	4.2
Day 1	5.7	7.0	4.4	4.4	4.8	4.6	4.5	3.7
Day 2	6.3	7.4	4.7	4.3	4.6	4.5	4.9	3.5
Day 3	6.0	7.4	4.3	4.5	4.7	4.6	4.5	3.6
Day 4	6.3	7.2	4.3	4.4	4.6	4.5	4.6	3.5
Day 5	6.0	7.5	4.2	4.3	5.0	4.8	4.6	3.9
Day 6	6.5	7.5	4.1	4.6	4.7	4.5	4.5	3.9
Day 7	6.7	7.4	4.0	4.3	4.8	4.6	4.5	3.8
Day 8	7.1	7.6	3.9	4.5	4.7	4.5	4.4	3.9
Day 9	6.7	7.6	3.9	4.4	5.4	4.7	4.6	3.8
Day 10	6.8	7.5	4.2	4.4	5.5	5.0	4.6	3.8

Table S3.5 PM and PS concentration in PM/PS system.

Time	Ctrl-PM		Ctrl-PS		PM/PS	
	PM concentration (g/L)	PS concentration (g/L)	PM concentration (g/L)	PS concentration (g/L)	PM concentration (g/L)	PS concentration (g/L)
Day 0	1.60	- [a]	-	0.50	1.60	NA [b]
Day 1	0.23	-	-	0.49	<MDL [c]	0.49
Day 2	<MDL [d]	-	-	0.49	<MDL	0.48
Day 3	<MDL	-	-	0.47	<MDL	0.47
Day 4	<MDL	-	-	0.47	<MDL	0.47
Day 5	<MDL	-	-	0.47	<MDL	0.46
Day 6	<MDL	-	-	0.47	<MDL	0.45
Day 7	<MDL	-	-	0.46	<MDL	0.44
Day 8	<MDL	-	-	0.45	<MDL	0.43
Day 9	<MDL	-	-	0.45	<MDL	0.42
Day 10	<MDL	-	-	0.44	<MDL	0.41
Day 11	<MDL	-	-	0.43	<MDL	0.41

Note:

a. Data is not applicable.
b. PS is not added into PM/PS system at Day 1.
c. PM concentration is below method detection method.
d. PS concentration is below method detection method.

Table S3.6 The effluent concentrations from Ctrl-GW column of the column experiments.

Operating conditions		Effluent (ml, eqv. mg) [a]	TCE concentration (mg/L)	TCE mass (mg)	1-methylnaphthalene concentration (mg/L)	1-methylnaphthalene mass (mg)
GW (3 PVs)	1st PV	4.7	687	3.2	4.4	0.02
	2nd PV	4.2	712	3.0	7.7	0.03
	3rd PV	4.1	960	4.0	8.4	0.04
GW (1 V)		4.1	949	3.9	8.3	0.03
Stop-flow-1 (1 day)		-	-	-	-	-
GW (1 PV)		4.2	1000	4.2	9.1	0.04
Stop-flow-2 (5 days)		-	-	-	-	-

Note:

a. The volume of effluent was equivalent to the mass of effluent.

Table S3.7 The effluent concentrations from Ctrl-PM column of the column experiments.

Operating conditions		Effluent (ml, eqv. mg)	TCE concentration (mg/L)	TCE mass (mg)	1-methylnaphthalene concentration (mg/L)	1-methylnaphthalene mass (mg)
GW (3 PVs)	1st PV	3.8	603	2.3	4.7	0.02
	2nd PV	3.7	753	2.8	8.2	0.03
	3rd PV	4.0	946	3.8	8.7	0.04
PM (1 PV)		4.0	233	0.9	8.2	0.03
Stop-flow (5 days)		-	-	-	-	-

Table S3.8 The effluent concentrations from Ctrl-PS column of the column experiments.

Operating conditions		Effluent (ml, eqv. mg)	TCE concentration (mg/L)	TCE mass (mg)	1-methylnaphthalene concentration (mg/L)	1-methylnaphthalene mass (mg)
GW (3 PVs)	1st PV	4.4	664	2.9	4.8	0.02
	2nd PV	4.1	781	3.2	7.8	0.03
	3rd PV	4.5	953	4.3	8.7	0.04
PS (1 PV)		3.6	420	1.5	10.2	0.04
Stop-flow (5 days)		-	-	-	-	-

Table S3.9 The effluent concentrations from PM/PS-1 column of the column experiments.

Operating conditions		Effluent (ml, eqv. mg)	TCE concentration (mg/L)	TCE mass (mg)	1-methylnaphthalene concentration (mg/L)	1-methylnaphthalene mass (mg)
GW (3 PVs)	1st PV	4.2	651	2.7	4.4	0.02
	2nd PV	4.1	753	3.1	7.5	0.03
	3rd PV	4.6	892	4.1	8.3	0.04
PM (0.25 PV) + GW (0.75 PV)		3.5	276	0.98	8.5	0.03
Stop-flow-1 (1 day)		-	-	-	-	-
PS (1 PV)		4.2	205	0.86	6.3	0.03
Stop-flow-2 (5 days)		-	-	-	-	-
GW (1 PV)		4.1	<MDL	-	4.1	0.02

Table S3.10 The effluent concentrations from PM/PS-2 column of the column experiments.

Operating conditions		Effluent (ml, eqv. mg)	TCE concentration (mg/L)	TCE mass (mg)	1-methylnaphthalene concentration (mg/L)	1-methylnaphthalene mass (mg)
GW (3 PVs)	1st PV	4.1	674	2.8	4.1	0.02
	2nd PV	4.8	701	3.3	8.0	0.04
	3rd PV	4.5	934	4.2	9.3	0.04
PM (0.25 PV) + GW (0.75 PV)		4.6	214	1.0	10.4	0.05
Stop-flow-1 (1 day)		-	-	-	-	-
PS (1 PV)		3.9	198	0.8	8.2	0.03
Stop-flow-2 (5 days)		-	-	-	-	-

Chapter 4

Chapter 4
Conclusions & Recommendations

4

4.1 Conclusions

The core findings of this research can be summarized as follows:

- $MnO_{2(s)}$ is an effective PS activator.
- In the $MnO_{2(s)}$ activated PS system, the 1-methylnaphthalene reaction rate coefficient is about one order-of-magnitude higher than in an equivalent unactivated PS system.
- Increasing the dosage of $MnO_{2(s)}$ increased the degradation kinetics of 1-methylnaphthalene.
- The degradation kinetics of 1-methylnaphthalene using the $MnO_{2(s)}$ activated PS system in synthetic groundwater is two- to three- fold higher than in Milli-Q water.
- PS activation by $MnO_{2(s)}$ resulted in 2 to 8 times faster degradation rate compared to unactivated PS for 1-methylnaphthalene treatment in batch experiments.
- $MnO_{2(s)}$ remain unaltered (visually) during the PS activation process.
- The pre-synthesized $MnO_{2(s)}$ experiments confirmed that some types of organic compounds are not able to produce effective $MnO_{2(s)}$ for PS activation. $MnO_{2(s)}$ with a K content higher than 7 % did not activate PS.
- The minimum PM to PS molar ratio for effective organic compound treatment is 13:1.

4.2 Recommendations

Based on this proof-of-concept study, the proposed dual oxidant system (PM/PS) is a promising system and should be investigated further.

The PM/PS system could be enhanced through multiple PS injection episodes since the $MnO_{2(s)}$ remains unaltered during the PS activation process. For the stop-flow column experiments, an addition flush of synthetic groundwater after the PM injection episode would have provided a buffered pH environment for improved PS activation. Increasing the reaction period might also be beneficial for the degradation of organics. The effluent PS concentration should be analyzed to provide an estimate of the PS decomposition during the treatment process.

Additional PM/PS batch tests for the treatment of probe contaminants (e.g., nitrobenzene, *tert*-butyl alcohol) are needed for the identification of radicals generated during the PS activation process. This work would be beneficial to understand the mechanisms and pathways underlying the PM/PS system.

It is thus necessary to identify whether other target organic compounds are able to generate effective MnO_2(s) after the reaction with PM to activate persulfate.

The minimum PM and PS molar ratio was determined as 13:1 in this study, but the optimal molar ratio was not identified. Excess PM will produce excess $MnO_{2(s)}$, which could reduce the NAPL dissolution rate, decrease the local permeability of the porous medium, and further adversely affect treatment. Future research is needed to explore the optimum PM to PS molar ratio.

References

Agency for Toxic Substances and Disease Registry; U.S. Department of Health and Human Services. (2007). *Toxicological Profile for Benzene: Potential for Human Exposure*. Atlanta, GA.

Ahmad, M., Teel, A. L., & Watts, R. J. (2010). Persulfate activation by subsurface minerals. *Journal of Contaminant Hydrology*, *115*(1–4), 34–45.

ASTM-D6520-06. (2012). Standard Practice for the Solid Phase Micro Extraction (SPME) of Water and its Headspace for the Analysis of Volatile and Semi-Volatile, 1–6.

Baciocchi, R., Boni, M. R., & D'Aprile, L. (2004). Application of H2O2 lifetime as an indicator of TCE Fenton-like oxidation in soils. *Journal of Hazardous Materials*, *107*(3), 97–102.

Ching, S., Petrovay, D. J., Jorgensen, M. L., & Suib, S. L. (1997). Sol−Gel Synthesis of Layered Birnessite-Type Manganese Oxides. *Inorganic Chemistry*, *36*(5), 883–890.

Chokejaroenrat, C., Comfort, S., Sakulthaew, C., & Dvorak, B. (2014). Improving the treatment of non-aqueous phase TCE in low permeability zones with permanganate. *Journal of Hazardous Materials*, *268*, 177–184.

Crimi, M. L., Quickel, M., & Ko, S. (2009). Enhanced permanganate in situ chemical oxidation through MnO2 particle stabilization: Evaluation in 1-D transport systems. *Journal of Contaminant Hydrology*, *105*(1–2), 69–79.

Crimi, M. L., & Siegrist, R. L. (2004). Impact of Reaction Conditions on MnO[sub 2] Genesis during Permanganate Oxidation. *Journal of Environmental Engineering*, *130*(5), 562.

Cui, J., Zhang, L., Xi, B., Zhang, J., & Mao, X. (2017). Chemical oxidation of benzene and trichloroethylene by a combination of peroxymonosulfate and permanganate linked by in-situ generated colloidal / amorphous MnO2. *Chemical Engineering Journal*, *313*, 815–825.

Do, S.-H., Kwon, Y.-J., & Kong, S.-H. (2010). Effect of metal oxides on the reactivity of persulfate/Fe(II) in the remediation of diesel-contaminated soil and sand. *Journal of Hazardous Materials*, *182*(1–3), 933–936.

Do, S. H., Kwon, Y. J., & Kong, S. H. (2010). Effect of metal oxides on the reactivity of persulfate/Fe(II) in the remediation of diesel-contaminated soil and sand. *Journal of Hazardous Materials*, *182*(1–3), 933–936.

Furman, O. S., Teel, A. L., & Watts, R. J. (2010). Mechanism of base activation of persulfate. *Environmental Science and Technology*, *44*(16), 6423–6428.

Gaines, R. V., Skinner, C. W., Foord, E. E., Mason, B., & Rosenzweig, A. (1997). *Dana's new mineralogy : the system of mineralogy of James Dwight Dana and Edward Salisbury Dana.* (8th ed.). New York, NY: John Wiley & Sons.

Gao, S., Cui, J., Xiong, Y., Xiao, W., Wang, D., Alshawabkeh, A. N., & Mao, X. (2015). Synergetic effect of the mineralization of organic contaminants by a combined use of permanganate and peroxymonosulfate. *Separation and Purification Technology*, *144*, 248–255.

Händel, M., Rennert, T., & Totsche, K. U. (2013). A simple method to synthesize birnessite at ambient pressure and temperature. *Geoderma*, *193–194*(February 2013), 117–121.

Heiderscheidt, J. L., Crimi, M., Siegrist, R. L., & Singletary, M. A. (2008). Optimization of full-scale permanganate ISCO system operation: Laboratory and numerical studies. *Ground Water Monitoring and Remediation*, *28*(4), 72–84.

Huang, K. C., Couttenye, R. a., & Hoag, G. E. (2002). Kinetics of heat-assisted persulfate oxidation of methyl tert-butyl ether (MTBE). *Chemosphere*, *49*(4), 413–420.

Huang, K. C., Hoag, G. E., Chheda, P., Woody, B. A., & Dobbs, G. M. (2002). Chemical oxidation

of trichloroethylene with potassium permanganate in a porous medium. *Advances in Environmental Research*, *7*(1), 217–229.

Huling, S. G., & Pivetz, B. E. (2006). *Engineering Issue In-Situ Chemical Oxidation*. Cincinnati, OH.

Huling, S. G., & Weaver, J. W. (1991). *Ground Water Issue: Dense Nonaqueous Phase Liquids*.

Jo, Y. H., Do, S. H., & Kong, S. H. (2014). Persulfate activation by iron oxide-immobilized MnO2 composite: Identification of iron oxide and the optimum pH for degradations. *Chemosphere*, *95*, 550–555.

Kim, K., & Gurol, M. D. (2005). Reaction of nonaqueous phase TCE with permanganate. *Environmental Science and Technology*, *39*(23), 9303–9308.

Krembs, F. J., Siegrist, R. L., Crimi, M. L., Furrer, R. F., & Petri, B. G. (2010). ISCO for Groundwater Remediation: Analysis of Field Applications and Performance. *Ground Water Monitoring & Remediation*, *30*(4), 42–53.

Li, W., Orozco, R., Camargos, N., & Liu, H. (2017). Mechanisms on the Impacts of Alkalinity, pH and Chloride on Persulfate-based Groundwater Remediation. *Environmental Science & Technology*, acs.est.6b04849.

Li, X. D., & Schwartz, F. W. (2002). Permanganate oxidation schemes for the remediation of source zone DNAPLs and dissolved contaminant plumes. In *Chlorinated Solvent and DNAPL Remediation* (Vol. 837, pp. 73–85). https://doi.org/10.1021/bk-2002-0837.ch005

Li, X. D., & Schwartz, F. W. (2004a). DNAPL mass transfer and permeability reduction during in situ chemical oxidation with permanganate. *Geophysical Research Letters*, *31*(6), 1–5.

Li, X. D., & Schwartz, F. W. (2004b). DNAPL remediation with in situ chemical oxidation using potassium permanganate. Part I. Mineralogy of Mn oxide and its dissolution in organic acids. *Journal of Contaminant Hydrology*, *68*(2004), 39–53.

Li, X. D., & Schwartz, F. W. (2004c). DNAPL remediation with in situ chemical oxidation using potassium permanganate. Part II. Increasing removal efficiency by dissolving Mn oxide precipitates. *Journal of Contaminant Hydrology*, *68*(2004), 269–287.

Liang, C., Bruell, C. J., Marley, M. C., & Sperry, K. L. (2004). Persulfate oxidation for in situ remediation of TCE. I. Activated by ferrous ion with and without a persulfate-thiosulfate redox couple. *Chemosphere*, *55*(9), 1213–1223.

Liang, C., Huang, C. F., Mohanty, N., & Kurakalva, R. M. (2008). A rapid spectrophotometric determination of persulfate anion in ISCO. *Chemosphere*, *73*(9), 1540–1543.

Liang, C. J., Bruell, C. J., Marley, M. C., & Sperry, K. L. (2003). Thermally Activated Persulfate Oxidation of Trichloroethylene (TCE) and 1,1,1-Trichloroethane (TCA) in Aqueous Systems and Soil Slurries. *Soil and Sediment Contamination*, *12*(2), 207–228.

Liang, C., Wang, Z. S., & Bruell, C. J. (2007). Influence of pH on persulfate oxidation of TCE at ambient temperatures. *Chemosphere*, *66*(1), 106–113.

Liu, H., Bruton, T. A., Doyle, F. M., & Sedlak, D. L. (2014a). In situ chemical oxidation of contaminated groundwater by persulfate: Decomposition by Fe(III)- and Mn(IV)-containing oxides and aquifer materials. *Environmental Science and Technology*, *48*(17), 10330–10336.

Liu, H., Bruton, T. A., Doyle, F. M., & Sedlak, D. L. (2014b). In situ chemical oxidation of contaminated groundwater by persulfate: Decomposition by Fe(III)- and Mn(IV)-containing oxides and aquifer materials. *Environmental Science and Technology*, *48*(17).

Liu, H., Bruton, T. A., Li, W., Buren, J. Van, Prasse, C., Doyle, F. M., & Sedlak, D. L. (2016). Oxidation of Benzene by Persulfate in the Presence of Fe(III)- and Mn(IV)-Containing Oxides: Stoichiometric Efficiency and Transformation Products. *Environmental Science &*

Technology, (Iii), acs.est.5b04815.
Ma, Y., Luo, J., & Sl, S. (1999). Syntheses of birnessites using alcohols as reducing reagents: Effects of synthesis parameters on the formation of birnessites. *Chemistry of Materials*, *11*(8), 1972–1979.
MacKinnon, L. K., & Thomson, N. R. (2002). Laboratory-scale in situ chemical oxidation of a perchloroethylene pool using permanganate. *Journal of Contaminant Hydrology*, *56*(1–2), 49–74.
McIsaac, A. (2013). Evaluation of persulfate for the treatment of manufactured gas plant residuals.
McKenzie, R. M. (1971). The Synthesis of Birnessite, Cryptomelane, and Some Other Oxides and Hydroxides of Manganese. *Mineralogical Magazine*, *38*(296), 493–502.
Mitchell, S. M., Ahmad, M., Teel, A. L., & Watts, R. J. (2014). Degradation of Perfluorooctanoic Acid by Reactive Species Generated through Catalyzed H2O2 Propagation Reactions. *Environmental Science & Technology Letters*, *1*(1), 117–121.
Newell, C. J., Acree, S. D., Ross, R. R., & Huling, S. G. (1995). *Ground Water Issue: Light Nonaqueous Liquids*. Houston, TX (United States).
Petri, B. G., Thomson, N. R., & Urynowicz, M. a. (2011). Fundamentals of ISCO Using Permangante. In R. L. Siegrist, M. Crimi, & T. J. Simpkin (Eds.), *In Situ Chemical Oxidation for Groundwater remediation* (pp. 89–146). New York, NY: Springer New York.
Petri, B. G., Watts, R. J., Aikaterini, T., Crimi, M. L., Thomson, N. R., & Teel, A. L. (2011). Fundamentals of ISCO Using Persulfate. In R. L. Siegrist, M. Crimi, & T. J. Simpkin (Eds.), *In Situ Chemical Oxidation for Groundwater remediation* (pp. 147–191). New York, NY: Springer New York.
Petri, B. G., Watts, R. J., Teel, A. L., Huling, S. G., & Brown, R. A. (2011). Fundamentals of ISCO Using Hydrogen Peroxide. In R. L. Siegrist, M. Crimi, & T. J. Simpkin (Eds.), *In Situ Chemical Oxidation for Groundwater remediation* (pp. 33–88). New York, NY: Springer New York.
Pivetz, B. (2012). *Framework for Site Characterization for Monitored Natural Attenuation of Volatile Organic Compounds in Ground Water*. Cincinnati.
Schroth, M. H., Oostrom, M., Wietsma, T. W., & Istok, J. D. (2001). In-situ oxidation of trichloroethene by permanganate: effects on porous medium hydraulic properties. *Journal of Contaminant Hydrology*, *50*(1–2), 79–98.
Siegrist, R. L., Crimi, M., & Brown, R. A. (2011). In Situ Chemical Oxidation: Technology Description and Status. In R. L. Siegrist, M. Crimi, & T. J. Simpkin (Eds.), *In Situ Chemical Oxidation for Groundwater Remediation* (pp. 1–32). New York, NY: Springer New York.
Siegrist, R. L., Urynowicz, M. a., Crimi, M. L., & Lowe, K. S. (2002). Genesis and Effects of Particles Produced during In Situ Chemical Oxidation Using Permanganate. *Journal of Environmental Engineering*, *128*(11), 1068–1079.
Siegrist, R. L., Urynowicz, M. a., West, O. R., Crimi, M. L., & Lowe, K. S. (2001). *Principles and practices of in situ chemical oxidation using permanganate*. Battelle Press (January 2001).
Sra, K. S. (2010). *Persulfate Persistence and Treatability of Gasoline Compounds*. University of Waterloo.
Sra, K. S., Thomson, N. R., & Barker, J. F. (2014). Stability of Activated Persulfate in the Presence of Aquifer Solids. *Soil and Sediment Contamination: An International Journal*, *23*(8), 820–837.
Thomson, N. R., Fraser, M. J., Lamarche, C., Barker, J. F., & Forsey, S. P. (2008). Rebound of a coal tar creosote plume following partial source zone treatment with permanganate. *Journal*

of Contaminant Hydrology, *102*(1–2), 154–171. https://doi.org/10.1016/j.jconhyd.2008.07.001

Tunnicliffe, B. S., & Thomson, N. R. (2004). Mass removal of chlorinated ethenes from rough-walled fractures using permanganate. *Journal of Contaminant Hydrology*, *75*(1–2), 91–114. https://doi.org/10.1016/j.jconhyd.2004.04.006

Urynowicz, M. A., & Siegrist, R. L. (2005). Interphase mass transfer during chemical oxidation of TCE DNAPL in an aqueous system. *Journal of Contaminant Hydrology*, *80*(3–4), 93–106. https://doi.org/10.1016/j.jconhyd.2005.05.002

USEPA. (2013). *Superfund Remedy Report: Fourteenth Edition*.

USEPA. (2016). NPL Site Totals by Status and Milestone. Retrieved September 17, 2016, from https://www.epa.gov/superfund/npl-site-totals-status-and-milestone

Waldemer, R. H., & Tratnyek, P. G. (2006). Kinetics of contaminant degradation by permanganate. *Environmental Science and Technology*, *40*(3), 1055–1061.

Watts, R. J., Asce, M., & Teel, A. L. (2006). Treatment of Contaminated Soils and Groundwater Using ISCO, *10*(1), 2–9.

Watts, R. J., Finn, D. D., Cutler, L. M., Schmidt, J. T., & Teel, A. L. (2007). Enhanced stability of hydrogen peroxide in the presence of subsurface solids. *Journal of Contaminant Hydrology*, *91*(3), 312–326.

Wilson, S., Farone, W., Leonard, G., Birnstingl, J., & Leombruni, A. (2013). CATALYZED PERSULFATE : Advancing In Situ Chemical Oxidation (ISCO) Technology. In *2013 REGENESIS Bioremediation Products* (pp. 1–16). San Clemente, CA.

Xu, X. (2006). *Interaction of Chemical Oxidants with Aquifer Materials*. University of Waterloo.

Xu, X., & Thomson, N. R. (2007). An evaluation of the green chelant EDDS to enhance the stability of hydrogen peroxide in the presence of aquifer solids. *Chemosphere*, *69*(5), 755–762.

Yan, Y. E., & Schwartz, F. W. (1999). Oxidative degradation and kinetics of chlorinated ethylenes by potassium permanganate. *Journal of Contaminant Hydrology*, *37*(3–4), 343–365.

Yan, Y. E., & Schwartz, F. W. (2000). Kinetics and mechanisms for TCE oxidation by permanganate. *Environmental Science and Technology*, *34*(12), 2535–2541.

Appendix A

The $MnO_{2(s)}$ Sample #2 applied as PS activator for benzene treatment

In order to verify the applicability of pre-synthesized $MnO_{2(s)}$ Sample #2 as PS activator for different types of organics' treatment, benzene (1.5 mg/L) is examined as treated organic with PS (1 g/L) at PS to $MnO_{2(s)}$ Sample #2 mass ratios of 1:20 over 10 days in synthetic groundwater. A series of batch reactors similar in principal to those discuss in Section 2.3.1.1 was conducted.

The normalized 1-methylnaphthalene, PS and pH temporal profiles are shown in Figure A1, A2, and A3. The removal percentage of benzene in Ctrl-PS system reaches to 89% at Day 10 (Figure A1; Table A1). According to the direct benzene oxidation by PS given in Eq 1.11, at least 0.06 g/L PS is required to oxidize 1.5 mg/L benzene, suggesting that the PS in the reactors is at sufficient amount to degrade benzene without any activators. In the PS-MnO_2 (1:20) system, benzene is completely removed at day 6, indicating the presence of $MnO_{2(s)}$ could enhance the benzene degradation. The PS decomposition with the presence of $MnO_{2(s)}$ is higher than that with Ctrl-PS system (Figure A2).

The pH of the Ctrl-PS system was about 7 (Figure A3). It might because that the buffering capacity of synthetic groundwater influences the pH, and the presence of benzene may also be having an effect. However, the $MnO_{2(s)}$ could activate PS to release ions (might be hydrogen ions) and decrease the pH in the reactors of 'PS-MnO_2 (1:20)' (Figure A3).

Benzene is effectively degraded in presence of $MnO_{2(s)}$ and PS. Especially, PM is very unreactive with benzene, while PM/PS system is highly reactive with benzene. It suggested that the dual oxidant (PM/PS) system is applicable for various types of organic contaminants.

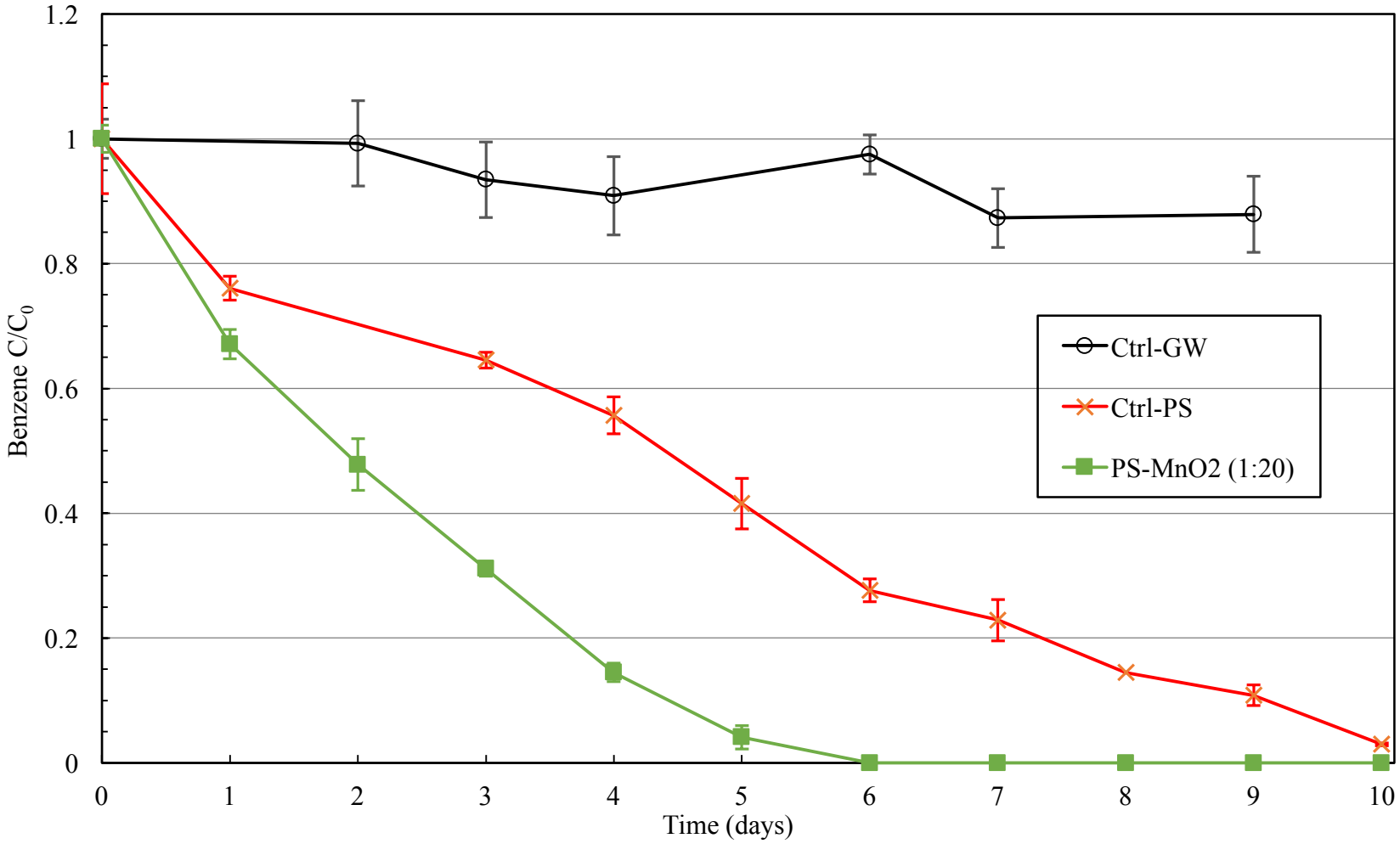

Figure A1 Normalized benzene temporal profiles in pre-synthesized $MnO_{2(s)}$ Sample #2 system (benzene as treated organic). The error bars represent the standard deviation from triplicate reactors.

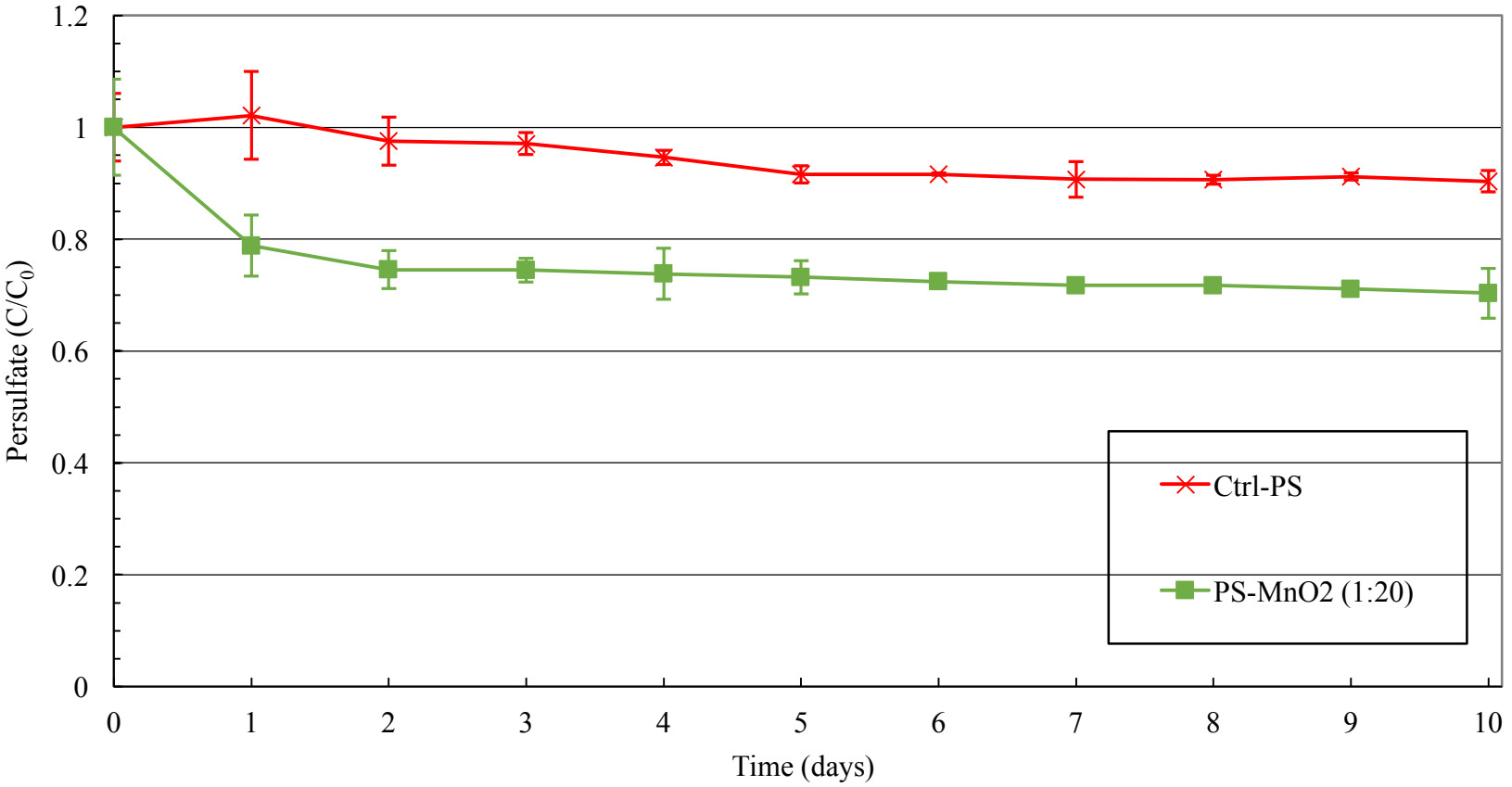

Figure A2 Normalized PS temporal profiles in pre-synthesized $MnO_{2(s)}$ Sample #2 system (benzene as treated organic). The error bars represent the standard deviation from triplicate reactors.

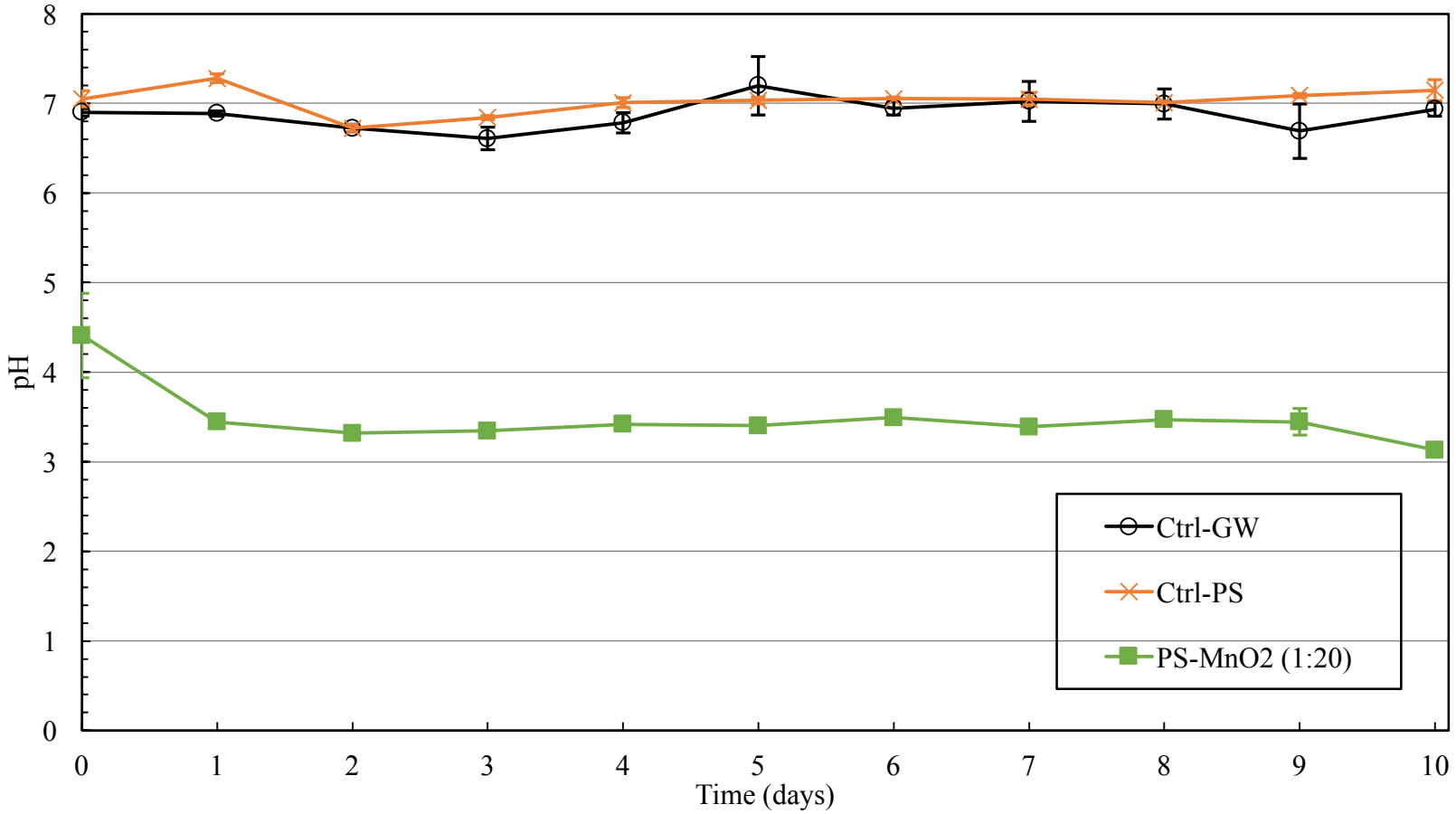

Figure A3 pH temporal profiles in pre-synthesized $MnO_{2(s)}$ Sample #2 system (benzene as treated organic). The error bars represent the standard deviation from triplicate reactors.

Table A1 Benzene concentration (mg/L) in pre-synthesized $MnO_{2(s)}$ Sample #2 system (benzene as treated organic).

Time	Ctrl-GW	Ctrl-PS	PS-MnO_2 (1:20)
Day 0	1.49	1.50	1.68
Day 1	-[a]	1.14	1.13
Day 2	1.47	-	0.80
Day 3	1.39	0.97	0.52
Day 4	1.35	0.84	0.24
Day 5	-	0.62	0.069
Day 6	1.45	0.42	<MDL
Day 7	1.30	0.34	<MDL
Day 8	-	0.22	<MDL
Day 9	1.31	0.16	<MDL
Day 10	-	0.045	<MDL
Reduction (%)	12.1%	89.2%	100%

Note:

a. Data was not applicable.

Appendix B

Table B1 Summary of ISCO studies using permanganate and persulfate.

Reference	Oxidants	System type	Target compounds	MnO_2 formation process	Persulfate activation mechanism	Summary of major findings
(Ahmad et al. 2010)	Persulfate	Aqueous	Oxidant probe, nitrobenzene; Reductant, hexachloroethane.	Manganese oxides mineral: birnessite [δ-MnO_2]	Soil and aquifer solids: Four iron and manganese oxides and two clay minerals	• The manganese oxide birnessite was the most effective initiator of persulfate for degrading the oxidant probe nitrobenzene, indicating that oxides are generated at both low and high pH regimes. • Manganese oxide: goethite [FeOOH], hematite [Fe_2O_3], ferrihydrite [$Fe_5HO_8{\cdot}4H_2O$], birnessite [δ-MnO_2], kaolinite [$Al_2Si_2O_5(OH)_4$], montmorillonite [(Na,Ca)(Al, $Mg)_6(Si_4O_{10})_3(OH)_6{\cdot}\ nH_2O$]. • Clay minerals: goethite [FeOOH], hematite [Fe_2O_3], ferrihydrite [$Fe_5HO_8{\cdot}4H_2O$]
(Crimi et al. 2009)	Permanganate	1-D column	TCE		NA	• Previous findings on the control and inhibition of MnO_2 particles deposition: increasing repulsive forces between porous media and particles. • HMP is a promising aid to stabilize MnO_2. With the use of HMP, a low mass of MnO_2 remained in the mobile phase. The use of HMP also can reduce the bypass flow of permanganate.
(Crimi and Siegrist 2004)	Permanganate (25 or 50 g/l)	Bench scale, batch experiments.	TCE (0, 10, 20, 40 mg/L)	With the increase of TCE and permanganate concentrations, reaction time, and the influence of	NA	• 'The presence of calcium results in larger, settleable solids than without calcium'. • The suspended particles (as opposed to soluble and/or settleable) were at a larger amount at pH 3 than at pH 7. • The manganese transformation progression: • $MnO_4^- \rightarrow MnO_2(soluble) \rightarrow MnO_2(colloidal) \rightarrow MnO_2(precipitate)$

				pH and matrix conditions, the MnO_2 transformed from soluble state, to colloidal state and precipitate state.		
(Cui et al. 2017)	Optimal combination: permanganate (1.8 mM), peroxymonosulfate (PMS, 2.4 mM)	Aqueous	Aqueous mixture of 0.3 mM benzene and TCE.	Colloidal MnO_2 in the initial stage of CUPP process, and the suspended MnO_2 after 4 h of CUPP reaction.	NA	• Combined use of PMS and permanganate (CUPP) exhibited favorable oxidizing capability because the in-situ colloidal and amorphous MnO_2 linked the two oxidants. • The suspended amorphous black MnO_2 and colloidal MnO_2 can activate PMS. • The combined use of two oxidants produced a synergetic effect on the removal of benzene.
(Do et al. 2010)	Persulfate	slurry	Diesel	Mineral, manganese oxide mineral pyrolusite (β-$MnO_{2(s)}$)	Fe(II) & metal oxides: goethite, hematite, magnetite, and manganese oxide ($\beta - MnO_2$, pyrolusite)	• Manganese oxide could increase the reactivity of PS most. Manganese oxide degraded diesel more than did any of the other metal oxides. • The highest diesel degradation by PS occurred when both manganese oxide and Fe(II) were used as activators.
(Gao et al. 2015)	Permanganate (2.9 mM) and peroxymonosulfate (PMS, Oxone; 5.8 mM)	Aqueous	Acid orange 7 (AO7; 50 mg/L)	Suspended particulate MnO_2: the particulate manganese dioxide with a brown-black color was formed.	Suspended particulate MnO_2 activate PMS. α-MnO_2 or Mn_3O_4 can effectively activate PMS	• Suspended particulate MnO_2, α-MnO_2 or Mn_3O_4 can effectively activate PMS.

(Huang et al. 2002)	Permanganate	Column tests	Dissolved phase and pure phase TCE	TCE-$KMnO_4$ reaction yield birnessite-type manganese oxide.	NA	• The MnO_x precipitates retained in columns reduced ~20% of the pore space in the columns.
(Jo et al. 2014)	Persulfate	aqueous	Carbon tetrachloride(CT) and benzene	Purchased pure, manganese oxide mineral pyrolusite (β-$MnO_{2(s)}$)	Iron oxide-immobilized manganese oxide (MnO_2)	• PS decomposed to produce oxidant sulfate radical ($SO_4^{\cdot-}$) under acidic conditions; oxidant hydroxyl radical ($OH^{\cdot}$) under basic conditions; reductant superoxide anion ($O_2^{\cdot-}$) under base-catalyzed PS system. The application of appropriate metal oxide composites in PS system might provide the reactive species (i.e. oxidant and reductant) effectively.
(Li and Schwartz 2002)	Permanganate	1-D column and 2-D flow tank	Dissolved TCE	MnO_2 rapidly formed a precipitation rind.	NA	• Once permanganate came in contact with dissolved TCE, MnO_2 was precipitated close to the zone with pure TCE DNAPL. • The zone of MnO_2 precipitation was in a light brown color. • With time, the precipitation of MnO_2 reduced the permeability across of the tanks through the formation of a precipitation rind above the DNAPL pool. • The experiment was haltered when MnO_2 was precipitated and a greater injection pressure was required to maintain the flow and subsequent permanganate injection.
(Li and Schwartz 2004a)	Permanganate	1-D columns	TCE	Light-brown color Mn oxide.	NA	• The column results suggested that the by-products CO_2 and MnO_2 could cause pore plugging and flow by-passing. • A hydraulic conductivity reduction as high as 80 % was quantified in a series of column experiments.
(Li and Schwartz 2004b)	Permanganate (30 g/L)	Batch experiments	TCE (75 g in 500 mL)	The solid by-product from the oxidation of TCE by	NA	• Organic acids including citric acid, oxalic acid and ethylenediaminetetraacetic acid (EDTA) could dissolve Mn oxide quickly.

				permanganate is semi-amorphous potassium-rich birnessite.		
(Li and Schwartz 2004c)	Permanganate (200 mg/L)	2-D flow-tank	Blue-dyed TCE (2 g)	-	NA	• The use of citrate and oxalate could control the plugging resulted from the precipitation of Mn oxide.
(Liu et al. 2014)	Persulfate (1 to 50 mM)	Aqueous	Benzene (0.1 to 1 mM)	Pyrolusite (β-$MnO_{2(s)}$) were obtained from Sigma-Aldrich	Minerals and clay materials.	• Iron- and manganese-containing minerals were able to decompose persulfate efficiently. • Minerals: Ferrihydrite ($Fe(OH)_{3(s)}$), Pyrolusite (β-$MnO_{2(s)}$), goethite (α-$FeOOH_{(s)}$), silica; The relative reactivity followed the order pyrolusite>ferrihydrite>goethite>silica. • The rate of persulfate decomposition accelerates when the injected oxidant reaches a contaminant plume. The decomposition rate of persulfate increased by as much as 100 times when benzene concentrations exceeded 0.1 mM. • $2S_2O_8^{2-} \xrightarrow{\text{Fe (III)or Mn(IV) oxide}} SO_4^{2-} + SO_4^{\cdot-} + S_2O_8^{\cdot-}$ • The persulfate decomposition could be enhanced when the aquifer solids contained greater approximately 2% of Fe(III)- or Mn(IV)-oxides.
(MacKinnon and Thomson 2002)	Permanganate	2-D saturated sand zone overlying a capillary barrier.	Dyed red perchloroethylene (PCE) with Sudan IV.	Black MnO_2 deposits.	NA	• The water flow velocity above the PCE pool decreased and the overall mass transfer rate from the remaining PCE pool also reduced due to the presence of MnO_2.

(Siegrist et al. 2002)	permanganate	Slurry	trichloroethylene (TCE)	-	NA	• The oxidant form of permanganate or reaction time had little effect on oxidant consumption or filterable solids (MnO_2) particles production. • ISCO with permanganate has the potential to yield system permeability loss. The magnitude of these effects is related the subsurface conditions (ambient silt/clay particles), target organic chemical mass, and permanganate dose and delivery method.
(Tunnicliffe and Thomson 2004)	Permanganate	Fracture aquifer system	TCE and PCE, dyed with Sudan IV.	Membrance-like $MnO_{2(s)}$	NA	• The MnO2 formation appeared and behaved like a flexiable 'membrance skin' varied between 1 and 15 mm over the DNAPL.
(Urynowicz and Siegrist 2005)	Permanganate		TCE	Manganese oxide solids formed a local deposition of film at the DNAPL interface.	NA	• The formation of $MnO_{2(s)}$ film could increase the interfacial resistance and decrease the TCE DNAPL dissolution rate, and further reduce the aqueous TCE concentration and the chemical oxidation rate.
(Yan and Schwartz 1999)	Permanganate	aqueous	Chlorinated ethylenes; tetrachloroethylene (PCE), trichloroethylene (TCE), three isomers of dichloroethylenes (DCEs)	By-products of chlorinated ethylenes and permanganate	NA	• In O_3/H_2O_2 system, key reactive intermediate hydroxyl radical, generated in this advanced oxidation process (AOP), strongly reacts with common inorganics species in ground water such as carbonate and bicarbonate. • The modeling results suggest that the effect of autocatalysis by MnO_2 on TCE degradation s significant when the system contains high concentration levels of MnO_4^- and TOC. • Competition of TOC for permanganate would be offset by the presence of a large quantity of MnO_2, which promotes the reaction between TCE and permanganate.